Title
Experimental investigations of photochemically-generated organic aerosols and applications to early Earth and Mars

Author
Chu, Emily Faye

Publication Date
2013

Peer reviewed|Thesis/dissertation

Experimental investigations of photochemically-generated organic aerosols and applications to early Earth and Mars

By

Emily Faye Chu

A dissertation submitted in partial satisfaction of the

requirements for the degree of

Doctor of Philosophy

in

Chemistry

in the

Graduate Division

of the

University of California, Berkeley

Committee in charge:

Professor Kristie A. Boering, Chair
Professor Stephen R. Leone
Professor Imke de Pater

Spring 2013

Abstract
Experimental investigations of photochemically-generated organic aerosols
and applications to early Earth and Mars

By

Emily Faye Chu

Doctor of Philosophy in Chemistry

University of California, Berkeley

Professor Kristie A. Boering, Chair

Aerosols in planetary atmospheres play a critical role in radiative transfer and thus also in determining the penetration depth of UV radiation and atmospheric temperatures. For early Mars and an anoxic early Earth, aerosols may have significantly influenced the stability of liquid water at the surface, as well as climate and habitability, yet the study of aerosol formation remains poorly constrained by models and experiments, making conclusions difficult. Significant progress can be made in reducing these uncertainties by providing additional laboratory constraints and tests for the photochemical and microphysical models used to generate the greatly varying predictions about aerosol formation in terrestrial-like atmospheres. Photochemistry experiments measuring gas- and condensed-phase species were conducted to determine (1) the extent to which a photochemical haze could have formed in Mars' and Earth's early atmospheres and (2) whether such aerosols might be depleted in carbon-13, providing a potentially false biosignature in organic matter in the Martian and terrestrial rock and meteorite records.

To gain a greater understanding of the fundamentals of aerosol formation in the CO_2-rich atmospheres of early Earth and Mars, methane (CH_4) and mixtures of CH_4 and carbon dioxide (CO_2) were irradiated with UV light in a static stainless steel reaction chamber, leading to the formation of aerosols. HeNe laser scattering was used to detect *in situ* the presence and relative amounts of aerosol produced, as well as the induction time required to form aerosols from the irradiation of the gases. Online mass spectrometry measurements were used to monitor the time evolution of gas phase species and, by difference, the relative amounts of carbon in the aerosol formed during an experiment. For comparison, particle samples were also collected during the irradiation experiments for "offline" analysis by elemental analyzer-isotope ratio mass spectrometry (EA-IRMS); the IRMS peak areas were used to quantify the relative amounts of carbon in the aerosols. From these three types of measurements, particle production was observed to be higher as the pressure of initial reactant $CH_4$was increased from 5 to 200 Torr, but little sensitivity to the CH_4/CO_2 ratio between 0.34 and 5 for a given CH_4 pressure was observed. This behavior is in contrast to what has been predicted by photochemical models, which suggest that aerosol production rates decrease as CO_2 levels increase. Furthermore, aerosol formation was detectable at a CH_4/CO_2 ratio down to 0.25 by *in situ* HeNe light scattering and down to 0.34 by offline EA-IRMS analysis of collected particles. These experimental ratios are significantly lower than the threshold ratios of 0.6 to 1 predicted by photochemical models for

particle production. This suggests that aerosol production in CO_2-rich atmospheres with feasible sources of CH_4 from mantle outgassing or methanogenic bacteria was likely to have been much more favorable than predicted by models. Further, more sophisticated photochemical models of early Earth's atmosphere will need to include reactions of organic species with oxygen in order to better predict the minimum CH_4/CO_2 threshold at which particles form as a function of CH_4/CO_2.

In addition to affecting atmospheric radiative transfer, organic aerosols that formed photochemically in the atmosphere could have deposited on the surface, and would thus have been incorporated in the rock record. If such aerosols were significantly lighter in carbon-13 than the CH_4 from which they formed, such a light isotopic signature might potentially be mistaken as a biomarker. To test this hypothesis, aerosols from the UV irradiation of CH_4 and mixtures of CH_4 and CO_2 were collected and analyzed for the carbon-13 isotopic composition by EA-IRMS. Compared to the isotopic composition of the reactant CH_4, the particle samples were depleted in ^{13}C by 6±3‰. While this is likely too small to account for the large isotopic depletions in ^{13}C observed between 2.5 to 3.0 billion years ago (which have been interpreted as the rise of methanotrophic bacteria), experimentation at lower temperatures is recommended to address whether the overall kinetic isotope effects in photochemical aerosol production might be larger at the temperatures in the upper atmosphere where CH_4 photolysis would have occurred.

Table of Contents

List of Figures

List of Tables

Acknowledgements

I would like to thank Dr. Kristie Boering for her advice and support as my advisor throughout my time as a graduate student. Maté Ádámkovics provided valuable advice at the start of my time in graduate school to help jump-start my research. My collaborators, Michael Kubo of the NASA Ames Astrobiology Institute and Professor Andrew Rice of Portland State University, assisted me by running carbon-13 isotopic analyses on the aerosol samples and reactant methane, respectively. John Randazzo helped me considerably by running errands as I juggled my duties as a lecturer at St. Mary's College of California with writing my dissertation in this last semester. In addition, with the encouragement of Dr. Michelle Douskey and Professor Heino Nitsche, I realized my passion for teaching and science education.

On the personal side, my brother, Ping Chu, taught me how to balance my studious academic side with a sense of humor and a *joie de vivre*. My friends, Mamie Thant, Lauren Comfort, and Mark Creelman, have been there for me from day one of orientation until the very end. My labmates, including Dr. Kathleen Mar, Dr. Katherine Hoag, Dr. Annalise van Wyngarden, Dr. Amanda Cole, Dr. Phil Croteau, Amadu Kanu, Aaron Wiegel, Lauren Garafolo, and Mica Smith, made each day more enjoyable, despite the frustrations that come with laboratory work. Matthew Leet, Jonathan Bardelline, and Konnor Robison-Williams gladly transported my methane samples during their road trip to Portland so they could be analyzed at Professor Rice's laboratory. In the last few years, Dr. Adam D. I. Kramer was always there for me, believing in me and supporting me through the trials and tribulations of completing this dissertation. Most of all, I would like to thank my parents, Show-Chiao Chu and Dr. Ching-Yu Chu, whose love always supported my curiosity and ambition. As I embark on a new chapter in my life, I know that I can always turn to them for guidance and support.

Chapter 1

Introduction

Astrophysical models of stellar evolution indicate that the luminosity of the Sun has increased by 30% over the last 4.5 billion years (Gya) [e.g. *Bahcall et al.*, 1995]. Assuming that the magnitude of the greenhouse effect has remained constant at its current value, calculations suggest that liquid water would not have existed on Earth more than 2.5 billion years ago [e.g., *Sagan and Mullen*, 1972; *Kasting*, 1993; *Sagan and Chyba*, 1997]. In addition, if the ice-albedo feedback is taken into consideration, liquid water would not have been stable on Earth as recently as 1 billion years ago [*Sagan and Chyba*, 1997]. In contrast, geological evidence suggests that liquid water has been present for more than 3.8 billion years [e.g., *Mojzsis et al.*, 1996; *Nutman et al.*, 1997, 2012; *Wilde et al.*, 2001; *Feulner*, 2012]. This apparent discrepancy between theory and geological evidence is known as the "Faint Young Sun Paradox." Mounting evidence from Mars observations and their analysis [e.g., *Mustard et al.*, 2001; *Jakosky et al.*, 2005] also point to the widespread influence of water on the martian surface over the course of martian history, yet the Faint Young Sun Paradox poses an even greater problem for Mars due to its greater distance from the Sun [e.g., *Fairén et al.*, 2012; *Feulner*, 2012].

Over the past 40 years, a number of solutions to the so-called paradox have been proposed, which have recently been reviewed by *Feulner* [2012]. Small perturbations to the standard solar model, such as a 7% increase in the early mass of the Sun [*Sackmann and Boothroyd*, 2003] or adjustments to the time-dependent gravitational constant [*Tomaschitz*, 2005], would result in a more luminous early Sun. However, the feasibility of these proposed changes to the standard solar models remains questionable, even after new scrutiny of young stars similar to the Sun [e.g., *Feulner*, 2012]. For example, measurements of solar analogs by *Minton and Malhotra* [2007] determined that the mass loss rate of the young Sun may have been lower than what was deemed necessary by *Sackmann and Boothroyd* [2003] for the young Sun to be luminous enough to sustain liquid water on Earth. Thus, although it is possible that the Sun may have exhibited slightly different properties than current solar analogs, the perturbations that can be successfully made to the standard solar model are too small to solve the Faint Young Sun Paradox [e.g., *Feulner*, 2012].

Other proposed resolutions to the paradox include changes in atmospheric composition, particularly higher concentrations of greenhouse gases, such as CO_2, CH_4, or NH_3, to provide a larger greenhouse effect to offset the lower solar luminosity. Analyses of siderite (an Fe(II) carbonate) in pre-1.8 Gya sediment beds suggest that CO_2 concentrations were up to 100 times that of present atmospheric levels, which would result in a large enough greenhouse effect needed to maintain liquid water on Earth's surface [*Ohmoto et al.*, 2004], although these results have been challenged [*Kasting*, 2004; *Sleep*, 2004; *Sheldon*, 2006]. More convincing studies have used the absence of siderite in other ~2.5 Gya paleosols [*Rye et al.*, 1995], the occurrence of Fe(II)-rich carbonates in ~3.2 Gya river gravels [*Hessler et al.*, 2004] and the coexistence of siderite with magnetite (Fe_3O_4) in Archean banded iron formations [*Rosing et al.*, 2010] to show that most geochemical constraints on CO_2 levels in the paleoatmosphere fall far short of what would be needed to solve the Faint Young Sun Paradox. Furthermore, even if the atmospheres of early Earth and Mars did have large concentrations of CO_2, CO_2 ice clouds in the upper atmosphere would likely form, creating a cooling rather than warming effect [e.g. *Kasting*, 1991], although the effects of CO_2 ice clouds on surface temperature remain highly uncertain for

both planets [*Forget and Pierrehumbert*, 1997; *Pierrehumbert and Erlick*, 1998; *Mischna et al.*, 2000; *Colaprete and Toon*, 2003]. Thus, it seems likely that increased CO_2 levels alone cannot solve the Faint Young Sun Paradox.

Higher concentrations of other greenhouse gases, such as methane and ammonia, have also been proposed; however, these are rapidly destroyed by UV light and thus the resulting fluxes of these gases to the atmosphere required to produce a substantial direct greenhouse effect has been thought to be unreasonably large [*Kasting et al.*, 1983; *Zahnle*, 1986; *Kasting*, 2005]. To allow for the accumulation of UV-labile greenhouse gases beyond what their emission fluxes and photochemical lifetimes would produce, *Sagan and Chyba* [1997] instead suggested that, if enough CH_4 were present so that a UV-shielding photochemical haze of organic particles could be generated, similar to the haze in the atmosphere of Saturn's moon Titan [e.g., *Yung and DeMore*, 1999; *Lavvas et al.*, 2008; *Cable et al.*, 2012], then the photochemical lifetimes of CH_4 and NH_3 in the lower atmosphere of early Earth and Mars may have increased enough in the presence of the UV shield to provide a larger overall greenhouse effect to warm the surfaces. The radical products from the UV irradiation of CH_4 recombine to form new hydrocarbons, such as ethane (C_2H_6) and acetylene (C_2H_2). Subsequent reactions as well as photoproducts of these species result in the formation of even larger hydrocarbons, and these larger hydrocarbons eventually condense to form organic aerosol particles after their saturation vapor pressures are reached [e.g., *Yung and DeMore*, 1999]. *Sagan and Chyba* [1997] hypothesized that the optical properties and size distribution of these aerosols might produce a UV-shield, allowing CH_4 and NH_3 to accumulate in the atmosphere below the haze layer and provide an enhanced greenhouse effect than in the absence of such a haze layer. More recent and more sophisticated model calculations by *McKay et al.* [1999] and *Pavlov et al.* [2000, 2001a], based on observations of the scattering properties of the photochemical haze on Titan, have suggested, though, that the resulting photochemical hazes would likely have provided neither a UV shield nor a greenhouse effect but an "anti-greenhouse" effect, thus exacerbating the Faint Young Sun Paradox rather than providing a solution. In model calculations, *Wolf and Toon* [2010] took into consideration fractal properties of organic particles on the radiative properties of the organic haze proposed by *Sagan and Chyba* [1997] to demonstrate that, in fact, a fractal haze might indeed have provided a UV shield with minimal “antigreenhouse” cooling effect on early Earth’s surface. In summary, while much progress has been made in the past 15 years exploring model sensitivities in the production and properties of a photochemical haze originating with CH_4 photolysis, whether or not such a haze directly or indirectly helps to solve or exacerbate the Faint Young Sun Paradox remains highly uncertain, in part due to lack of a fundamental understanding of the kinetics and properties of these haze particles.

For completeness, we note that other solutions to the Faint Young Sun Paradox have also been proposed, particularly recently resulting in a flurry of activity on the subject. These proposals include (1) additional greenhouse gases such as C_2H_6 [*Haqq-Misra et al.*, 2008] and OCS [*Ueno et al.* 2009]; (2) enhanced greenhouse effects due to non-greenhouse gas interactions (e.g., collisional broadening of CO_2 and H_2O absorptions due to a hypothesized higher paleoatmospheric N_2 pressure by at least a factor of 2 [*Goldblatt et al.*, 2009] or to collision-induced rotational transitions in H_2 [*Kasting*, 2013; *Wordsworth and Pierrehumbert*, 2013]; (3) Archean cloud characteristics [*Rosing et al.*, 2010]; and (4) rotational and continental effects [See *Feulner*, 2012 and references therein]. At least several of these ideas are in dispute (e.g. OCS [*Domagal-Goldman et al.*, 2011] or Archean cloudiness [*Goldblatt and Zahnle*, 2011]) or have been discounted as not applicable (e.g., fossil raindrops constraining paleoatmospheric N_2

close to today's [*Som et al.*, 2012]). Perhaps most importantly, however, none of these appears to have a large enough effect alone to compensate for the Faint Young Sun.

Overall, the most attractive and conceptually simplest solution still appears to be an enhanced greenhouse effect through atmospheric composition [*Feulner*, 2012]. Given this assessment, it is thus imperative that we understand more about the formation of hydrocarbon aerosols on early Earth and whether, if present, they warm or cool the surface and under what conditions. Even for haze on Titan, for which there are now a number of direct observations [*Israël et al.*, 2005; *Tomasko et al.*, 2005; *Cable et al.*, 2012], the kinetics of haze formation and the microphysical/optical properties are still uncertain [*Lavvas et al.*, 2008; *Bézard*, 2009]. These uncertainties are even greater for early Earth and Mars, for which there are no direct atmospheric observations, of course, and for which there is the added complexity of the chemistry of organic aerosol formation in a CO_2-rich atmosphere, distinct from Titan's anoxic atmosphere. *Kasting et al.* [1983] and *Zahnle* [1986] used photochemical models to investigate such chemistry and predicted that photolysis of CH_4 in a CO_2-rich atmosphere would result in significantly less to no aerosol formation than in a CO_2-free atmosphere. In their models, this is the result of photolysis of CO_2, which produces oxygen atoms that oxidize gas-phase hydrocarbons, thus competing with polymerization to form larger hydrocarbons and condensation to form particles. Their model results predicted that a CH_4/CO_2 ratio larger than 1 is necessary to form aerosols [*Kasting et al.*, 1983; *Zahnle*, 1986], which would be difficult to achieve in the CO_2-rich atmospheres of early Mars and Earth [*Kasting*, 1993]. In more recent modeling efforts, *Pavlov et al.* [2000, 2001a, 2001b] reported that a ratio of 0.6 to 1 is needed, a range making aerosol haze formation slightly more feasible. Results by *Trainer et al.* [2006] for photochemical generation of particles in the laboratory analyzed by Aerosol Mass Spectrometry yielded a significantly lower threshold ratio down to at least 0.2, apparently the lowest ratio at which experiments were performed, while laboratory experiments by *Ádámkovics* [2004] demonstrated particle formation at a CH_4/CO_2 ratio of 0.25 but no detectable formation for a ratio of 0.10. The lower the value at which aerosol particles can form, the more likely it is that hydrocarbon hazes were present and played an important role in radiative transfer in early Earth's and Mars' atmospheres. Thus, the experimental results suggest a larger role for aerosols in CO_2-rich atmospheres than would be predicted from photochemical models and indicate the need for further experimental testing to understand the effects of CO_2 on particle formation and whether a photochemical haze could have been present in the atmospheres of early Earth and Mars.

If a photochemical haze did form in early Earth's CO_2-rich atmosphere, the aerosols could have settled to the surface and, if their abundances were large enough, may have left a detectable isotopic signature in organic matter found in the geologic record. Specifically, if isotope effects in the photochemical formation of the organic aerosols formed from CH_4 photolysis resulted in haze that was significantly isotopically depleted in carbon-13 relative to carbon-12, such an isotopically light carbon signature could have been incorporated into the rock record, an idea suggested by *Pavlov et al.* [2001a] and made feasible by the identification of oxygen and sulfur isotope signatures derived from atmospheric photochemistry in the rock and meteorite record of Earth and Mars [*Farquhar et al.*, 1998, 2000; *Farquhar and Thiemens*, 2000]. Indeed, *Pavlov et al.* [2001a] proposed that isotopically light carbon produced abiotically in the atmosphere may account for the isotopically light carbon in ancient kerogens (organic material) in rocks from 2.5 to 3.0 Gya ago, which had until their proposal been considered a clear sign of biology -- the rise of methanotrophic bacteria [*Hayes*, 1983, 1994]. Measurements of the carbon isotopic composition of particles formed from photolysis of CH_4 in the laboratory are

thus needed to provide a test of the hypothesis that such a signature may instead be produced by atmospheric photochemistry, with clearly dramatic implications for the search for and characterization of life on Mars and Earth in the first 2 to 3 billion years of solar system history.

Given how ubiquitous aerosols are in planetary atmospheres and how significant a role they are known to play in radiative transfer, the current inability to predict with confidence even the presence or absence of aerosols on early Mars and Earth, much less their optical properties and effect on radiative transfer, is a wildcard in understanding the history of climate and habitability on Mars and Earth. Much more must be known in order to assess whether one or multiple solutions to the Faint Young Sun Paradox are feasible, especially given the newly appreciated complex feedbacks between haze formation, surface temperatures, CH_4 emissions, UV-labile greenhouse gas lifetimes, and so on [e.g. *Feulner*, 2012]. The work presented in this dissertation was undertaken to gain a greater fundamental understanding of aerosol formation in terrestrial-like atmospheres and provides additional laboratory constraints and tests for the photochemical and microphysical models used to generate the greatly-varying predictions noted above.

In Chapter 2, I describe experimental methods. In Chapter 3, I describe and interpret results for experiments in which organic aerosols are formed from the photolysis of CH_4 and of CH_4 in the presence of varying amounts of CO_2. Results from online mass spectrometry measurements of H_2 and C_2H_6 and *in situ* laser light scattering from aerosol particles all produced in a 13L stainless steel reaction chamber by irradiation of the gas mixtures with a deuterium lamp, as well as "offline" elemental analyzer-isotope ratio mass spectrometry (EA-IRMS) measurements of the relative amounts of particulate carbon collected during the course of an experiment, are presented and compared with previous experimental and modeling results. These results have important implications for the presence and prevalence of aerosols in the atmospheres of Early Earth and Mars. First, the fact that aerosols are easily observed to form down to CH_4/CO_2 ratios of at least 0.25 means that aerosols likely played a more important role in the atmospheres of these planets than previously predicted by photochemical models, which currently predict that aerosols do not form when the CH_4/CO_2 ratio is below 0.6 [*Pavlov et al.*, 2000] or below 1 [*Zahnle*, 1986]. Second, the multi-faceted disagreement between the experimental results and model results mean that more sophisticated photochemical models of early Earth's atmosphere that incorporate many more reactions of organic species with oxygen than are currently included in the models need to be developed, both to better predict the minimum CH_4/CO_2 threshold at which particles form and to better describe the production rates as a function of CH_4/CO_2. Third, if the results from our long integration time experiments (50+ hours) are robust – that is, if particle production rates are as insensitive to the CH_4/CO_2 ratio as the results here suggest – then these results, with their long irradiation times and long timescales for chemistry to occur, may be more relevant for aerosols in a planetary atmosphere, in which the aerosol lifetimes should be many days, much longer than the instantaneous chemical timescales in the previous results of Trainer *et al.* [2006] yet allowing the chemistry to occur over relatively long periods. Additional experiments as well as photochemical modeling of these results, both on the reaction chamber scale and on an atmospheric scale, are needed to further explore these implications for the atmosphere and to aid in determining whether and under what conditions the production of a photochemical haze may warm or cool Earth's surface, thus resolving or exacerbating the Faint Young Sun Paradox.

In Chapter 4, I describe and interpret results for measurements of the carbon isotopic composition (i.e., the ratio of carbon-13 to carbon-12) of the aerosol particles collected from the

photolysis of CH_4 and mixtures of CH_4 and CO_2, which are used to test the extent to which atmospheric photochemistry could have been an important abiotic source of isotopically light carbon, which could be preserved in the rock and meteorite records on Earth and Mars. I found that, relative to the initial isotopic composition of the reactant CH_4, the particle samples were depleted in ^{13}C by 6±3‰ and showed little sensitivity to the pressure of CH_4 irradiated from 10 Torr to 200 Torr and for CH_4/CO_2 ratios down to 0.34. An overall isotope fractionation of −6±3‰ is significantly smaller than the ^{13}C depletions observed in the geological record 2 to 3 billion years ago for which *Pavlov et al.* [2001] were seeking an abiotic explanation. Thus, unless the normal kinetic isotope effects in the formation of increasingly large and increasingly ^{13}C-depleted hydrocarbons initiated by CH_4 photolysis are much larger at the much lower temperatures in the upper atmosphere than in our room temperature laboratory experiments, the abiotic production of photochemical haze in Earth's early atmosphere is not likely to account for observations of the isotopically light carbon in Earth's rock record from 2.5 to 3.0 billion years ago. Measurements of the isotopic composition of particles formed by the UV irradiation of CH_4 at lower temperatures are therefore critically needed to address this remaining uncertainty.

Overall, the measurements in these two chapters improve our understanding of how the presence of CO_2 affects organic aerosol formation in terrestrial-like atmospheres, distinct from the formation of hazes on Titan, and will guide a more accurate and less parameterized representation of haze in models in order to better predict the presence and properties of aerosols, their effect on radiative transfer, and their complex feedbacks with surface temperature, which in turn will help inform their role in resolving or compounding the Faint Young Sun Paradox for early Earth and Mars. The carbon isotope results suggest that an isotopic signature of organic aerosol photochemistry may be too small to detect in kerogens contained in ancient rocks and therefore move us further towards being able to trust large excursions in carbon-13/carbon-12 ratios as being "biomarkers," although they do not rule out other abiotic processes and, importantly, need to be confirmed at lower temperatures characteristic of upper atmospheres.

Chapter 1 References

Ádámkovics, M. (2004), Hydrocarbon Photochemistry in Planetary Atmospheres: Laboratory and Observational Investigations of Organic Aerosols, University of California, Berkeley, Berkeley, CA.

Bahcall, J. N., M. H. Pinsonneault, and G. J. Wasserburg (1995), Solar models with helium and heavy-element diffusion, *Rev. Mod. Phys.*, *67*(4), 781–808, doi:10.1103/RevModPhys.67.781.

Bézard, B. (2009), Composition and chemistry of Titan's stratosphere, *Philos. Trans. R. Soc. London, Ser. A*, *367*(1889), 683–695, doi:10.1098/rsta.2008.0186.

Cable, M. L., S. M. Horst, R. Hodyss, P. M. Beauchamp, M. A. Smith, and P. A. Willis (2012), Titan Tholins: Simulating Titan Organic chemistry in the Cassini-Huygens Era, *Chem. Rev.*, *112*, 1882–1909, doi:dx.doi.org/10.1021/cr200221x.

Colaprete, A., and O. B. Toon (2003), Carbon dioxide clouds in an early dense martian atmosphere, *J. Geophys. Res.*, *108*, E4, doi:10.1029/2002JE001967.

Domagal-Goldman, S. D., V. S. Meadows, and M. W. Claire (2011), Using Biogenic Sulfur Gases as Remotely Detectable Biosignatures on Anoxic Planets, *Astrobiology*, *11*(5), 419–441, doi:10.1089/ast.2010.0509.

Fairén, A. G., J. D. Haqq-Misra, and C. P. McKay (2012), Reduced albedo on early Mars does not solve the climate paradox under a faint young Sun, *Astronomy and Astrophysics*, *540*, A13, doi:10.1051/0004-6361/201118527.

Farquhar, J., and M. H. Thiemens (2000), Oxygen cycle of the Martian atmosphere-regolith system: 17O of secondary phases in Nakhla and Lafayette, *J. Geophys. Res.*, *105*(E5), 11991–7, doi:10.1029/1999JE001194.

Farquhar, J., M. H. Thiemens, and T. Jackson (1998), Atmosphere-surface interactions on Mars: Δ17O measurements of carbonate from ALH 84001, *Science*, *280*(5369), 1580–1582, doi:10.1126/science.280.5369.1580.

Farquhar, J., J. Savarino, T. L. Jackson, and M. H. Thiemens (2000), Evidence of atmospheric sulphur in the martian regolith from sulphur isotopes in meteorites, *Nature*, *404*, 50–52, doi:10.1038/35003517.

Feulner, G. (2012), The Faint Young Sun Problem, *Rev. Geophys.*, *50*, RG2006, doi:8755-1209/12/2011RG000375.

Forget, F., and R. Pierrehumbert (1997), Warming Early Mars with Carbon Dioxide Clouds that Scatter Infrared Radiation, *Science*, *278*(5341), 1273–1276, doi:10.1126/science.278.5341.1273.

Goldblatt, C., and K. J. Zahnle (2011), Clouds and the Faint Young Sun Paradox, *Climate of the Past*, *7*, 203–220, doi:10.5194/cp-7-203-2011.

Goldblatt, C., M. W. Claire, T. M. Lenton, A. J. Matthews, A. J. Watson, and K. J. Zahnle (2009), Nitrogen-enhanced greenhouse warming on early Earth, *Nature Geoscience*, *2*, 891–896, doi:10.1038/NGEO692.

Haqq-Misra, J. D., S. D. Domagal-Goldman, P. J. Kasting, and J. F. Kasting (2008), A Revised, Hazy Methane Greenhouse for the Archean Earth, *Astrobiology*, *8*(6), 1127–1137, doi:10.1089/ast.2007.0197.

Hayes, J. M. (1983), Geochemical evidence bearing on he origin of aerobiosis, a speculative hypothesis, in *Earth's earliest biosphere*, pp. 291–301, Princeton University Press, Princeton, N.J.

Hayes, J. M. (1994), Global methanotrophy at the Archean-Proterozoic transition, in *Early life on Earth*, pp. 220–236, Columbia University Press, New York.
Hessler, A. M., D. R. Lowe, R. L. Jones, and D. K. Bird (2004), A lower limit for atmospheric carbon dioxide levels 3.2 billion years ago, *Nature*, *428*, 736–738, doi:10.1038/nature02471.
Israël, G. et al. (2005), Complex organic matter in Titan's atmospheric aerosols from in situ pyrolysis and analysis, *Nature*, *438*, 796–799, doi:10.1038/nature04349.
Jakosky, B. M., R. M. Haberle, and R. E. Arvidson (2005), The changing picture of volatiles and climate on Mars, *Science*, *301*, 1439–1440, doi:10.1126/science.1118031.
Kasting, J. F. (1991), CO2 condensation and the climate of early Mars, *Icarus*, *94*, 121–148, doi:10.1016/0019-1035(91)90137-I.
Kasting, J. F. (1993), Earth's early atmosphere, *Science*, *259*, 920–926, doi:10.1126/science.11536547.
Kasting, J. F. (2004), Paleoclimatology: Archaean atmosphere and climate, *Nature*, *432*, 1, doi:10.1038/nature03166.
Kasting, J. F. (2005), Methane and climate during the Precambrian era, *Precambrian Res.*, *137*, 119–129, doi:10.1016/j.precamres. 2005.03.002.
Kasting, J. F. (2013), How Was Early Earth Kept Warm?, *Science*, *339*, 44–45, doi:10.1126/science.1232662.
Kasting, J. F., K. J. Zahnle, and J. C. G. Walker (1983), Photochemistry of methane in the Earth's early atmosphere, *Precambrian Res.*, *20*, 121–148, doi:10.1016/0301-9268(83)90069-4.
Lavvas, P. P., A. Coustenis, and I. M. Vardavas (2008), Coupling photochemistry with haze formation in Titan's atmosphere, Part II: Results and validation with Cassini/Huygens data, *Planet Space Sci.*, *56*(1), 67–99, doi:10.1016/j.pss.2007.05.027.
McKay, C. P., R. D. Lorenz, and J. I. Lunine (1999), Analytic Solutions for the Antigreenhouse Effect: Titan and the Early Earth, *Icarus*, *137*, 56–61, doi:10.1006/icar.1998.6039.
Minton, D. A., and R. Malhotra (2007), Assessing the Massive Young Sun Hypothesis to Solve the Warm Young Earth Puzzle, *Astrophys. J.*, *660*, 1700–1706, doi:10.1086/514331.
Mischna, M. A., J. F. Kasting, A. A. Pavlov, and R. Freedman (2000), Influence of carbon dioxide clouds on early martian climate, *Icarus*, *145*, 546–554, doi:10.1006/icar.2000.6380.
Mojzsis, S. J., G. Arrhenius, K. D. McKeegan, T. M. Harrison, A. P. Nutman, and C. R. L. Friend (1996), Evidence for life on Earth before 3,800 million years ago, *Nature*, *384*, 55–59, doi:10.1038/384055a0.
Mustard, J. F., C. D. Cooper, and M. K. Rifkin (2001), Evidence for recent climate change on Mars from the identification of youthful near-surface ground ice, *Nature*, *412*(6845), 411–414, doi:10.1038/35086515.
Nutman, A. P., S. J. Mojzsis, and C. R. L. Friend (1997), Recognition of ≥3850 Ma water-lain sediments in West Greenland and their significance for the early Archaean Earth, *Geochim. Cosmochim. Acta*, *61*, 2475–2484, doi:10.1016/S0016-7037(97)00097-5.
Nutman, A. P., V. C. Bennett, and C. R. L. Friend (2012), Waves and weathering at 3.7 Ga: Geological evidence for an equitable terrestrial climate under the faint early Sun, *Aust. J. Earth Sci.*, *59*(2), 167–176, doi:10.1080/08120099.2012.618512.

Ohmoto, H., Y. Watanabe, and K. Kumazawa (2004), Evidence from massive siderite beds for CO_2-rich atmosphere before ~1.8 billion years ago, *Nature*, *429*, 395–399, doi:10.1038/nature02573.

Pavlov, A. A., J. F. Kasting, L. L. Brown, K. A. Rages, and R. Freedman (2000), Greenhouse warming by CH4 in the atmosphere of early Earth, *J. Geophys. Res.*, *105*(E5), 11981–11990, doi:10.1029/1999JE001134.

Pavlov, A. A., J. F. Kasting, J. L. Eigenbrode, and K. H. Freeman (2001a), Organic haze in Earth's early atmosphere: Source of low-^{13}C Late Archean kerogens?, *Geology*, *29*(11), 1003–1006, doi:10.1130/0091-7613(2001)029<1003:OHIESE>2.0.CO;2.

Pavlov, A. A., L. L. Brown, and J. F. Kasting (2001b), UV Shielding of NH_3 and O_2 by organic hazes in the Archean atmosphere, *J. Geophys. Res.*, *106*(E10), 23267–23287, doi:10.1029/2000JE001448.

Pierrehumbert, R. T., and C. Erlick (1998), On the scattering greenhouse effect of CO_2 ice clouds, *J. Atmos. Sci.*, *55*, 1897–1903, doi:10.1175/1520-0469(1998)055<1897:OTSGEO>2.0.CO;2.

Rosing, M. T., D. K. Bird, N. H. Sleep, and C. J. Bjerrum (2010), No climate paradox under the faint early Sun, *Nature*, *464*, 744–747, doi:10.1038/nature08955.

Rye, R., P. H. Kuo, and H. Holland (1995), Atmospheric carbon dioxide concentrations before 2.2 billion years ago, *Nature*, *378*, 603–605, doi:10.1038/378603a0.

Sackmann, I. J., and A. I. Boothroyd (2003), Our Sun. V. A bright young Sun consistent with helioseismology and warm temperatures on ancient Earth and Mars, *Astrophys. J.*, *583*, 1024–1039, doi:10.1086/345408.

Sagan, C., and C. Chyba (1997), The Early Faint Sun Paradox: Organic Shielding of Ultraviolet-Labile Greenhouse Gases, *Science*, *276*, 1217–1221, doi:10.1126/science.276.5316.1217.

Sagan, C., and G. Mullen (1972), Earth and Mars - Evolution of Atmospheres and Surface Temperatures, *Science*, *177*(4043), 52–56, doi:10.1126/science.177.4043.52.

Sheldon, N. D. (2006), Precambrian paleosols and atmospheric CO_2 levels, *Precambrian Res.*, *147*(1-2), 148–155, doi:10.1016/j.precamres.2006.02.004.

Sleep, N. H. (2004), Palaeoclimatology: Archaean palaeosols and Archaean air, *Nature*, *432*, 1, doi:10.1038/nature03167.

Som, S. M., D. C. Catling, J. P. Harnmeijer, P. M. Polivka, and R. Buick (2012), Air density 2.7 billion years ago limited to less than twice modern levels by fossil raindrop imprints, *Nature*, *484*, 359–362, doi:10.1038/nature10890.

Tomaschitz, R. (2005), Faint young Sun, planetary paleoclimates and varying fundamental constants, *Int. J. Theor. Phys.*, *44*, 195–218, doi:10.1007/s10773-005-1492-4.

Tomasko, M. G. et al. (2005), Rain, winds and haze during the Huygens probe's descent to Titan's surface, *Nature*, *438*(7069), 765–778, doi:10.1038/nature04126.

Trainer, M. G., A. A. Pavlov, H. L. DeWitt, J. L. Jimenez, C. P. McKay, O. B. Toon, and M. A. Tolbert (2006), Organic haze on Titan and the early Earth, *Proc. Natl. Acad. Sci. U.S.A.*, *103*(48), 18035–18042, doi:10.1073/pnas.0608561103.

Ueno, Y., M. S. Johnson, S. O. Danielache, C. Eskebjerg, A. Pandey, and N. Yoshida (2009), Geological sulfur isotopes indicate elevated OCS in the Archean atmosphere, solving faint young sun paradox, *Proc. Natl. Acad. Sci. U.S.A.*, *106*(35), 14784–14789, doi:10.1073_/pnas.0903518106.

Wilde, S. A., J. W. Valley, W. H. Peck, and C. M. Graham (2001), Evidence from detrital zircons for the existence of continental crust and oceans on the Earth 2.6 billion years ago, *Nature*, *409*, 175–178, doi:10.1038/35051550.

Wolf, E. T., and O. B. Toon (2010), Fractal Organic Hazes Provided an Ultraviolet Shield for Early Earth, *Science*, *328*, 1266–1268, doi:10.1126/science.1183260.

Wordsworth, R., and R. Pierrehumbert (2013), Hydrogen-Nitrogen Greenhouse Warming in Earth's Early Atmosphere, *Science*, *339*, 64–67, doi:10.1126/science.1225759.

Yung, Y. L., and W. B. DeMore (1999), *Photochemistry of Planetary Atmospheres*, Oxford University Press, New York.

Zahnle, K. J. (1986), Photochemistry of Methane and the Formation of Hydrocyanic Acid (HCN) in the Earth's Early Atmosphere, *J. Geophys. Res.*, *91*(D2), 2819–2834, doi:10.1029/JD091iD02p02819.

Chapter 2

Methods

In this chapter, the experimental apparatus used to generate organic aerosols from the photolysis of CH_4 and mixtures of CH_4 and CO_2 is described, along with the "online" mass spectrometry and *in situ* HeNe laser scattering measurement detection schemes for gaseous and particulate species, respectively, and the method for collection and analysis of aerosol particles over the course of a photolysis experiment for "offline" measurements of the relative amount of carbon in aerosols produced and their carbon isotopic composition by Elemental Analyzer-Isotope Ratio Mass Spectrometry. Details of the analysis of the online mass spectrometry raw data are also discussed.

2.1. Instrumentation and Procedures

2.1.1 Aerosol Generation Chamber

The aerosol generation chamber consisted of a stainless steel cylinder with a height of 36 cm and a diameter of 21 cm, resulting in a volume of about 13 L (Figure 2.1). Copper gaskets were used on all flanges and connections instead of rubber O-rings that could potentially contaminate the system with hydrocarbons from out-gassing. The deuterium lamp irradiation source and a gas manifold for the introduction of the reactants were attached to the top flange of the chamber. A separate manifold for the residual gas analyzer mass spectrometer (RGA-MS) with a volume of 1.8 L was connected to the chamber through a precision leak valve (Kurt J. Lesker VZMD9538) approximately 10 cm from the irradiation source. A cold cathode/Pirani gauge (Pfeiffer PKR 251) was used to measure the pressure within the RGA-MS manifold.

A turbomolecular pump (Pfeiffer TSU 261) with a diaphragm backing pump (Pfeiffer MVP-055-3) was used to evacuate the reaction chamber and RGA-MS manifold before and after experiments. A diaphragm backing pump was used instead of an oil-sealed rough pump to avoid hydrocarbon contamination. The chamber typically reached 5 x 10^{-7} Torr within a day of pumping down from atmospheric pressure, and baking out the chamber overnight further reduced the background pressure to ~1 x 10^{-8} Torr. A gate valve (MDC GV-4000V) separated the reaction chamber from the turbomolecular pump. This gate valve was opened when pumping down the chamber and closed while filling the chamber with the reactant gases and during experiments. Although in principle, the experiments could be run by flowing gases through the chamber, the rates at which gas phase species and aerosol are produced given the photon fluxes of the deuterium lamps (and most other broadband UV light sources available for routine laboratory use) are such that experiments reported here were run in a static mode with the gate valve closed, as in *Ádámkovics and Boering* [2003]. The gate valve between the mass spectrometer region and the vacuum pump was always left open, including during experiments, to yield a time-dependent signal from the main reaction chamber.

2.1.2 UV Irradiation Source

For the experiments reported here, either a Hamamatsu L2D2 L7292 “low-brightness” or a Hamamatsu L2D2 L9841 “high-brightness” deuterium lamp was used as the irradiation source. The MgF_2 window of the lamps allowed transmission of wavelengths down to 110 nm, including the Lyman-α line at 121.6nm and the peak output of the lamp at 160 nm. The Hamamatsu L9841 lamp (“high-brightness”) was also used in some of the experiments. The photon intensity is similar for both lamps, but the high-brightness lamp has an aperture of only 0.05 mm, instead of

the 0.1 mm aperture for the low-brightness lamp, thus spreading the photons across a smaller area.

To measure the photon output of the lamps, N_2O actinometry [*Calvert and Pitts*, 1966] was used. According to measurements by *Greiner* [1967], 1.00 ± 0.05 molecule is generated per quantum absorbed in the photolysis of N_2O at 184.9 nm; thus, the photon intensity of the lamp can be determined by measuring the increase in pressure during irradiation of N_2O. Note that N_2O actinometry only yields the photon intensity between 135.0 and 210.0 nm, which does not include the Lyman-α line at 121.6 nm. Actinometry results for the high-brightness Hamamatsu deuterium lamp in the reaction chamber are shown in Figure 2.2. For the experiment in this figure, N_2O (Praxair, 99.998%) was introduced into the reaction chamber to a pressure of 8.1 Torr and photolyzed for 6.5 hours. During the course of the experiment, the chamber pressure was monitored with a capacitance manometer (MKS; 10 Torr full range, 0.12% accuracy). The linear portion of chamber pressure versus the irradiation time was fitted and, using the ideal gas law, the volume of the chamber (13 L), and the yield of one molecule generated per quantum absorbed, the photon intensity was calculated, yielding 5.4 ± 0.4 x 10^{15} photons s^{-1}. This is comparable to but slightly smaller than previously reported measurements for the low-brightness lamp of 8.8 ± 0.8 x 10^{15} photons s^{-1} by *Ádámkovics and Boering* [2003]. The difference, if significant, may reflect differences in the operational hours on the lamp prior to the actinometry measurements. The manufacturer-specified lifetime of the lamp, defined as the elapsed operating time at which the photon flux at 240 nm drops to 50% of its initial value, was 2000 hours, although at Lyman-α the lifetime is only 600 hours. In another actinometry experiment performed (not shown), the low-brightness lamp after it had been operated for nearly 1200 hours yielded a photon intensity of 3.7 ± 0.2 x 10^{15} photons s^{-1}, less than half that of the value reported by *Ádámkovics and Boering* [2003]. The differences between the low and high brightness lamps, and their operational usage before any given aerosol generation experiment, may lead to additional uncertainties in some of the results presented in Chapters 3 and 4 since the photon intensities and intensity distributions with respect to space and wavelength may have varied more than anticipated. However, these lamp intensity differences are unlikely to affect the primary conclusions in these chapters, although they may add to the apparent noise of the results. In fact, the photon intensities and distributions with respect to space and wavelength also varied during a single experiment as aerosol formed on the MgF_2 window; the latter issue is discussed in *Ádámkovics and Boering* [2003].

2.1.3 Mass Spectrometry

A residual gas analyzer mass spectrometer (Stanford Research Systems, SRS-RGA 300) was used to measure the concentrations of stable gas phase species during the irradiation experiments. The RGA-MS was placed in a manifold connected to the chamber through a precision leak valve. Before each experiment, a background spectrum was taken. After filling the chamber with reactants, the leak valve was opened until the pressure in the manifold increased to 5 x 10^{-5} Torr, chosen because it is below 10^{-4} Torr, the maximum operating pressure for the RGA-MS, and low enough that fewer repairs due to hydrocarbon contamination of the quadrupole rods were needed than at the maximum pressures used in *Adamkovics and Boering* [2003], although necessarily yielding a lower sensitivity. The system was then allowed to equilibrate for 2 hours until the lamp was turned on to start the experiment at time t=0.

Within the RGA-MS, gases were ionized by electron impact by 70 eV electrons from a hot filament, an iridium (Ir) wire coated with thorium oxide (ThO_2). Ions were filtered using a

quadrupole mass analyzer before being detected by a Faraday cup. One spectrum from 1 to 100 amu was run and collected by the SRS-Labview data acquisition software every 1.5 minutes throughout the 50+ hours of the experiments.

Extended use of the RGA-MS (often after only several experiments of ~100 hours each) led to contamination of the quadrupole rods and ionizer by hydrocarbon deposition. This contamination lowered the sensitivity of the instrument and prevented the filament from achieving the emission voltage of 70 eV. When this occurred, the instrument was baked out under vacuum to vaporize the hydrocarbon residue or returned to Stanford Research Systems for cleaning and maintenance.

A triple filter quadrupole mass spectrometer from Hiden Analytical (RC HAL/3F PIC Quadrupole Mass Spectrometer) was also purchased and incorporated into the design and operation of the apparatus in an attempt to achieve higher sensitivity and larger dynamic range than the RGA-MS. Instead of just one set of quadrupole rods, the triple filter mass spectrometer has two sets of quadrupole rods with a collision cell between them [*de Hoffmann*, 1996]. In addition, the secondary electron multiplier detector in the Hiden mass spectrometer in principle could have provided greater sensitivity than the Faraday cup detectors used in the RGA-MS [*Herbert*, 2003]. Despite the potential advantages of the Hiden triple filter mass spectrometer, however, it was determined that, like the RGA-MS, hydrocarbons contamination of the detectors affected the performance of the mass spectrometer. Furthermore, the Hiden QMS signals frequently dropped to zero as the detectors became contaminated over the course of a single experiment, unlike the RGA-MS that would lose sensitivity only after several long experimental runs. Thus, the Hiden Analytical triple-filter mass spectrometer was untenable for our experiments, and only the results for the RGA-MS from Stanford Research Systems are presented in Chapter 3.

2.1.4 *In situ* detection of optical scattering from particles

To investigate the real-time formation of the particles during the experiment, a Mie scattering optical scattering system was utilized. This experimental set-up was previously described in detail in *Ádámkovics and Boering* [2003] and *Ádámkovics* [2004]. In brief, for the CH_4-only experiments, a 1kHz mechanically chopped, 15 mW, 632.8 nm HeNe laser entered the chamber through fiber optic waveguides. For irradiation of mixtures of CH_4 and CO_2, an 8 mW, 613 nm HeNe laser was used instead since H_2O, which can be produced photochemically when both CH_4 and CO_2 are irradiated, can fluoresce at 632 nm, thus obscuring elastic scattering from the particles. Within the chamber, the laser light interacted with aerosol particles in a 4.2 mm^3 region (given the 0.65 mm laser beam diameter and the 1 cm diameter field of view for the detector). The output fiber waveguide was coupled to a photomultiplier tube (Hamamatsu R928) operating at a bias voltage of 1.1 kV with a HeNe laser line filter to ensure measurement of elastic scattering. A multichannel scaler/averager (MSA, Stanford Research Systems Model SR430) collected the scattered light and used a signal from the optical chopper to sort it into laser "on" and laser "off" bins. The SRS-MSA data acquisition software calculated the net scattering as the difference between the laser "on" and laser "off" bins, which was stored along with the raw photon-counting data. Light scattering signals reached up to 2700 counts/min during the irradiation of 70 Torr of CH_4 with the 16 mW HeNe laser [*Ádámkovics and Boering*, 2003].

2.1.5 EA-IRMS Measurements

Elemental Analyzer-Isotope Ratio Mass Spectrometry (EA-IRMS) was used to measure the stable carbon isotopic composition (Chapter 4) and the relative amounts (Chapter 3 and 4) of organic carbon in aerosol generated and collected over the course of separate photolysis experiments. To collect the particles for EA-IRMS analysis, a square piece of tin (Sn) foil (30 mm x 30 mm) was placed within the reaction chamber before chamber evacuation on a stainless steel platform approximately 16 cm below the deuterium lamp. Within 10 minutes of the end of an experiment (i.e., when the deuterium lamp was turned off), the foil was collected with a clean pair of tweezers and wrapped in another piece of foil. The particle samples were kept in a vacuum dessicator until they were analyzed on an EA-IRMS instrument, described below, in the laboratory of David Des Marais at the NASA Ames Astrobiology Institute.

In preparation for EA-IRMS analysis, the particle samples were placed in a larger tin foil cup with vanadium oxide (V_2O_5), added to facilitate clean, complete combustion. Additional "blank" samples consisting only of a tin foil blank and V_2O_5 were included in each analysis run. The samples then underwent flash combustion in a Carlo Erba CHN 1108 Elemental Analyzer at 1000 to 1050°C, which quantitatively converted all the organic carbon in the samples into CO_2. The resulting CO_2 was then purified in a flow of helium in a series of oxidation and reduction steps then through a gas chromatography column before entering a Finnigan Delta Plus XL isotope ratio mass spectrometer for measurement of the stable carbon isotopic composition [*Matthews and Hayes*, 1978; *Brenna et al.*, 1997]. Standards and precisions for the carbon isotopic compositions are discussed in Chapter 4. In addition to the carbon isotopic composition, the IRMS results also included integrated peak areas for the Faraday cup signal at mass-to-charge 44. Although uncertain to ± 40%, these peak areas provide a proxy for the relative amounts of carbon in particulate matter collected over the course of an experiment; the results and corresponding uncertainties and caveats are discussed in detail in Chapters 3 and 4.

2.1.6 Experimental Procedures

The protocol for the irradiation experiments was as follows. Before evacuating the chamber, a piece of Sn foil for collecting particles for EA-IRMS analysis was placed on a platform within the chamber, approximately 16 cm below the window of the D_2 lamp. The chamber was evacuated to a background pressure of about 1 x 10^{-8} Torr after baking out for 12 hours or longer. In preparation for an irradiation experiment, the background signals for optical scattering and RGA mass spectrometer were measured. The reaction chamber was isolated from the turbomolecular pump and the mass spectrometer manifold, and gases (CH_4, Scott Gas, 99.99%; CO_2, Scott Gas, 99.997%) were introduced through a valved inlet. The total chamber pressure was measured with a capacitance manometer (MKS 627D; 1000 Torr full range, 0.12% accuracy). The precision leak valve between the chamber and the MS manifold was opened until the pressure in the mass spectrometer manifold reached approximately 5 x 10^{-5} Torr. After a two hour equilibration period, the lamp was turned on, a fan was placed externally next to the lamp for cooling, and the data acquisition software for the laser detection scheme (SRS MSA) and the RGA-MS (RGA-Labview) were initiated. Both the RGA-Labview and SRS MSA programs collected data every 90 seconds. Within 10 minutes or less of the end of each experiment (i.e., when the lamp was turned off), the formation of particles was confirmed by opening the chamber and observing a visible brown residue on the window of the lamp, which was then cleaned with acetone and optical grade cloths (Fisher Scientific 06-665-29). The tin foil containing the particles that had settled onto it during the experiment was collected from the chamber with a

clean pair of tweezers, wrapped in another piece of foil, and kept in a vacuum desiccator until analysis at NASA Ames. Before the next experiment, another piece of foil was placed in the chamber and the chamber was evacuated and baked again.

2.2 Analysis of the RGA-MS measurements

Mass spectra from the RGA-MS were used to derive the net concentrations of H_2 and C_2H_6 produced over the course of an experiment to use as a proxy for net formation of C-C bonds in both the gas phase and particulates. To obtain quantitative information, each mass spectrum was deconvolved using the analysis procedures described below in section 2.1, with the calibration data that were obtained through the procedures outlined below in section 2.2. Using the deconvolved values, the gas phase species concentrations were calculated (section 2.3 and 2.4) in order to determine the changes in H_2 and/or C_2H_6 over the course of an experiment (section 2.5).

2.2.1 Deconvolution of the Mass Spectra

During the irradiation experiments, the gaseous mixture from the reaction chamber was introduced into the RGA mass spectrometer through a precision leak valve. Upon electron impact ionization, some of the parent ions representing molecular species in the gaseous mixture from the reaction chamber fragmented into ions. A given mass-to-charge value (m/z) may thus result from the parent ion of a gas-phase molecule in the chamber and/or from the fragmentation of one or several different parent ions; the mass spectra therefore need to be deconvolved in order to determine the concentrations of each separate species in the reaction chamber. Additionally, the ionization efficiencies of each species vary and also need to be taken into account during deconvolution.

This procedure to deconvolve the measured mass spectra outlined below has been previously described in detail by *Ádámkovics and Boering* [2003]. First, Gaussian multi-peak fitting was used to calculate the peak heights for each mass spectrum. For a pure gas, the signal intensity at a given m/z ratio (h_i) depends on the gas' true pressure (p), the gas' ionization efficiency relative to N_2 (known as the sensitivity factor, s), and the normalized fragment intensity itself (r_i):

$$h_i = r_i \bullet p \bullet s \qquad (2.1)$$

For a gaseous mixture, many of the species can in principle result in some of the same ion fragments, so the series of h_i's represents the contribution of each species to a m/z value (h_m). That is,

	Species 1	Species 2	Species *n*	
$h_1 =$	$r_{11} \bullet p_1 \bullet s_1 +$	$r_{12} \bullet p_2 \bullet s_2 +$	$\ldots + r_{1n} \bullet p_n \bullet s_n$	(2.2)
$h_2 =$	$r_{21} \bullet p_1 \bullet s_1 +$	$r_{22} \bullet p_2 \bullet s_2 +$	$\ldots + r_{1n} \bullet p_n \bullet s_n$	(2.3)
…				

In a generalized form, where m is m/z and there are n species:

$$h_m = r_{m1} \bullet p_1 \bullet s_1 + r_{m2} \bullet p_2 \bullet s_2 + \ldots + r_{mn} \bullet p_n \bullet s_n \qquad (2.4)$$

This matrix can be written as:

$$\mathbf{H} = \mathbf{R} \bullet \mathbf{P} \qquad (2.5)$$

where **R** is a matrix of all the fragmentation patterns and **P** is the product of the sensitivity factor, s_i, and the partial pressures of the gases in the RGA, p_i:

$$\boldsymbol{R} = \begin{pmatrix} r_{11} & \cdots & r_{1n} \\ \vdots & \ddots & \vdots \\ r_{m1} & \cdots & r_{mn} \end{pmatrix} \text{ and } \boldsymbol{P} = \begin{bmatrix} p_1 \cdot s_1 \\ \vdots \\ p_n \cdot s_n \end{bmatrix}$$

The fragmentation patterns **R**, obtained through calibration of the RGA-MS, are given in Table 2 of *Ádámkovics and Boering* (2003) and in Table 2.1 here. **P**, which represents the partial pressures of each parent species, can be solved with matrix equations:

$$\mathbf{R} \bullet \mathbf{P} = \mathbf{H} \qquad (2.6)$$

$$\mathbf{R^T} \bullet \mathbf{R} \bullet \mathbf{P} = \mathbf{R^T} \bullet \mathbf{H} \qquad (2.7)$$

$$\mathbf{P} = (\mathbf{R^T} \bullet \mathbf{R})^{-1} \bullet \mathbf{R^T} \bullet \mathbf{H} \qquad (2.8)$$

The pressure of species *i* in the MS manifold, p_i, can be solved for by dividing each element of the matrix **P** by the sensitivity factor (s_i), which were also obtained through calibration and shown again in Table 2.2:

$$p_i = \frac{P_i}{s_i} \qquad (2.9)$$

Using the p_i values for H_2 and C_2H_6, the concentrations of H_2 and C_2H_6 were calculated (sections 2.3 and 2.4), along with the net change in H_2 and C_2H_6 concentrations over the course of an irradiation experiment, denoted as $\Delta[H_2]$ and $\Delta[C_2H_6]$.

2.2.2 Calibration using mass spectra of pure gases

To obtain the fragmentation patterns (**H**) and sensitivity factors of the gases (s_i) for the RGA-MS, the RGA-MS was calibrated using pure gases. This calibration procedure is summarized here and described in detail in *Ádámkovics and Boering* [2003]. Initially, the reaction chamber was filled to 70 Torr with a pure gas, such as H_2 or C_2H_6. The precision leak valve between the MS manifold and the reaction chamber was opened until the manifold pressure was between 10^{-6} to 10^{-4} Torr as measured by a capacitance manometer (MKS model 627B; 0.020 Torr full range, 0.25% accuracy). The mass spectrum for each pure gas was measured by the RGA-MS and recorded by the RGA Labview program, and the precision leak valve was closed again to evacuate the manifold. This procedure was repeated at four additional pressures between 10^{-6} and 10^{-4} Torr, resulting in five mass spectra at five different pressures. For each calibration gas, the fragmentation patterns shown in Table 2.1 were obtained by normalizing the peak heights in each spectrum and then averaging the five spectra. There were no calibration gases available for C_3H_4 (1,2-propadiene) and C_4H_2 (1,3-butadiyne) so their fragmentation patterns were obtained from the NIST Chemistry WebBook (http://webbook.nist.gov/chemistry). For each gas, the sensitivity factor, s_i, was derived from the the linear fit of the RGA gas pressure, the sum of the measured peak heights, versus the absolute pressure measured by a capacitance manometer. The sensitivities are also listed in Table 2.1.

2.2.3 Calculation of H_2 and C_2H_6 concentrations in the CH_4 irradiation experiments

In Chapter 3, time-dependent measurements of the H_2 and C_2H_6 concentrations over the course of the CH_4 irradiation experiments are reported. The number density of H_2 in the reaction chamber at time t, n_t, was calculated from the partial pressures of H_2 and CH_4 in the RGA mass spec manifold based on the deconvolved RGA mass spectral data using Equation 2.9, where p_t and $p_{CH4,t}$ are the partial pressures of H_2 and CH_4 in the MS manifold at time t and P_{TOT} is the measured total pressure in the reaction chamber:

$$n_t = \frac{\frac{p_t}{p_{CH4,t}} \cdot P_{TOT}}{RT} \qquad (2.10)$$

To account for any small amounts of H_2 contaminants in the reaction chamber from small impurities derived from the reactant gases before irradiation, the H_2 concentration at the start of the irradiation (n_0) was subtracted from all subsequent concentration values. In addition, the parent ion for CH_4 at *m/z* 16 was used to scale $n_{H2,0}$ to account for both fluctuations and decreases in the chamber pressure over the course of an experiment using Equation 2.10.

$$n_{t,corrected} = n_t - n_0 \cdot \frac{(m/z\ 16)_t}{(m/z\ 16)_0} \qquad (2.11)$$

2.2.4 Calculation of $[H_2]$ in the CH_4/CO_2 irradiation experiments

In Chapter 3, time-dependent measurements of the H_2 concentrations over the course of the irradiation experiments in which CH_4 and CO_2 are irradiated are reported. To calculate $[H_2]$ for these experiments, the analysis procedure was adjusted from that used in the irradiation of pure CH_4 (Section 2.3). Photochemistry occurring during the photolysis of a mixture of CO_2 and CH_4 creates additional species beyond the hydrocarbons listed in the table of fragmentation patterns (Table 2.1), including a potentially large number of oxygenated species [e.g., *Trainer et al.*, 2006]. However, the contributions of the oxygenated species to m/z 1 and 2 are expected to be negligible in comparison to those from H_2. Acetic acid and formic acid, for example, do not contribute at all to m/z 1 and 2, according to the NIST database (http://webbook.nist.gov/chemistry), and, furthermore, the concentrations of oxygenated molecules that could form should be significantly lower than that of H_2.

For these experiments with added CO_2, Equation 2.10 has been modified to account for the fact that CO_2 can be a major species in order to relate the partial pressure for H_2 derived from the RGA mass spec data to the total pressure in the reaction chamber. To do so, it was assumed, as should be the case, that the CH_4/CO_2 ratio (β) remained constant throughout a given experiment so that:

$$p_{CO2,t} = \frac{p_{CH4,t}}{\beta} \qquad (2.12)$$

The mixing ratio of H_2 at time t was then calculated by dividing p_t by $P_{CH4,t} + P_{CO2,t}$ so that number density of H_2, n_t, can then be calculated in a manner similar to that in section 2.3 but modified for the presence of CO_2 as:

$$n_t = \frac{\frac{p_t}{\left(p_{CH4,t} + {}^{p_{CH4,t}}/_{\beta}\right)} \cdot P_{TOT}}{RT} \qquad (2.13)$$

2.2.5 Calculation of $\Delta[H_2]$, $\Delta[C_2H_6]$ and ΔC-C

The net change in H_2 and C_2H_6 concentrations, $\Delta[H_2]$ and $\Delta[C_2H_6]$, respectively, were used to calculate the net number of carbon-carbon bonds formed in the particulate matter, which we denote as $\Delta_{C\text{-}C}$. Due to noise issues in some runs, the initial $[H_2]$, $[H_2]_i$, was derived from the y-intercept of the linear regression of the first 8 to 15 hours of $[H_2]$ versus irradiation time rather than using the initial $[H_2]$ concentration value, which could be quite noisy for some runs (Figure 2.3) For the final H_2 concentration, $[H_2]_f$, out of the typically 60 to 100 hour experiments, the 8 to 15 hours preceding the highest peak for H_2 was fit with a linear regression. $\Delta[H_2]$ was then calculated by taking the difference between these final and initial H_2 values. This fitting procedure was also followed to calculate $\Delta[C_2H_6]$.

For the CH_4 irradiation experiments, values for $\Delta_{C\text{-}C}$, an estimate of the amount of carbon-carbon bonds in particulate matter, were calculated by subtracting $\Delta[C_2H_6]$ from $\Delta[H_2]$ (i.e., $\Delta H_2 - \Delta C_2H_6$). ΔH_2 serves as proxy for the total number of carbon-carbon bonds formed in both gaseous and particulate matter since the photolysis of CH_4 and the formation of each carbon-carbon bond produces 2H or H_2. $\Delta[C_2H_6]$, the gaseous hydrocarbon present at the largest and detectable concentrations in these experiments (given the lower operating pressure of the RGA mass spectrometer), was subtracted from $\Delta[H_2]$ to obtain an estimate of the number of carbon-carbon bonds in particulate matter. This calculation is numerically comparable to those in *Ádámkovics and Boering* [2003] in which other hydrocarbons (C_2H_4, C_2H, C_3H_4, C_4H_2 and C_4H_{10}) were also subtracted from ΔH_2, weighted by the number of carbon-carbon bonds in each, since the net production of hydrocarbons other than C_2H_6 are so small. For example, using $\Delta H_2 - \Delta C_2H_6$, $\Delta_{C\text{-}C}$ from the data in *Ádámkovics and Boering* [2003] was 1.33×10^{17} cm^{-3}, which is close to their reported value of 1.25×10^{17} cm^{-3} taking all other detectable hydrocarbons into account.

Chapter 2 References

Ádámkovics, M. (2004), Hydrocarbon Photochemistry in Planetary Atmospheres: Laboratory and Observational Investigations of Organic Aerosols, University of California, Berkeley, Berkeley, CA.

Ádámkovics, M., and K. A. Boering (2003), Photochemical formation rates of organic aerosols through time-resolved in situ laboratory measurements, *J. Geophys. Res. E: Planets*, *108*(E8), 5092, doi:10.1029/2002JE002028.

Brenna, J. T., T. N. Corsco, H. J. Tobias, and R. J. Caimi (1997), High-precision continuous-flow isotope ratio mass spectrometry, *Mass Spectrom. Rev.*, *16*(5), 227–258, doi:10.1002/(SICI)1098-2787(1997)16:5<227::AID-MAS1>3.0.CO;2-J.

Calvert, J. G., and J. N. Pitts (1966), *Photochemistry*, Wiley, New York.

Greiner, N. R. (1967), Photochemistry of N_2O Essential to a Simplified Vacuum-Ultraviolet Acintometer, *J. Chem. Phys.*, *47*(11), 4373–4377, doi:10.1063/1.1701640.

Herbert, C. G. (2003), *Mass spectrometry basics*, CRC Press, Boca Raton.

De Hoffmann, E. (1996), Tandem Mass Spectrometry: a Primer, *J. Mass Spectrom.*, *31*, 129–137.

Matthews, D. E., and J. M. Hayes (1978), Isotope-Ratio-Monitoring Gas Chromatography-Mass Spectrometry, *Anal. Chem.*, *50*(11), 1465–1473, doi:10.1021/ac50033a022.

Trainer, M. G., A. A. Pavlov, H. L. DeWitt, J. L. Jimenez, C. P. McKay, O. B. Toon, and M. A. Tolbert (2006), Organic haze on Titan and the early Earth, *Proc. Natl. Acad. Sci. U.S.A.*, *103*(48), 18035–18042, doi:10.1073/pnas.0608561103.

Table 2.1: Mass Fragmentation Patterns and Sensitivities of Gases. Adapted from *Ádámkovics and Boering* [2003].

m/z	H_2 Hydrogen	CH_4 Methane	C_2H_2 Acetylene	C_2H_4 Ethylene	C_2H_6 Ethane	C_3H_4 1,2-propadiene	C_3H_8 n-propane	C_4H_2 1,3-butadiyne	C_4H_{10} n-butane
1	0.0206	0.0044	0.0028	0.0034	0.0048	0	0.0014	0	0.0009
2	0.9794	0.0245	0.0066	0.0089	0.0702	0	0.0203	0	0.021
12	0	0.004	0.0083	0.0038	0.0013	0.013	0.0006	0	0.0006
13	0	0.0122	0.2263	0.0068	0.0035	0.0108	0.0014	0	0.0012
14	0	0.3022	0.0022	0.0135	0.01	0.0127	0.0035	0	0.0019
15	0	0.2861	0.0044	0.0017	0.0153	0.001	0.0139	0	0.0108
16	0	0.3598	0.0006	0.0004	0.0013	0.0003	0.0055	0	0.0043
17	0	0.0068	0	0	0	0.0003	0	0	0
18	0	0	0.0011	0	0	0.0003	0	0	0
19	0	0	0	0	0	0.0099	0.0029	0	0
20	0	0	0	0	0	0.0121	0.0035	0	0
24	0	0	0.0304	0.011	0.0031	0.0086	0.0009	0	0.0003
25	0	0	0.112	0.0397	0.0175	0.0146	0.0041	0	0.0046
26	0	0	0.5519	0.2421	0.1043	0.0153	0.0324	0	0.0325
27	0	0	0.0116	0.2379	0.1361	0.0022	0.1043	0.0008	0.0983
28	0	0	0.0408	0.4225	0.4363	0.0006	0.1892	0.0127	0.1088
29	0	0	0.0011	0.0084	0.0864	0.0003	0.2897	0	0.1286
30	0	0	0	0	0.1082	0	0.0052	0	0.0028
36	0	0	0	0	0.0017	0.0299	0.0012	0.0067	0.0003
37	0	0	0	0	0	0.1038	0.0078	0.0143	0.0025
38	0	0	0	0	0	0.129	0.0133	0.0014	0.0049
39	0	0	0	0	0	0.3063	0.0458	0	0.0325
40	0	0	0	0	0	0.3181	0.0075	0	0.0059
41	0	0	0	0	0	0.0105	0.0423	0	0.0955
42	0	0	0	0	0	0.0003	0.0145	0	0.0501
43	0	0	0	0	0	0	0.0892	0	0.3091
44	0	0	0	0	0	0	0.0997	0.001	0.009
48	0	0	0	0	0	0	0	0.0553	0
49	0	0	0	0	0	0	0	0.2446	0.0012
50	0	0	0	0	0	0	0	0.6336	0.004
51	0	0	0	0	0	0	0	0.0297	0.0028
52	0	0	0	0	0	0	0	0	0.0009
53	0	0	0	0	0	0	0	0	0.0022
54	0	0	0	0	0	0	0	0	0.0006
55	0	0	0	0	0	0	0	0	0.0028
56	0	0	0	0	0	0	0	0	0.0022
57	0	0	0	0	0	0	0	0	0.0083
58	0	0	0	0	0	0	0	0	0.0467
sensitivity, *s*	1.68	3.72	2.46	4.1	4.36	5.58 †	5.58	6.25 †	6.25

† For C_3H_4 and C_4H_2, we assumed their sensitivities were comparable to C_3H_8 (n-propane) and C_4H_{10} (n-butane), respectively.

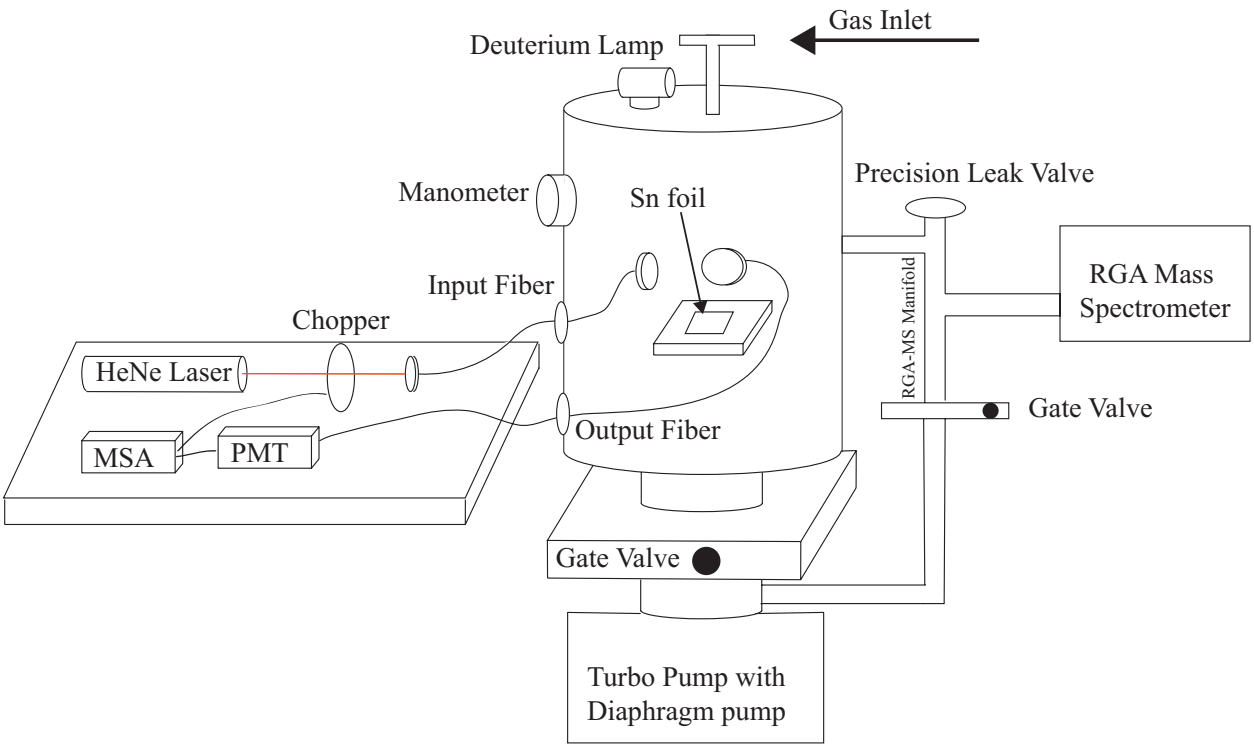

Figure 2.1: Experimental setup including stainless steel reaction chamber, mass spectrometer for detection of stable gas phase species and optical scattering detection scheme for detection of aerosol.

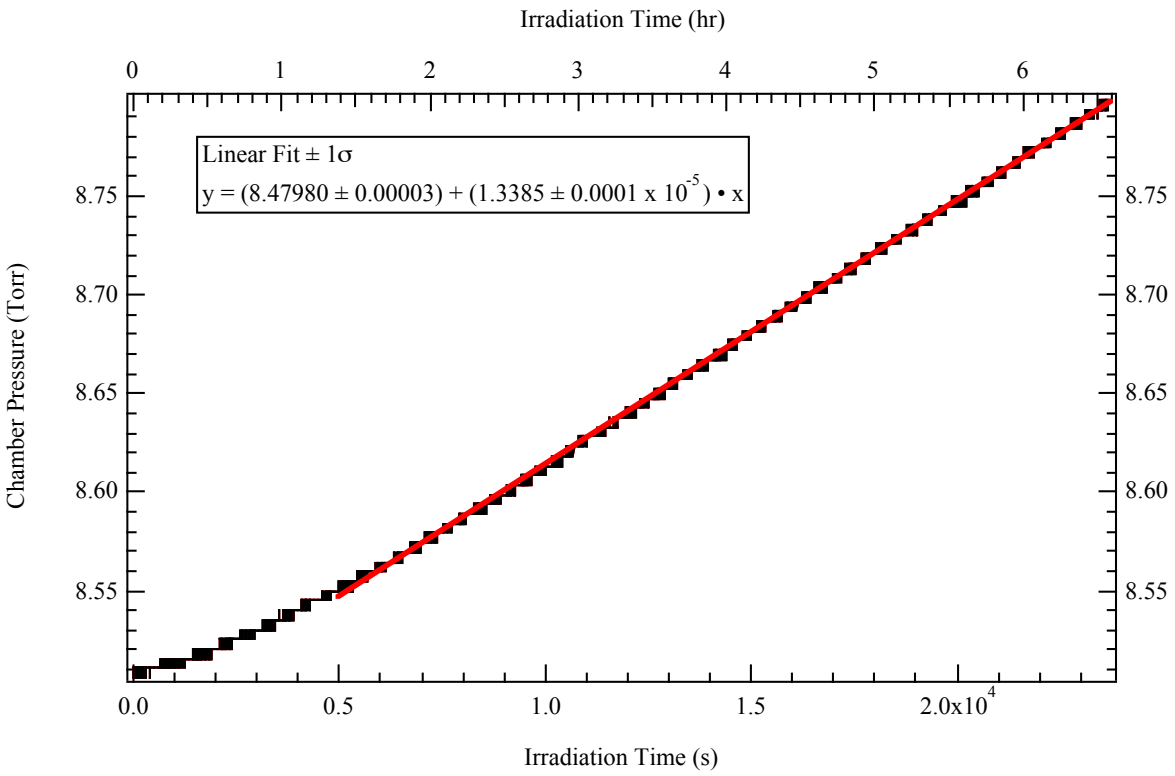

Figure 2.2: N_2O actinometry measurements for the high-brightness (L9841) D_2 lamp. As N_2O was photolyzed, the pressure in the chamber increased. The slope of the linear fit was used to calculate the photon intensity (see text).

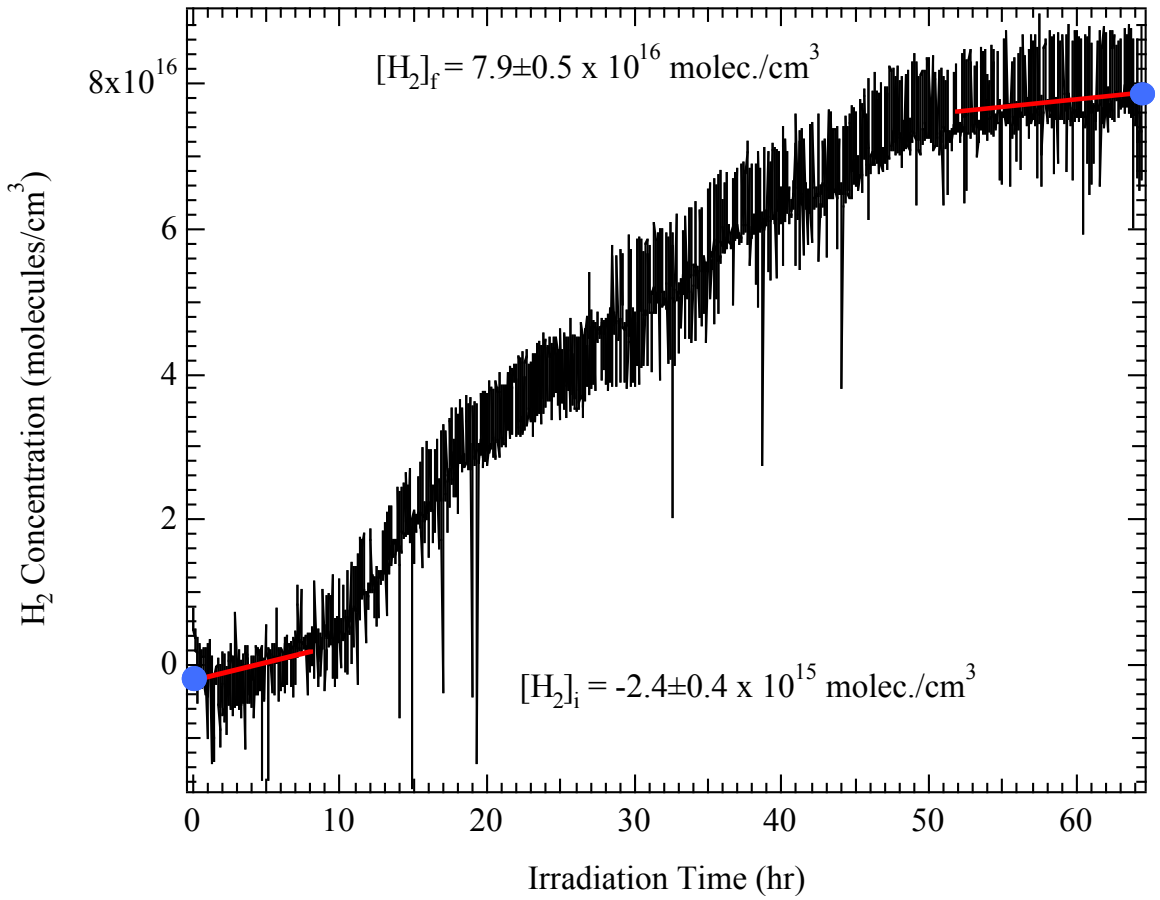

Figure 2.3: H_2 concentration as a function of time for the irradiation of 70.8 Torr CH_4. In cases in which the data are noisy, $[H_2]_i$ and $[H_2]_f$ were determined from linear fits and then extrapolating to the y-intercept and the 8 -15 hours preceding the highest peak, respectively (see text).

Chapter 3

Photochemical generation of organic aerosols in CH_4 and CH_4-CO_2 gas mixtures

3.1 Introduction

For the atmospheres of early Mars and an anoxic early Earth, the presence of aerosols may have significantly influenced climate, habitability and the stability of liquid water at the surface due to their potential for altering atmospheric radiative transfer [e.g., *Lovelock*, 1988; *Sagan and Chyba*, 1997; *McKay et al.*, 1999; *Pavlov et al.*, 2000, 2000; *Trainer et al.*, 2006; *DeWitt et al.*, 2009; *Wolf and Toon*, 2010]. *Sagan and Chyba* [1997], for example, suggested that the photolysis of CH_4 might have produced a UV-shielding haze of organic particles that would have in turn extended the photochemical lifetimes of CH_4 and NH_3 in the lower atmosphere of early Earth, thus increasing the concentrations of these greenhouse gases and perhaps compensating for the so-called "Faint Young Sun Paradox" [e.g., *McKay et al.*, 1991; *Kasting*, 2005, 2013] enough so that liquid water could have existed at Earth's surface, as the geologic record confirms [e.g., *Mojzsis et al.*, 1996; *Nutman et al.*, 1997, 2012; *Wilde et al.*, 2001; *Valley et al.*, 2002]. The formation of this haze would have been initiated by the UV irradiation of CH_4, which produces radical products that recombine to form new hydrocarbons, such as ethane (C_2H_6) and acetylene (C_2H_2), while further photolysis and reactions lead to even larger hydrocarbons that eventually condense into particles after their saturation vapor pressures are reached. This process of photochemical aerosol formation is common, if still not well-quantified, and is known to occur in the atmospheres of the Giant Planets and Saturn's moon, Titan [e.g., *Yung and DeMore*, 1999; *Lavvas et al.*, 2008; *Cable et al.*, 2012]. Using more sophisticated models than that of *Sagan and Chyba* [1997], as well as constraints from observations of the haze on Titan, however, *McKay et al.* [1991, 1999] and *Pavlov et al.* [2000, 2001b] suggested that, if indeed enough CH_4 were present and aerosols did form from the irradiation of CH_4 to produce higher hydrocarbons, the resulting photochemical hazes (in particular, their size distribution) would have provided neither a UV shield nor a greenhouse effect but an "anti-greenhouse" effect, thus exacerbating the Faint Young Sun Paradox rather than providing a solution. On the other hand, more recent model calculations by *Wolf and Toon* [2010] that take into consideration the fractal properties of particles suggest that the initial hypothesis of *Sagan and Chyba* [1997] (if not their model of it) may be correct – that is, if the haze particles were fractal, the resulting effect on atmospheric radiative transfer could indeed have served as an effective UV shield, allowing for the accumulation of UV-labile greenhouse gases and thus allowing Earth's surface temperature to rise above the freezing point despite a fainter young Sun. Thus, the presence or absence of aerosols in a planetary atmosphere as well as their optical properties and size distribution can have a dramatic influence on atmospheric radiative transfer and in turn UV fluxes at the surface, surface temperatures, and the stability of liquid water at the surface. Clearly, much remains to be understood and quantified regarding the prevalence and properties of aerosols formed by atmospheric photochemistry on early Earth and Mars and thus to what degree they may have influenced climate and habitability.

Photochemical models of the formation of organic hazes on early Earth and Mars [*Zahnle*, 1986; *Pavlov et al.*, 2000, 2001a, 2001b] are still somewhat rudimentary, due in part to a lack of fundamental kinetics data from laboratory experiments. For example, condensation of gas-phase species to form aerosol has been grossly simplified (e.g., *Zahnle* [1986] state that "the species C_3H_4, C_4H_2 and HC_3N were allowed to go to soot at an arbitrary rate"). Furthermore, an

additional complication for organic aerosol formation in terrestrial-like planetary atmospheres is that CO_2 is also present, and it can photolyze to produce $O(^1D)$. The oxygen atoms can react with the gas phase hydrocarbons, breaking them down into smaller hydrocarbons and thus competing with further polymerization to form higher hydrocarbons and subsequent condensation to form particles. The overall model prediction for terrestrial-like atmospheres is that a CH_4/CO_2 ratio larger than 1 is necessary for aerosol formation [*Zahnle*, 1986; *Pavlov et al.*, 2000, 2001a, 2001b]-- a value considered to be difficult to achieve in the CO_2-rich atmospheres of early Mars and Earth, given ranges of estimates for CH_4 fluxes from the mantle degassing and, later biogenic emissions [e.g., *Kasting*, 1993, 2005; *Sagan and Chyba*, 1997; *Pavlov et al.*, 2000]. *Pavlov et al.* [2000, 2001a, 2001b] predicted that a CH_4/CO_2 ratio of 0.6 to 1 was needed, a range making aerosol haze formation slightly more feasible but not dramatically so. Yet the CH_4/CO_2 ratio at which particle formation can happen is critical – the lower the ratio, the more likely a haze can form in the atmospheres of early Earth and Mars.

Importantly, however, experiments performed to date show that photochemically-generated aerosol can be produced at significantly lower CH_4/CO_2 ratios than the 0.6 to >1 thresholds predicted by photochemical models. *Trainer et al.* [2006] measured aerosol produced by irradiating flowing gaseous mixtures of N_2, CH_4, and CO_2 with broadband UV light from a deuterium lamp and detecting the aerosol by Aerosol Mass Spectrometry (AMS). Their study demonstrated aerosol production down to a CH_4/CO_2 ratio of 0.20, presumably the lowest ratio at which they performed an experiment. *Ádámkovics* [2004] measured particle production by irradiating mixtures of CH_4 and CO_2 with a deuterium lamp in a static reaction chamber and detecting aerosol *in situ* by HeNe laser light scattering. The laser scattering results demonstrated that particles were detectable down to CH_4/CO_2 ratios as low as 0.25; although no particles were detected by laser light scattering at a CH_4/CO_2 ratio of 0.1, it was unclear if longer irradiation times and/or higher absolute CH_4 pressures at the same CH_4/CO_2 ratio might ultimately have produced a detectable signal. These two experimental studies showing aerosol formation at much lower CH_4/CO_2 ratios than predicted by photochemical models suggest a larger role for aerosols in radiative transfer in early Earth's atmosphere than predicted by photochemical models. The Trainer *et al.* [2006] results, however, were limited by a 10-minute residence time for the irradiation of the CH_4 and CO_2 gas mixtures while the mixture was flowed continuously into their aerosol mass spectrometer; a longer irradiation time might have produced aerosol at lower CH_4/CO_2 ratios than they detected if the overall gas-phase kinetics to form higher hydrocarbons at lower CH_4/CO_2 ratios is slower, as is expected. In addition, the short irradiation time dictated by their experimental setup resulted in a dependence of their aerosol production rates on the CH_4 optical depth in their flowing reaction cell [Trainer *et al.*, 2006] and not necessarily on the underlying chemistry, which we wish to probe. In the *Ádámkovics* [2004] experiments, the CH_4/CO_2 ratio was varied by changing both CH_4 and CO_2 to keep the total pressure in the reaction chamber at 100 Torr. This experimental design makes it difficult to distinguish changes in particle production due to a dependence on the CH_4/CO_2 ratio from changes due to a dependence on the absolute amount of CH_4 being irradiated. Thus, constraints from additional experiments are needed to better understand particle production in controlled mixtures of gases relevant for early Earth and Mars and, hence, to better predict the prevalence or absence of photochemical hazes in the atmospheres of early Earth and Mars given various possible atmospheric compositions and conditions.

In this study, aerosols were produced by irradiating CH_4 or mixtures of CH_4 and CO_2 at room temperature with a broadband VUV light source for 50 to 100 hours in the static reaction

chamber used in *Ádámkovics and Boering* [2003] and *Ádámkovics* [2004]. In some experiments, HeNe laser scattering was used both to detect the presence and relative amount of particles and to measure the induction time from gaseous precursors to the initial particle detection at different initial CH_4 pressures and CH_4/CO_2 ratios. These particle scattering results are compared with measurements of the net production of H_2 and/or C_2H_6 in the gas phase over the course of an irradiation experiment by time-resolved mass spectrometry, which we then use as a proxy for the number of carbon-carbon bonds in particulate form for a given CH_4 pressure and CH_4/CO_2 ratio. In addition, in some experiments particles were also collected for "offline" measurements of the integrated relative aerosol amounts using peak areas from an elemental analyzer-isotope ratio mass spectrometer (EA-IRMS). The combined results are compared and contrasted with each other as well as with the results of *Trainer et al.* [2006] to derive new constraints on and insights into photochemical aerosol formation as a function CH_4 pressure and CH_4/CO_2 mixing ratio in the laboratory and implications for terrestrial-like planetary atmospheres.

3.2 Methods

The reaction chamber, laser light scattering, and mass spectrometer have been described previously [*Ádámkovics and Boering*, 2003; *Ádámkovics*, 2004] and in Chapter 2, and are shown schematically in Figure 3.1. A stainless steel reaction chamber with a leak valve to the Residual Gas Analyzer mass spectrometer (RGA 300, Stanford Research Systems) was used. The reaction chamber was 36 cm tall and 21 cm in diameter, with a total volume of about 13 L. The irradiation source for most of the experiments reported here was a "high-brightness" D_2 lamp (Hamamatsu Model L9841), installed in the top flange of the reaction chamber with a MgF_2 window that allowed transmittance of wavelengths longer than 110 nm into the chamber. Using N_2O actinometry [*Greiner*, 1967], the total lamp intensity from 120 to 300 nm was determined to be $5.4 \pm 0.4 \times 10^{15}$ photons s^{-1} with maximum output near 160 nm. In some previous experiments with this reaction chamber, a "low brightness" Hamamatsu Model L7292 deuterium lamp was used [*Ádámkovics and Boering*, 2003; *Ádámkovics*, 2004]. The intensity of the low brightness lamp, $8.8 \pm 0.8 \times 10^{15}$ photons s^{-1} as reported in *Ádámkovics and Boering* [2003], was the same magnitude as the "high brightness" lamp, but its aperture was 1.0 mm, twice that of the high brightness lamp, so photons were spread over a wider area.

Before each experiment, a turbomolecular pump (Pfeiffer TSU 261) was used to evacuate the chamber to $\sim 10^{-8}$ Torr (1.3×10^{-6} Pa), as monitored with a cold cathode gauge (Pfeiffer PKR 251). During evacuation, heating tape wrapped around the chamber was used to bake out the chamber for two days. At the start of an irradiation experiment, the reaction chamber was isolated from the turbomolecular pump, and CH_4 (Scott Gas, 99.99%) and CO_2 (Scott Gas, 99.997%) were introduced through an evacuated valved inlet. The total chamber pressure was monitored with a capacitance manometer (MKS; 1000 Torr full range, 0.12% accuracy). Two types of experiments were conducted: irradiation of pure CH_4 and irradiation of mixtures of CH_4 and CO_2. The pressures used in the CH_4 and CH_4/CO_2 experiments, along with the irradiation times, are shown in Table 3.1. During the experiments, a fan external to the reaction chamber was used to prevent the deuterium lamp from overheating.

At the end of each experiment, the deuterium lamp was turned off and, always within 10 minutes, the chamber was evacuated with the turbomolecular pump. A brown residue on the window of the deuterium lamp (i.e., the particulate matter which formed directly on the window of the lamp) was cleaned using optical grade cloths (Fisher Scientific 06-665-29) and acetone. The chamber was then evacuated and baked out in preparation for the next experiment.

3.2.1 Online mass spectrometry

The time evolution of H_2 and C_2H_6 over the course of some of the irradiation experiments was monitored with the RGA mass spectrometer. After filling the chamber with the gases for irradiation, the precision leak valve that connected the reaction chamber to the mass spectrometer manifold was opened until the pressure in the manifold was approximately 5 x 10^{-5} Torr, less than 1 x 10^{-4} Torr, the maximum operating pressure of the RGA. After two hours of equilibration, the deuterium lamp was turned on to start the experiments. Each mass spectral scan from 1 to 100 amu in 0.1 amu intervals took approximately 1 minute to complete and was repeated, digitized, and recorded in 1.5 minute intervals using the RGA Labview program.

Since the gaseous mixture from the reaction chamber was composed of a mixture of H_2 and various hydrocarbons, and since the parent hydrocarbon ions can fragment into smaller ions with overlapping m/z values, deconvolution of the mass spectral peaks, as well as a correction for the relative ionization efficiences (i.e., "sensitivities") of the different parent species, was necessary in order to obtain the concentrations of stable (i.e., non-radical) species in the chamber from the raw data from the mass spectrometer. Calibration of the mass spectrometer was achieved by measuring the fragmentation patterns and relative ionization efficiencies of pure gases individually placed into the reaction chamber that we thought might be produced in the reaction chamber during CH_4 irradiation: H_2, CH_4, C_2H_2, C_2H_4, C_2H_6, C_3H_8, and C_4H_{10}. The raw mass spectral data obtained during an experimental run at each time step were first fitted using a multi-Gaussian function, then deconvolved using calibrated fragmentation patterns and divided by their sensitivity values in order to derive the concentrations for H_2 and C_2H_6 (as noted below, other gaseous hydrocarbons, while likely produced, were not detected above the detection limit, in the experiments reported here except for those shown in Figure 3.3). Additional details of the mass spectral analyses are described in *Ádámkovics and Boering* [2003], *Ádámkovics* [2004] and in Chapter 2 of this dissertation.

3.2.2 HeNe light scattering apparatus

In some irradiation experiments, optical scattering from photochemically generated aerosol particles was obtained. Details of the particle detection scheme have been described previously [*Ádámkovics and Boering*, 2003; *Ádámkovics*, 2004] and in Chapter 2 of this dissertation. In brief, a HeNe laser entered the chamber through fiber optic waveguides. For most experiments in which pure CH_4 was irradiated, a 15 mW, 632.8 nm HeNe laser was used (except as noted below). For experiments in which mixtures of CH_4 and CO_2 were irradiated, an 8 mW, 613 nm laser was used instead since H_2O produced photochemically in a mixture of CH_4 and CO_2 can fluorescence at 632 nm, interfering with the scattering signal from the particles. Within the chamber, the laser light interacted with the aerosol particles in a 4.2 mm^3 region (given the 0.65 mm laser beam diameter and the 1 cm diameter field of view for the detector) approximately 16 cm below the window of the deuterium lamp. The collection optics were mounted perpendicular to the incident HeNe radiation. The output fiber waveguide was coupled to a photomultiplier tube (Hamamatsu: R928) operating at a bias voltage of 1.1 kV with a HeNe laser line filter to ensure measurement of elastic scattering. A multichannel scaler/averager (MSA, Stanford Research Systems: Model SR430) collected the scattered light and used a signal from the optical chopper to sort it into laser “on” and laser “off” bins; net scattering was determined by averaging the measurements in the laser “on” and “off” bins and taking the difference, which was stored along with the raw photon-counting data.

3.2.3 Offline EA-IRMS peak area measurements

In some irradiation experiments, particles were collected for offline analysis by elemental analyzer-isotope ratio mass spectrometry (EA-IRMS) by placing a 3 cm x 3 cm piece of tin (Sn) foil on a stage in the chamber, approximately 16 cm below the window of the deuterium lamp at the top of the reaction chamber. Within 10 minutes of the end of an irradiation experiment, the reaction chamber was opened and the tin foil was collected with a pair of clean tweezers. The sample was folded into another piece of tin foil to preserve all the particles, then labeled and stored in a desiccator until analysis on a Finnigan Delta Plus XL isotope ratio mass spectrometer at the NASA Ames Astrobiology Institute.

At NASA Ames, each aerosol sample was placed individually in a tin cup containing vanadium oxide (V_2O_5), a reagent that facilitates complete combustion. In the elemental analyzer portion of the instrument, the particle samples (in tin foil) were flash-combusted between 1000 and 1050°C, converting all carbon in the sample to CO_2. In a flow of helium, the CO_2 produced by combustion of the aerosol sample was purified in a series of oxidation and reduction steps, purified further by injection onto a gas chromatography column, and then injected into the IRMS portion of the instrument for measurement of the bulk carbon-13 isotopic composition of the aerosol particles. The $\delta^{13}C$ values for the particle samples are reported in Chapter 4. In this chapter, measurements of the peak areas – i.e., the integrated IRMS voltages for m/z 44 as measured by a Faraday cup detector – are used as a measure of the relative amount of particulate carbon produced in the irradiation experiments under different conditions. The uncertainties in the relative carbon amounts from the peak areas are as large as 40% due to changes in, e.g., IRMS source parameters, both from run to run and over time. The large uncertainty is not particularly surprising since the EA-IRMS was not designed to measure amount of carbon and the peak area is more of a housekeeping measurement to check, for example, the appropriateness of the relative standard and sample sizes and instrument performance in general, but is useful here nevertheless when comparing different CH_4 and CH_4/CO_2 runs. Uncertainties of ±40% (±1σ) are therefore given in tables, figures, and the results and discussion below.

3.3 Results and Discussion

3.3.1 CH_4 irradiation experiments

HeNe light scattering from the particles suspended in the gas phase, mass spectrometry of the time evolution of the gas-phase species H_2 and C_2H_6, and offline measurements of the EA-IRMS peak areas from particles collected during the irradiation experiments were used to study the time evolution and relative total amounts of particulate organic carbon formed during the irradiation of pure CH_4 at different starting concentrations in the reaction chamber. The results from all three of these types of measurements suggest that the formation of higher hydrocarbons and the total amount of organic carbon produced in particulate form increased as the initial pressure of reactant CH_4 in an irradiation experiment was increased.

3.3.1.1 CH_4 irradiation experiments: RESULTS

Measurements of *in situ* HeNe light scattering from particles produced from the irradiation of pure CH_4 at reaction chamber pressures of 35, 50, and 70 Torr are shown in Figure 3.2. Both the amplitude and peak area of the light scattering signals increased with larger initial pressures of CH_4. For example, the peak scattering intensity from the irradiation of 70 Torr CH_4 was approximately 2800 counts/min, while the peak scattering intensity from the irradiation of 35 Torr CH_4 was much lower, at 800 counts/min (Figure 3.2 and Table 3.2). We infer that a

higher number density of particles was formed in experiments with larger initial CH_4 pressures. In addition, it is also apparent in Figure 3.2 that, as the initial CH_4 pressure is increased from 35 to 70 Torr, the onset of first detection of light scattering from particles moves to shorter irradiation times – that is, the relative "induction time" between the start of irradiation and detection of first light scattering decreases on going from an initial CH_4 pressure of 35 to 50-70 Torr. For example, the induction time for the irradiation of 35 Torr CH_4 was 20 hours, in comparison to 15 hours for 50 and 70 Torr CH_4 (Table 3.2). Note that as irradiation continues in each experiment, the scattering signal increases to a maximum and then begins to decrease, eventually decreasing to the background level. As explained in *Adamkovics and Boering* [2003], the concentrations of higher gas-phase hydrocarbons level off to their final values (i.e., their production stops) as the D_2 lamp window becomes coated with a brown UV-attenuating film (i.e., the same material that is also produced as aerosol), while aerosol production also ceases and the remaining aerosol settles out to the bottom of the chamber so that eventually the scattering signal drops to its light-off value.

To determine whether the variation in relative induction times results from the timescale for production of the larger gas-phase hydrocarbons necessary for particle formation and/or from some other timescale, such as the timescale for particles to settle into the laser scattering measurement region if, for example, they formed near the window of the D_2 lamp, another experiment was conducted. In this experiment, pure CH_4 at 100 Torr was photolyzed as before and then the deuterium lamp was turned off after 30.65 hours – a time at which light scattering from particles was clearly detected but long before the window of the lamp had been coated with particulate matter; results are shown in Figure 3.3. Upon turning off the D_2 lamp, the HeNe scattering signal started to decrease immediately, while the RGA-MS signals for the gaseous stable hydrocarbon precursors increased for approximately 20 minutes before leveling off and then remaining constant in time. After the laser scattering signal was observed to decrease back to background values, the lamp was turned on again at 46 hours. The gaseous hydrocarbon abundances from the RGA-MS measurements started increasing again within 30 minutes, while the laser scattering signal started to rise again 3 hours after the light was turned on again. This timing suggests that in the 23 hour induction time at the beginning of this experiment, gaseous hydrocarbon precursors produced from CH_4 photolysis and subsequent photochemistry accumulated in the reaction chamber within the first 19 hours; while particle formation may have also occurred during this time, it took an additional 3 hours of irradiation before the scattering became large enough to detect the particles. The latter effect may be a combination of the time it took to create particles large enough to scatter the laser light and the time it took particles to settle into the HeNe laser interaction region 16 cm below the deuterium light. (This interpretation is also consistent with the particle scattering induction time being a function of the HeNe laser used – i.e., there is a difference in the absolute induction times, as well as scattering intensity, between the 16 mW 632 nm laser and the 8 mW 613 nm laser results in Figure 3.2 vs 3.3). In any case, however, it seems clear from the results in Figure 3.3 that the majority of the induction time measured from the first light-on period is due to the relatively long time it takes to create the larger gaseous hydrocarbons starting from pure CH_4; once much of these have been produced in the first UV light-on period, particles are detected again after only 3 hours. Thus, we interpret the relative induction times for the irradiation of different pressures of CH_4 in Figure 3.2 to mean that the shorter the induction time, the higher the initial rate of particle production (although the 50 Torr and 70 Torr data cannot be differentiated within the sensitivity of the HeNe scattering instrumentation). Overall, the shorter induction time combined with the larger scattering

amplitude and larger integrated scattering area for larger initial pressures of CH_4 (for a given HeNe laser) suggest that the particle production rate and total particle production increase as the CH_4 pressure in the chamber is increased.

For comparison with the *in situ* particle scattering data, mass spectrometry was used in separate experiments to study the growth of H_2 and C_2H_6 and, from their difference, to obtain a rough estimate of the amount of carbon-carbon bonds in particulate matter. The time-dependent concentrations of H_2 and C_2H_6 from the irradiation of varying initial pressures of CH_4 are shown in Figure 3.4, while the net production of H_2 and C_2H_6 (i.e., the difference between the initial and final concentrations in each irradiation experiment, ΔH_2 and ΔC_2H_6) and the difference between them (i.e., $\Delta H_2 - \Delta C_2H_6$) are shown in Figure 3.5 as a function of initial CH_4 pressure for each experiment. The rate at which H_2 is formed is an indication of the CH_4 photolysis rate in an experiment and, hence, for the rate of formation of higher hydrocarbons, while ΔH_2 is a proxy for the total number of carbon-carbon bonds formed in gaseous and particulate matter. This concept is illustrated in Figure 3.6, where it is shown that either an H_2 molecule or two H atoms are produced initially in the photolysis of CH_4 as well as upon the formation of every carbon-carbon bond in higher molecular-weight hydrocarbons, such as ethane and diacetylene. Generalizing to all reaction schemes relevant to the formation of higher hydrocarbons and hydrocarbon aerosol, 2H or H_2 is produced for each carbon-carbon bond formed regardless of the specific reaction pathway and can be used to characterize the particle formation [*Yung and DeMore*, 1999; *Ádámkovics and Boering*, 2003; *Ádámkovics*, 2004]. In this study, we use the quantity ($\Delta H_2 - \Delta C_2H_6$) as a rough estimate for the total number of carbon-carbon bonds formed in particulate matter, which we will denote $\Delta_{C\text{-}C}$. (The values for $\Delta_{C\text{-}C}$ in this study are roughly comparable to those in *Adamkovics and Boering* [2003] since no gas-phase hydrocarbons were detected larger than C_2H_6 in this study, while C_2H_2 as well as larger hydrocarbon gases species were above the detection limit yet they were present in such small concentrations that they made only a very small contribution to their $\Delta_{C\text{-}C}$ values; the lower sensitivity of the mass spec results in Figure 3.4 and other more recent results is likely due to the necessity of running the RGA at a lower pressure than earlier studies to avoid serious damage to the detector.) Given the values for ΔH_2, ΔC_2H_6, and $\Delta_{C\text{-}C}$ as a function of initial CH_4 pressure in Figure 3.5, the higher the initial CH_4 pressure, the greater the net production of carbon-carbon bonds in both gaseous and particulate species. As for the laser scattering data, then, particle production increases with increasing initial CH_4 pressure.

The conclusions based on the laser light scattering by particles and the mass spectrometry data for H_2 and C_2H_6 are also consistent with results for the relative amounts of carbon in particulate form inferred from the peak areas measured by EA-IRMS on particles collected over the course of an irradiation experiment. Measured EA-IRMS peak areas as a function of initial pressure of CH_4 in the reaction chamber are shown in Figure 3.7: EA-IRMS peak area increased with initial CH_4 pressure, which suggests an increased production of aerosols at higher initial CH_4 pressures. Thus, the HeNe light scattering from particles, the gaseous mass spectrometry data, and the EA-IRMS peak areas on collected particles all indicate that both the particle production rate and the total amount of organic carbon in particulate form increase as the initial CH_4 pressure in the CH_4 irradiation experiments is increased.

3.3.1.2 CH_4 irradiation experiments: DISCUSSION

The results from HeNe scattering, mass spectrometry, and EA-IRMS measurements all suggest that particle production and the total amount of organic carbon produced by CH_4

photolysis increase with higher initial pressures of CH_4. At first glance, these conclusions appear to differ from the results of *Trainer et al.* [2006]; they found that the aerosol mass loading of particles produced photochemically from the UV irradiation of CH_4 in their flowing reaction cell and then detected after the cell by Aerosol Mass Spectrometry at first increased as the initial CH_4 pressure increased but then significantly decreased at higher CH_4 pressures. *Trainer et al.* [2006] attributed this behavior to the CH_4 creating optically thick conditions in their reaction cell: at low CH_4 pressures, aerosol production was CH_4-limited, and increasing CH_4 increased the particle production rate. At higher CH_4 pressures, however, their reaction cell became optically thick for CH_4 photolysis (that is, much of the UV radiation was absorbed a short distance from the deuterium lamp and so did not penetrate deeper into their flowing reaction cell), and the particle production rate became photon-limited instead of CH_4-limited. Thus, at the higher pressures (starting at about 0.1 Torr in their reaction cell), increasing the initial CH_4 pressure irradiated decreased the particle production rate.

In our experiments here, the reaction cell was always optically thick with respect to CH_4 photolysis (e.g., reaching an optical depth of 1 within 30 mm of the D_2 lamp window at the lowest CH_4 pressure we tested of 4.9 Torr), and yet we observe that particle production still increases as the initial CH_4 pressure is increased, even up to 200 Torr in the EA-IRMS measurements in Figure 3.7 – in other words, in our experiment, particle production is always CH_4-limited. The difference between our results and those of *Trainer et al.* [2006] can be understood in terms of the very different time-scales for the irradiation experiments and the timescales for mixing of gases in the two different reaction cells. In our static irradiation experiments lasting for ~50 to 100 hours, CH_4 and its photolysis products can diffuse in and out of the narrow optically thin region near the lamp (see Figure 4.5 in Chapter 4), and photochemistry and particle production can continue in spite of the optical thickness for most of the chamber. (In fact, the light-on, light-off, light-on experiment shown in Figure 3.3 yields an estimate for a mixing time for the entire chamber of $\leq$ 20 minutes.) Integrated over the course of many hours, then, we see that particle production is always proportional to CH_4 concentration. In the *Trainer et al.* [2006] experiments, the particle production rate and total aerosol mass loading become severely limited due to the short 10-minute residence time of precursor gases in the photolysis cell once the CH_4 pressure is high enough to create optically thick conditions.

3.3.2 CH_4/CO_2 irradiation experiments

As for the irradiation of pure CH_4, HeNe light scattering, mass spectrometry, and EA-IRMS peak areas were used to estimate relative particle production rates and the relative amounts of organic carbon formed in particulate matter in experiments in which mixtures of CH_4 and CO_2 were irradiated. The results suggest that, while the initial particle production rate appears to increase when CO_2 is first added (i.e., at a high CH_4/CO_2 ratio) based on shorter initial induction times for particle detection, over a longer timescale the total amount of organic carbon in particles is not sensitive to the CH_4/CO_2 ratio, at least down to a ratio of 0.34 and to within the noise of our dataset.

3.3.2.1 CH_4/CO_2 irradiation experiments: RESULTS

First, we revisit and reanalyze the HeNe light scattering from particles formed during the irradiation of mixtures of CH_4 and CO_2 from *Adamkovics* [2004], shown in Figure 3.8. Particles were detectable down to CH_4/CO_2 ratios as low as 0.25, which is significantly lower than 0.6 to 1, the values predicted by photochemical models [*Zahnle*, 1986; *Pavlov et al.*, 2000, 2001a,

2001b]. In these light scattering experiments, the total pressure in the reaction cell was kept at 100 Torr, with the CO_2 and CH_4 partial pressures varied in each experiment to yield the CH_4/CO_2 ratios noted in the figure. The induction times from the start of irradiation to time of first particle detection by scattering are given in Table 3.3. Interestingly, the induction times as CO_2 is first added decrease from that for pure CH_4 (i.e., the induction times for CH_4/CO_2 ratios of 3 and 1 were 16 and 15 hours, respectively, while that for pure CH_4 at 100 Torr is 22 hours). Furthermore, the induction times decrease despite the fact that the CH_4 pressure in these runs are 75 and 50 Torr, which are significantly lower than the 100 Torr pure CH_4 run. Given our results and conclusions in section 3.1 above that particle production rates and total particulate carbon decrease with decreasing initial CH_4 pressure, the amount of additional CO_2 in runs with CH_4/CO_2 ratios of 3 and 1 therefore more than compensates for the "CH_4-limited" photochemistry in the pure CH_4 experiment at 100 Torr (if we assume that the particle scattering properties are similar for the CH_4 versus the CH_4/CO_2 experiments). As the mixing ratio of CO_2 is increased even further in additional experimental runs, the induction times do finally increase (i.e., the induction times for CH_4/CO_2 ratios of 0.33 and 0.25 were 40 and 90 hours, respectively). Finally, particles were not detected by scattering at a CH_4/CO_2 ratio of 0.11, although a longer irradiation time may have been required at the CH_4 partial pressure of only 10 Torr or the laser scattering system was not sensitive enough to detect particles at the number density of particles produced. To view the relative induction times versus the CH_4/CO_2 ratio in a more compact manner, we plot the "normalized particle formation time scale," which we define as the induction time for particle detection in pure CH_4 at 100 Torr, t_{CH4}, divided by the observed induction time for a given CH_4/CO_2 ratio, t, or t_{CH4}/t, in Figure 3.9. Again, the normalized time scale for particle production can be seen to first increase as the mixing ratio of CO_2 is increased from 0 for the pure CH_4 experiment (i.e., $t_{CH4}/t > 1$) and then to decrease (i.e., $t_{CH4}/t < 1$) as the mixing ratio of CO_2 is further increased beyond some threshold value, which for this dataset appears to be for $CH_4/CO_2 < 1$. For comparison, normalized AMS aerosol mass loading results from *Trainer et al.* [2006] are also shown in Figure 3.9.

As noted earlier, however, it is difficult to separate the effects of an increasing CO_2 mixing ratio versus a decreasing CH_4 partial pressure in the light scattering experiments above. In order to facilitate comparisons between particle production in experiments in which the CH_4/CO_2 ratio was varied but the CH_4 pressure was the same, we measured the time evolution and the net production of H_2 (Figures 3.10 and 3.11). In each experiment, CO_2 was added to 10 Torr of CH_4 to reach the desired CH_4/CO_2 ratio, ranging from 0.50 and 4.28. Over the course of irradiation, H_2 concentrations increased, similar to what was measured in the irradiation of pure CH_4 (Figure 3.4). The net H_2 production, $\Delta[H_2]$, in these experiments is shown as a function of the CH_4/CO_2 ratio in Figure 3.11. Within 2σ in this set of measurements, $\Delta[H_2]$ did not vary with the CH_4/CO_2 mixing ratio, and the average of $3.5 \pm 2.2 \times 10^{16}$ molecules cm^{-3} of H_2 produced is similar to the average (3.3×10^{16} molecules cm^{-3} of H_2) and range (2.5 to 4.1 $\times 10^{16}$ molecules cm^{-3} of H_2) from the pure CH_4 irradiation experiments shown in Figure 3.5. Although it is tempting to interpret the ΔH_2 results in a similar manner as the induction times above if the data point at a CH_4/CO_2 ratio of 2.40 is for some reason an outlier -- that is, particle production may initially increase as CO_2 is added and enhance particle production before it eventually begins to inhibit particle production for CH_4/CO_2 below 1 – there is no reason to suspect the 2.40 datum as an outlier beyond the noise of the experiments in general. Thus, the mass spectrometry results suggest that, for a given CH_4 pressure, the total amount of carbon-carbon bonds produced in the

particulate and gaseous phase does not vary significantly within the CH_4/CO_2 ratio range of these experiments nor from that for pure CH_4.

This result that varying the CH_4/CO_2 ratio did not change the total amount of carbon in particulate matter formed over the course of a long irradiation experiment for the mass spectrometry dataset is consistent with the EA-IRMS peak areas for particulates collected during experiments. EA-IRMS peak areas representing the relative amounts of carbon in particulate matter produced in experiments irradiating CH_4 at a partial pressure of 10 Torr and varying the amount of CO_2 to vary the CH_4/CO_2 ratio are shown in Figure 3.12. All the data points fall within 2σ of the average value of the CH_4/CO_2 runs as well as within 2σ of the average of the CH_4-only runs between 5 and 20 Torr. Again, although it is tempting to find a trend of increasing and then decreasing peak areas as the CH_4/CO_2 ratio decreases, such a trend would be within the noise of the current datasets for both $\Delta[H_2]$ and peak areas. Thus, both the mass spectrometry and the EA-IRMS peak area measurements suggest that the total amount of organic carbon produced throughout an entire experiment does not vary within the CH_4/CO_2 ratio range of these experiments from 0.34 to 4.8, at least to within the precision of the measurements.

3.3.2.2 CH_4/CO_2 irradiation experiments: DISCUSSION

The most important result for the data shown here is that particles were detected at CH_4/CO_2 ratios down to 0.25, significantly lower than the lowest threshold values predicted by photochemical models of 0.6 to 1 [*Zahnle*, 1986; *Pavlov et al.*, 2000, 2001a, 2001b], which in turn suggest a larger role for aerosols in early Earth's atmosphere than expected based on model results alone. Indeed, *Trainer et al.* [2006] measured particles down to a CH_4/CO_2 ratio of 0.20 (although it is not clear whether they performed experiments below this ratio and neglected to report negative results or whether this was the lowest ratio at which they attempted to make measurements). The lower the CH_4/CO_2 ratio at which particles can form, the easier it is for natural CH_4 emissions from degassing of the early mantle and/or from methanogenic bacteria to have been sufficiently high that the CH_4/CO_2 ratio would exceed the aerosol production threshold [e.g., *Pavlov et al.*, 2000].

Speculation on the reasons for the inadequacy of the model chemistry for particle formation at lower CH_4/CO_2 ratios is informed by a more in-depth look at the light scattering results as a function of CH_4/CO_2 and comparing those with the aerosol mass spectrometer results of Trainer *et al.* In Figure 3.9, the induction times from the light scattering experiments shown in Figure 3.8, normalized to the CH_4-only induction time, as a function of CH_4/CO_2 ratio are compared with the aerosol mass loading results measured by *Trainer et al.*[2006] normalized to their CH_4-only aerosol mass loading. Both the normalized induction time to first detection of particles by light scattering and the total mass of particles formed during the 10-minute residence time of the gas mixture irradiated and then introduced into an AMS show that the aerosol production rate as CO_2 is added to the irradiated gas mixture stays the same as, or is larger than, the CH_4-only irradiation results. Both datasets show a maximum increase in aerosol production rates at CH_4/CO_2 values near 1. This has been surprising since model predictions do not show such an increase as CO_2 levels are increased, predicting that any added CO_2 will inhibit aerosol formation and yet the experimental results of both groups show a maximum aerosol production rate at a ratio 1. Indeed, in the light scattering experiments, CO_2 enhances initial particle production rates for CH_4/CO_2 values between 1 and 3 that the enhanced chemistry overcomes the lower initial CH_4 pressures in these experiments, which, if acting alone, should have resulted in a lower particle production rate and hence longer induction time, given our results in section 3.1

above. The large discrepancy between the measurements and model predictions for aerosol production as a function of CH_4/CO_2 is likely due to a lack of detailed chemistry in the models involving the production of oxygenated organic species, which have a lower vapor pressure for a given number of carbon atoms than the corresponding hydrocarbon species and so would condense more readily, which the models are not currently taking into account. Indeed, the Aerosol Mass Spectrometry measurements of *Trainer et al.* [2006] show substantial peaks associated with oxygenated species in the aerosol, such as CH_3O^+ and COO^+. The models, however, largely consist of reactions that oxidize the organic species from $O(^1D)$ produced by CO_2 photolysis and have not included details of the oxygenation of the larger organic species being produced. Clearly, more sophisticated chemical reaction pathways including the formation of oxygenated compounds such as aldehydes, ethers, and carboxylic acids need to be included in the models to more accurately predict the formation of aerosol as a function of CH_4/CO_2.

It is also interesting to compare and contrast these more "time-dependent" results from the AMS and the light scattering results with the results presented here that are integrated over much longer time scales – i.e., the $\Delta[H_2]$ and peak area results from Figures 3.11 and 3.12, respectively. The $\Delta[H_2]$ and EA-IRMS peak area measurements are a proxy for the amount of organic carbon produced over an entire 50 to 100 hour irradiation experiment in a static reaction chamber with ample time for mixing. In contrast, the induction times from light scattering and the aerosol mass produced in a reaction chamber with only a 10-minute residence time are probing the initial aerosol production rates and do not necessarily represent the integrated aerosol production over longer to much-longer timescales. More specifically, in the AMS results of *Trainer et al.* [2006], the aerosol production rates are both photon-limited and residence-time-limited. In the light scattering results in Figure 3.8, the aerosol production rates are likely to be at least somewhat photon-limited (given that the reaction chamber is optically thick with respect to CH_4 photolysis to within millimeters of the lamp) and may therefore also be convolved with diffusion and mixing timescales within the chamber as well as with the changing CH_4 pressures as the CH_4/CO_2 ratio is changed in the separate runs. Despite these differences and complications, however, these two types of measurements appear to be probing the initial particle production rates – beginning with the synthesis of all higher hydrocarbons from CH_4 – and both show similar behavior with respect to changing the CH_4/CO_2 ratio in the irradiated gas mixture: first an increase in initial particle production rates as CO_2 is increased, followed by a decrease as CO_2 is increased further. It is tempting to interpret the $\Delta[H_2]$ and peak area measurements in Figures 3.11 and 3.12 in a similar manner. For example, if it were not for the datum at a CH_4/CO_2 ratio of 2.4 in Figure 3.11, one could argue for an increase then decrease in organic carbon production as the CH_4/CO_2 ratio is decreased, similar to behavior for the light scattering induction times and the aerosol mass loading results. Likewise, the peak area measurements are suggestive that the peak area as CO_2 is added is first increased above that for the CH_4-only experiments and stays elevated as more CO_2 is added until it begins to drop at a ratio of 0.34, the lowest ratio for which peak area for collected particles was measured. However, in the cases of both $\Delta[H_2]$ and peak area, there is no reason to ignore any data points, and the measurements are all within the 2σ noise of the entire datasets. Thus, one interpretation is that there might be similar behavior to the light scattering and AMS results for particle production rates as a function of the CH_4/CO_2 ratio but that more highly precise measurements for $\Delta[H_2]$ and EA-IRMS peak area are needed to detect such behavior. An opposing interpretation is that these two sets of measurements represent particle production integrated over much longer time scales and that, on these longer timescales, total particle production is less sensitive to the CH_4/CO_2

ratio than the initial production rates when photons and mixing times are limited, as in the light scattering induction times and AMS results. This is an important distinction to work out since, as long as the overall particle production rates in an atmosphere are faster than the atmospheric settling time of the aerosols formed (which is likely to be at least several days or longer), then particles will be efficiently formed, regardless of the initial induction times required to form more complex hydrocarbons from CH_4 photolysis or the photon- and diffusion-limited results from the light scattering or AMS results. In other words, in this latter interpretation, the experimental results for $\Delta[H_2]$ and peak areas, which are effectively integrated over the equivalent of many days and are not sensitive to optical thickness issues and short residence and/or diffusion and mixing times, may be more relevant for atmospheric applications.

3.3.3 Additional issues

3.3.3.1 Wall effects

In this experimental study of photochemical particle production, CH_4 and mixtures of CH_4 and CO_2 were irradiated in a static stainless steel reaction chamber for ~50 to 100 hours. Under these experimental conditions, the walls of the reaction chamber could potentially catalyze some chemical reactions that would not occur in the gas phase, affecting the concentrations of both gas phase and particulate species. To check for wall effects, pure CH_4 was irradiated with the same deuterium lamp in a quartz reaction cell with a much smaller volume (~1L). The behaviors of all gas-phase species measured (H_2, C_2H_2, C_2H_4, C_2H_6, C_3H_4, C_4H_2, C_3H_6, and C_4H_{10}) were indistinguishable from those measured in the 13L stainless steel reaction chamber, apart from expected and calculable differences due to the smaller volume itself [*Ádámkovics*, 2004]. The similar results in the 1L quartz volume and the 13L stainless steel volume suggests that wall effects (such as radical losses and possible catalysis at the walls), while likely occurring, are likely not dominating the chemistry we are monitoring.

3.3.3.2 Effects of large hydrogen concentrations

It has been shown [*Moses et al.*, 2000] that the presence of H_2 can inhibit the formation of larger molecular-weight hydrocarbons and particles through saturation reactions:

$$C_2H_5 + H_2 \rightarrow C_2H_6 + H$$
$$C_3H + H_2 \rightarrow C_3H_2 + H$$
$$C_3H_7 + H_2 \rightarrow C_3H_8 + H$$

In these reactions, H_2 saturates radicals, preventing them from forming larger molecular weight hydrocarbons. *DeWitt et al.* [2009] observed this effect in their experimental studies: irradiating mixtures of CH_4 and CO_2 with increasing concentrations of H_2 decreased the measured aerosol mass loading, as measured by Aerosol Mass Spectrometry. In their experiments, however, the H_2 concentration required to inhibit particle production was 40 times that of CH_4, while the H_2 mixing ratios in our reaction in the experiments reported here, between 0.05 and 0.22, were well below that threshold. Therefore, although saturation reactions can occur, we do not expect them to be a significant factor in our results.

In addition, heterogeneous reactions of H_2 with species on the surface of aerosol particles can also potentially affect the concentration of H_2 in the gas phase. Experimental and modeling studies by *Sekine et al.* [2008a, 2008b] highlighted two significant types of heterogeneous reactions involving H_2: abstraction and saturation reactions. In abstraction, gaseous H_2 reacts with saturated carbon-carbon bonds on the surface of the aerosols to produce two moles of H_2, thus increasing the amount of H_2 in the gas phase. In contrast, heterogeneous saturation reactions

decrease the H_2 concentration in the gas phase by incorporating it into unsaturated carbon-carbon bonds in species on the surfaces of the aerosol particles. For these reactions to occur to any significant extent, the particles must be exposed a high flux of H_2. In the experiments conducted by *Sekine et al.* [2008a], particles were irradiated with D_2 (instead of H_2 in order to monitor its incorporation into the particles with IR spectroscopy and other techniques) with a flux of $8 \pm 2 \times 10^{16}$ atoms/cm^2 • min for 15 minutes. This flux is significantly greater than the production of H_2 in our UV irradiation experiments. For example, for the irradiation of 70 Torr CH_4, it takes approximately 60 hours to form approximately 5×10^{16} molecules of H_2. As a result, although heterogeneous reactions, in addition to saturation reactions, can occur during the photochemical generation of organic aerosols, we do not expect them to be significant factors since H_2 is produced at a much slower rate than what is necessary for these reactions to occur and the background H_2 levels are extremely low.

3.4 Conclusions

Using the irradiation chamber instrumentation developed by *Ádámkovics and Boering* [2003], we conducted a series of experiments to demonstrate how the photochemical production of organic aerosol from the UV irradiation of CH_4 varies with the absolute CH_4 pressure and the ratio of CH_4 to CO_2. The measurement techniques included *in situ* HeNe laser scattering for monitoring of aerosol suspended in the gas phase in the chamber, online RGA mass spectrometry for monitoring the evolution of gas phase species (in particular, H_2 and C_2H_6), and collection of aerosol on a tin foil substrate in the chamber for offline analysis by EA-IRMS for quantifying the relative amounts of carbon contained in the collected aerosol from the peak areas measured.

For experiments irradiating pure CH_4, the 3 types of measurements are all consistent with particle production increasing with increasing initial CH_4 pressure. These results differ from measurements in a flowing reaction chamber with a 10-minute residence time [*Trainer et al.*, 2006], in which particle production first increased at low CH_4 concentrations and then decreased at higher CH_4 concentrations as the chamber became optically thick against CH_4 photolysis. The difference is explained by the long irradiation times in our experiment of 50 to 100 hours and a mixing time in the chamber of <20 minutes in which gases could move in and out of the optically thin CH_4 photolysis region near the deuterium lamp; thus our results for particle production as a function of CH_4 pressure always scaled with CH_4 concentration, despite the reaction chamber being optically thick at all CH_4 pressures measured.

For experiments in which mixtures of CH_4 and CO_2 were irradiated, aerosol formation was observed by HeNe light scattering at CH_4/CO_2 ratios as low as 0.25 and in offline EA-IRMS analyses of particulate carbon as low as 0.34 (the lowest ratio for which offline analyses were attempted). These levels are significantly lower than the threshold of 0.6 to 1 predicted by photochemical models, and similar to the lowest ratio reported by *Trainer et al.* [2006] of 0.20. Interestingly, the results from *Trainer et al.* [2006] in a flowing photochemical reactor with a 10-minute residence time and the induction time between the start of irradiation and detection of light scattering by particles in this study both showed an increase in particle production rates over the pure CH_4 experiments as CO_2 was first added. The particle production rates from both sets of studies appear to maximize at a CH_4/CO_2 ratio of ~1 and then begin to decrease as CO_2 is increased further. This has been attributed at least in part to the production of oxygenated organic compounds, which may condense more easily to form aerosol since their vapor pressures are lower, especially for a given carbon number [*Trainer et al.*, 2006]. In comparison, the measurements in this study that integrate particle production over the entire 50 to 100 hour

period of irradiation – that is, the net production of H_2 (a proxy for formation of carbon-carbon bonds) and the relative amounts of carbon in collected particulate matter by EA-IRMS analysis appear to be much less sensitive to the CH_4/CO_2 ratio over the range of measurements that cover ratios from 0.34 to 4.8 and up to pure CH_4, at least to within the 2σ experimental uncertainties. Two interpretations were explored: (1) that the sensitivities of the latter experiments are not sufficient to show the same dependence of the particle production rates on the CH_4/CO_2 ratio as the HeNe light scattering experiments and AMS results of *Trainer et al.* [2006] show; or (2) that the $\Delta[H_2]$ and EA-IRMS peak area measurements are measuring integrated particle production over long time periods while the light scattering induction time measurements and the short-residence time AMS results are measuring only the initial production rates, not the integrated particle production of the longer time-scale measurements.

These results have important implications for the presence and prevalence of aerosols in the atmospheres of Early Earth and Mars. First, the fact that aerosols are easily observed to form down to CH_4/CO_2 ratios of at least 0.25 means that aerosols likely played a more important role in these planets' atmospheres than previously predicted by photochemical models, which currently predict that aerosols do not form when the CH_4/CO_2 ratio is below 0.6 [*Pavlov et al.*, 2000] or below 1 [*Zahnle*, 1986]. Second, more sophisticated photochemical models of early Earth's atmosphere that incorporates many reactions of organic species with oxygen that are currently not included in models need to be developed, both to better predict the minimum CH_4/CO_2 threshold at which particles form and to better describe the production rates as a function of CH_4/CO_2. Third, if the results from the long integration time experiments for $\Delta[H_2]$ and EA-IRMS peak area remain robust – that is, if particle production rates are as insensitive to the CH_4/CO_2 ratio as the results here suggest they might be – then these results, with their long irradiation times and long timescales for chemistry to occur, may be more relevant for aerosols in a planetary atmosphere, in which the aerosol lifetimes should be many days, much longer than the instantaneous chemical timescales in Trainer *et al.* [2006] yet allowing the chemistry to occur over relatively long periods. Additional experiments as well as photochemical modeling of these results, both on the reaction chamber scale and on an atmospheric scale, are needed to further explore these implications for the atmosphere and to aid in determining whether and under what conditions the production of a photochemical haze may warm or cool Earth's surface, thus resolving or exacerbating the Faint Young Sun Paradox.

Chapter 3 References

Ádámkovics, M. (2004), Hydrocarbon Photochemistry in Planetary Atmospheres: Laboratory and Observational Investigations of Organic Aerosols, University of California, Berkeley, Berkeley, CA.

Ádámkovics, M., and K. A. Boering (2003), Photochemical formation rates of organic aerosols through time-resolved in situ laboratory measurements, *J. Geophys. Res. E: Planets*, *108*(E8), 5092, doi:10.1029/2002JE002028.

Cable, M. L., S. M. Horst, R. Hodyss, P. M. Beauchamp, M. A. Smith, and P. A. Willis (2012), Titan Tholins: Simulating Titan Organic chemistry in the Cassini-Huygens Era, *Chem. Rev.*, *112*, 1882–1909, doi:dx.doi.org/10.1021/cr200221x.

DeWitt, H. L., Melissa G. Trainer, and A. A. Pavlov (2009), Reduction in Haze Formation Rate on Prebiotic Earth in Presence of Hydrogen, *Astrobiology*, *9*(5), 447–453, doi:10.1089/ast.2008.0289.

Greiner, N. R. (1967), Photochemistry of N2O Essential to a Simplified Vacuum-Ultraviolet Acintometer, *J. Chem. Phys.*, *47*(11), 4373–4377, doi:10.1063/1.1701640.

Kasting, J. F. (1993), Earth's early atmosphere, *Science*, *259*, 920–926, doi:10.1126/science.11536547.

Kasting, J. F. (2005), Methane and climate during the Precambrian era, *Precambrian Res.*, *137*, 119–129, doi:10.1016/j.precamres. 2005.03.002.

Kasting, J. F. (2013), How Was Early Earth Kept Warm?, *Science*, *339*, 44–45, doi:10.1126/science.1232662.

Lavvas, P. P., A. Coustenis, and I. M. Vardavas (2008), Coupling photochemistry with haze formation in Titan's atmosphere, Part II: Results and validation with Cassini/Huygens data, *Planet Space Sci.*, *56*(1), 67–99, doi:10.1016/j.pss.2007.05.027.

Lovelock, J. (1988), *The Ages of Gaia*, W. W. Norton, New York.

McKay, C. P., J. B. Pollack, and R. Courtin (1991), The Greenhouse and Antigreenhouse Effects of Titan, *Science*, *253*(5024), 1118–1121, doi:10.1126/science.11538492.

McKay, C. P., R. D. Lorenz, and J. I. Lunine (1999), Analytic Solutions for the Antigreenhouse Effect: Titan and the Early Earth, *Icarus*, *137*, 56–61, doi:10.1006/icar.1998.6039.

Mojzsis, S. J., G. Arrhenius, K. D. McKeegan, T. M. Harrison, A. P. Nutman, and C. R. L. Friend (1996), Evidence for life on Earth before 3,800 million years ago, *Nature*, *384*, 55–59, doi:10.1038/384055a0.

Moses, J. I., B. Bézard, E. Lellouch, G. R. Gladstone, and H. Feuchtgruber (2000), Photochemistry of Saturn's Atmosphere: I. Hydrocarbon Chemistry and Coparison with ISO Observations, *Icarus*, *143*, 244–298, doi:10.1006/icar.1999.6270.

Nutman, A. P., S. J. Mojzsis, and C. R. L. Friend (1997), Recognition of ≥3850 Ma water-lain sediments in West Greenland and their significance for the early Archaean Earth, *Geochim. Cosmochim. Acta*, *61*, 2475–2484, doi:10.1016/S0016-7037(97)00097-5.

Nutman, A. P., V. C. Bennett, and C. R. L. Friend (2012), Waves and weathering at 3.7 Ga: Geological evidence for an equitable terrestrial climate under the faint early Sun, *Aust. J. Earth Sci.*, *59*(2), 167–176, doi:10.1080/08120099.2012.618512.

Pavlov, A. A., J. F. Kasting, L. L. Brown, K. A. Rages, and R. Freedman (2000), Greenhouse warming by CH4 in the atmosphere of early Earth, *J. Geophys. Res.*, *105*(E5), 11981–11990, doi:10.1029/1999JE001134.

Pavlov, A. A., J. F. Kasting, J. L. Eigenbrode, and K. H. Freeman (2001a), Organic haze in Earth's early atmosphere: Source of low-13C Late Archean kerogens?, *Geology*, *29*(11), 1003–1006, doi:10.1130/0091-7613(2001)029<1003:OHIESE>2.0.CO;2.

Pavlov, A. A., L. L. Brown, and J. F. Kasting (2001b), UV Shielding of NH3 and O2 by organic hazes in the Archean atmosphere, *J. Geophys. Res.*, *106*(E10), 23267–23287, doi:10.1029/2000JE001448.

Sagan, C., and C. Chyba (1997), The Early Faint Sun Paradox: Organic Shielding of Ultraviolet-Labile Greenhouse Gases, *Science*, *276*, 1217–1221, doi:10.1126/science.276.5316.1217.

Sekine, Y., H. Imanaka, T. Matsui, B. N. Khare, E. L. O. Bakes, C. P. McKay, and S. Sugita (2008a), The role of organic haze in Titan's atmospheric chemistry I. Laboratory investigation of heterogeneous reaction of atomic hydrogen with Titan tholin, *Icarus*, *194*, 186–200, doi:10.1016/j.icarus.2007.08.031.

Sekine, Y., S. Lebonnois, H. Imanaka, T. Matsui, E. L. O. Bakes, C. P. McKay, B. N. Khare, and S. Sugita (2008b), The role of organic haze in Titan's atmospheric chemistry II. Effect of heterogeneous reaction to the hydrogen budget and chemical composition of the atmosphere, *Icarus*, *194*, 201–211, doi:10.1016/j.icarus.2007.08.030.

Trainer, M. G., A. A. Pavlov, H. L. DeWitt, J. L. Jimenez, C. P. McKay, O. B. Toon, and M. A. Tolbert (2006), Organic haze on Titan and the early Earth, *Proc. Natl. Acad. Sci. U.S.A.*, *103*(48), 18035–18042, doi:10.1073/pnas.0608561103.

Valley, J. W., W. H. Peck, E. M. King, and S. A. Wilde (2002), A cool early Earth, *Geology*, *30*, 351–354, doi:10.1130/0091-7613(2002)030<0351:ACEE>2.0.CO;2.

Wilde, S. A., J. W. Valley, W. H. Peck, and C. M. Graham (2001), Evidence from detrital zircons for the existence of continental crust and oceans on the Earth 2.6 billion years ago, *Nature*, *409*, 175–178, doi:10.1038/35051550.

Wolf, E. T., and O. B. Toon (2010), Fractal Organic Hazes Provided an Ultraviolet Shield for Early Earth, *Science*, *328*, 1266–1268, doi:10.1126/science.1183260.

Yung, Y. L., and W. B. DeMore (1999), *Photochemistry of Planetary Atmospheres*, Oxford University Press, New York.

Zahnle, K. J. (1986), Photochemistry of Methane and the Formation of Hydrocyanic Acid (HCN) in the Earth's Early Atmosphere, *J. Geophys. Res.*, *91*(D2), 2819–2834, doi:10.1029/JD091iD02p02819.

Table 3.1: Pressures and irradiation times for irradiation experiments

A. CH_4 irradiation experiments

CH_4 (Torr)	Irradiation Time (hr)
4.9	67
5.6	84
10.7	83
11.2	44
20.5	91
41.5	69
70.8	59
102.1	71
125.0	137
150.0	115
200.2	90

B. CH_4/CO_2 irradiation experiments

CH_4/CO_2	CH_4 (Torr)	CO_2 (Torr)	Total Pressure (Torr)	Irradiation Time (hr)
0.34	10.3	30.3	40.6	114
0.50	10.7	21.5	32.2	114
0.50	10.7	21.5	32.2	95
0.96	10.2	10.7	20.9	91
1.67	10.7	6.4	17.1	118
2.40	10.3	4.3	14.6	89
3.44	11.7	3.4	15.1	110
4.28	10.7	2.5	13.2	86

Table 3.2: HeNe light scattering measurements from particles produced during the irradiation of pure CH_4. A 16 mW, 632.8 nm laser was used for these experiments.

CH_4 pressure (Torr)	Peak intensity (counts/min)	Induction Time (hr)
35	800	20
50	1300	15
70	2800	15

Table 3.3: HeNe light scattering measurements from particles produced during the irradiation of mixtures of CH_4 and CO_2 ratios. An 8 mW, 613 nm laser was used for these experiments.

CH_4/CO_2	CH_4 pressure (Torr)	CO_2 pressure (Torr)	Induction Time (hr)
---	100	0	23
3	75	25	16
1	50	50	15
0.33	25	75	40
0.25	20	80	90

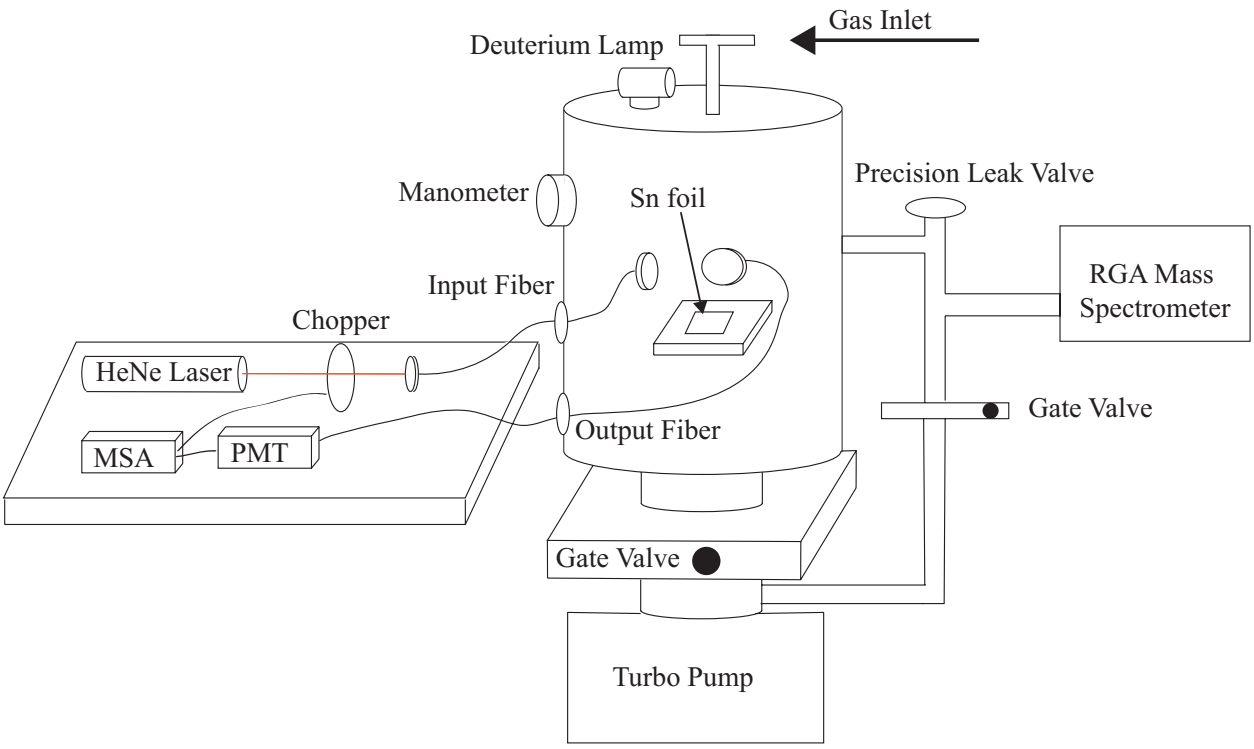

Figure 3.1: Schematic showing the photochemical reaction chamber, broadband UV light source, RGA mass spectrometer for detection of gas phase species, and laser light scattering set-up for detection of aerosol (Adapted from *Ádámkovics and Boering* [2003]).

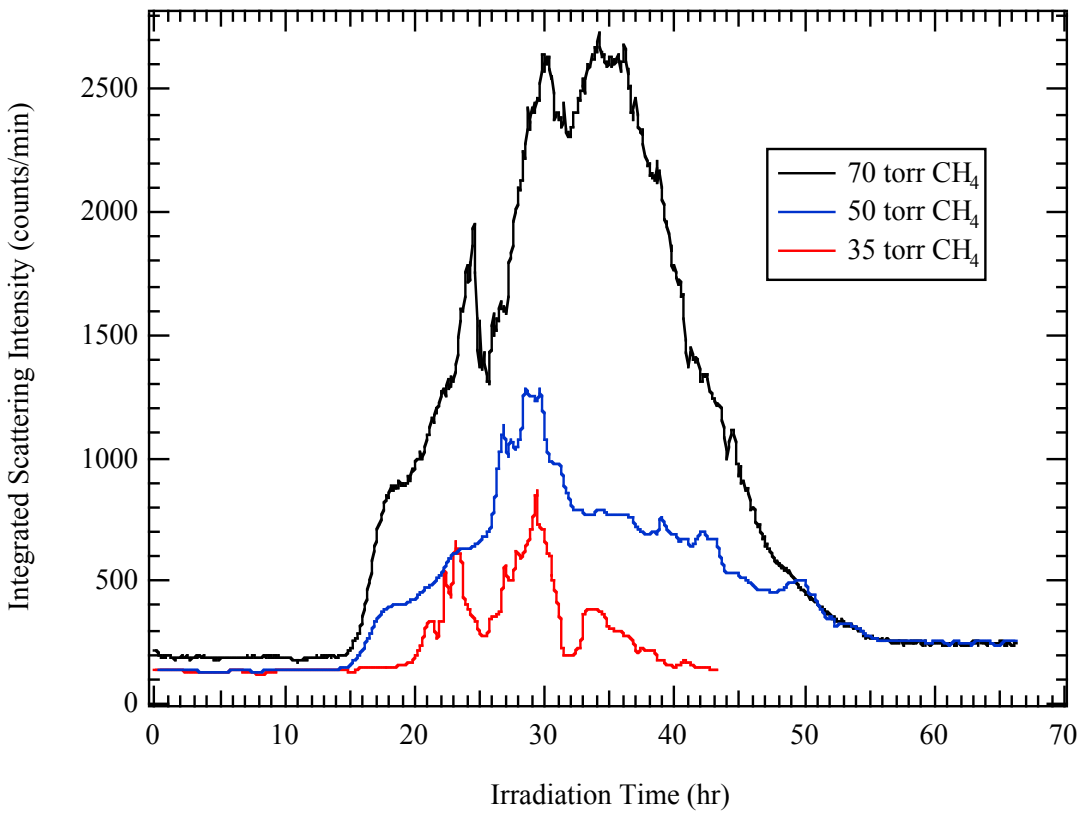

Figure 3.2: The amplitudes of the light scattering intensities and the integrated scattering signals over time are larger for larger initial CH_4 pressures, while the relative induction times (see text) are shorter. A 16 mW, 632.8 nm HeNe laser was used.

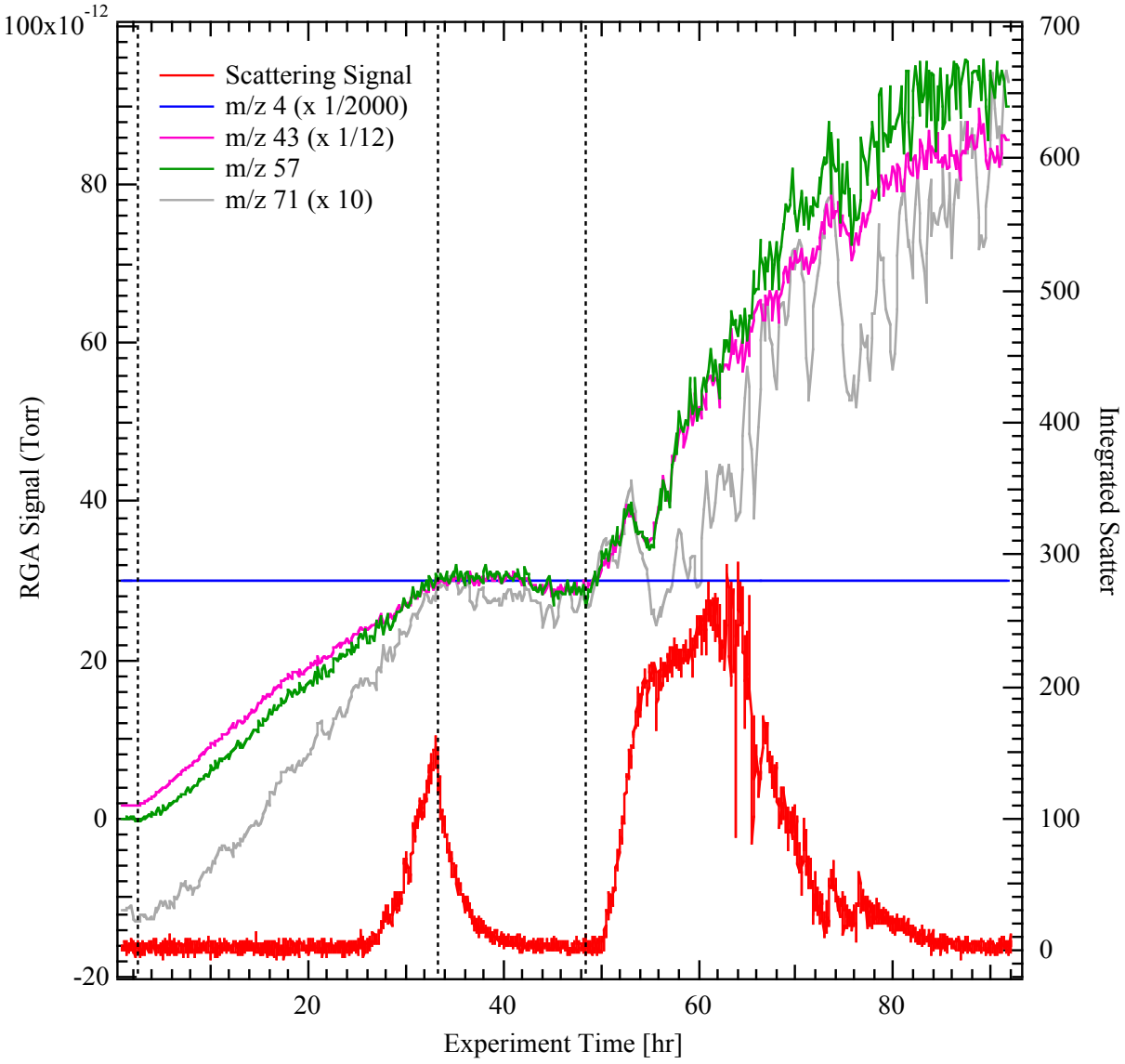

Figure 3.3: RGA mass spectrometer data at m/z values representative of several photochemically-generated hydrocarbons (normalized to m/z = 4 from a 1 mTorr spike of He), along with simultaneous *in situ* HeNe laser light scattering by aerosol particles in the chamber in an experiment in which 100 Torr of CH_4 was irradiated. The deuterium lamp was switched off at 30.65 hours and turned on again at 46 hours, as noted by the dashed vertical lines. Note that an 8 mW, 613 nm laser was used for this experiment so the relative induction time and scattering signal intensities cannot be directly compared with those in Figure 3.2. (Adapted from Figure 3.2 of *Ádámkovics* [2004].)

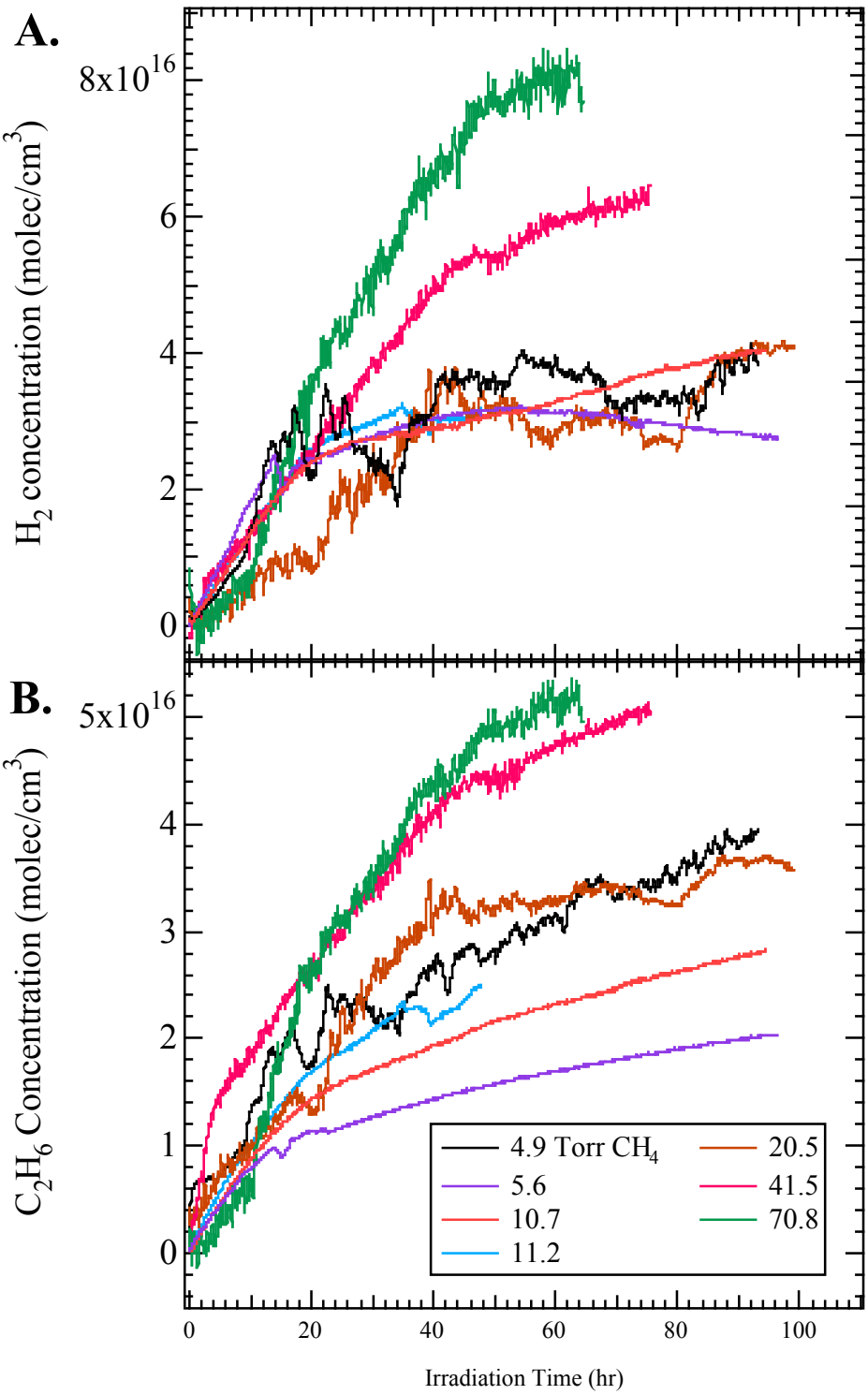

Figure 3.4: Time dependence of the net production of (A) H_2 and (B) C_2H_6 from a deconvolution of the RGA mass spectrometer data in experiments irradiating pure CH_4 at the pressures given in the legend. The data have been smoothed with 4th order Savitzky-Golay for this figure and offset by the initial concentration values.

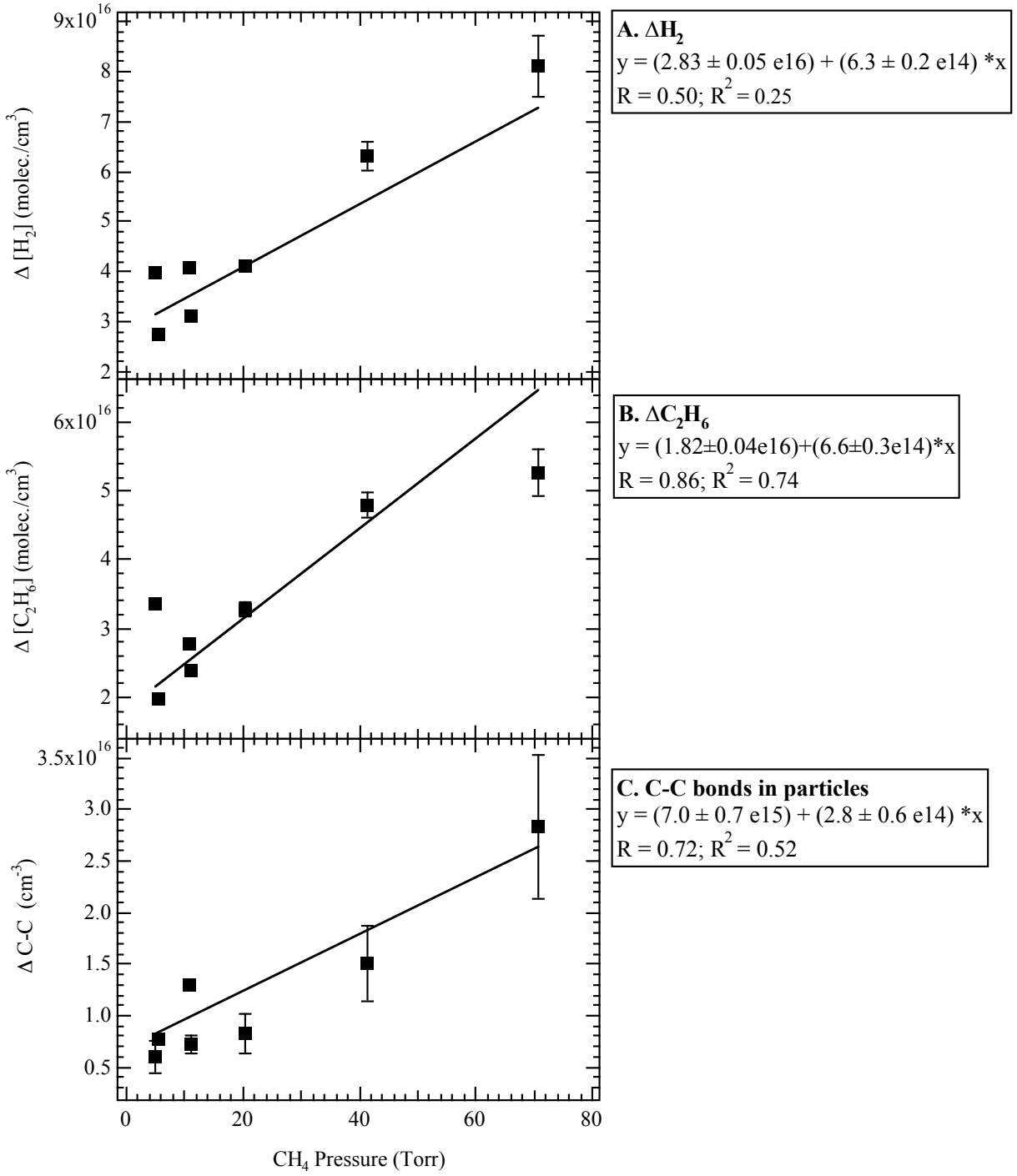

Figure 3.5: Net production for (A) H_2, (B) C_2H_6, and (C) number of carbon-carbon bonds in particles from the time-resolved mass spectrometry measurements as a function of the initial CH_4 pressure for the experiments shown in Figure 3.4. Error bars ($\pm 1\sigma$) are estimates of the error based on uncertainties in determining the initial and final concentrations for H_2 and C_2H_6.

Photolysis of CH_4

$CH_4 + h\upsilon$	$\rightarrow$	$^1CH_2 + H_2$	$q_1 = 0.41$
	$\rightarrow$	$CH_2 + 2H$	$q_2 = 0.51$
	$\rightarrow$	$CH + H + H_2$	$q_3 = 0.08$
	$\rightarrow$	$CH_3 + H$	$q_4 = 0.00$

Formation of Ethane (C_2H_6)

$2\ (CH_4 + h\upsilon$	$\rightarrow$	$^1CH_2 + H_2)$
$2\ (^1CH_2 + H_2$	$\rightarrow$	$CH_3 + H)$
$CH_3 + CH_3 + M$	$\rightarrow$	$C_2H_6 + M)$
net $2CH_4$	$\rightarrow$	$C_2H_6 + 2H$

Formation of Diacetylene from C_2H_2

$CH + C_2H_2$	$\rightarrow$	$C_3H_2 + H$
$C_3H_2 + C_2H_2$	$\rightarrow$	$C_4H_2 + CH_2$
$CH_2 + H$	$\rightarrow$	$CH + H_2$
net $2C_2H_2$	$\rightarrow$	$C_4H_2 + H_2$

The chain reaction to form polyacetylenes likewise results in a continued production of H atoms:

$C_{2n}H_2 + h\upsilon$	$\rightarrow$	$C_{2n}H + H$
$C_{2n}H + C_2H_2$	$\rightarrow$	$C_{2n+2}H_2 + H$
net $C_2H_2 + C_{2n}H_2$	$\rightarrow$	$C_{2n+2}H_2 + 2H$

Figure 3.6: Examples of reaction schemes that lead to the production of H_2 or 2H for every new carbon-carbon bond that is formed.

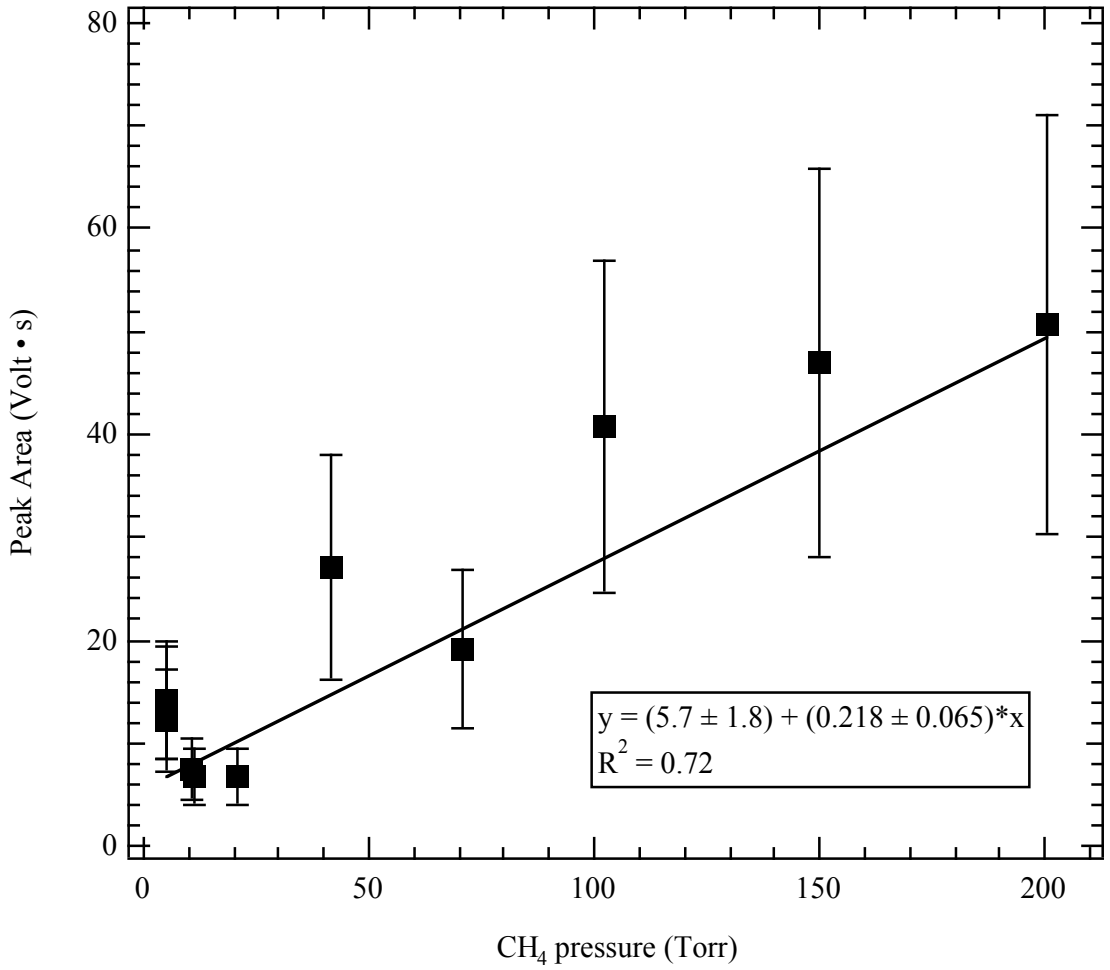

Figure 3.7: Measurements of the peak area from "offline" EA-IRMS analysis of particle samples collected over the course of a 50- to 100-hour irradiation experiment as a function of the initial CH_4 pressure in the reaction chamber. The peak area is proportional to the total carbon content of the samples, which increases as the initial CH_4 pressure in the reaction chamber. Error bars are ±40%, the expected 1σ uncertainty in the EA-IRMS peak areas.

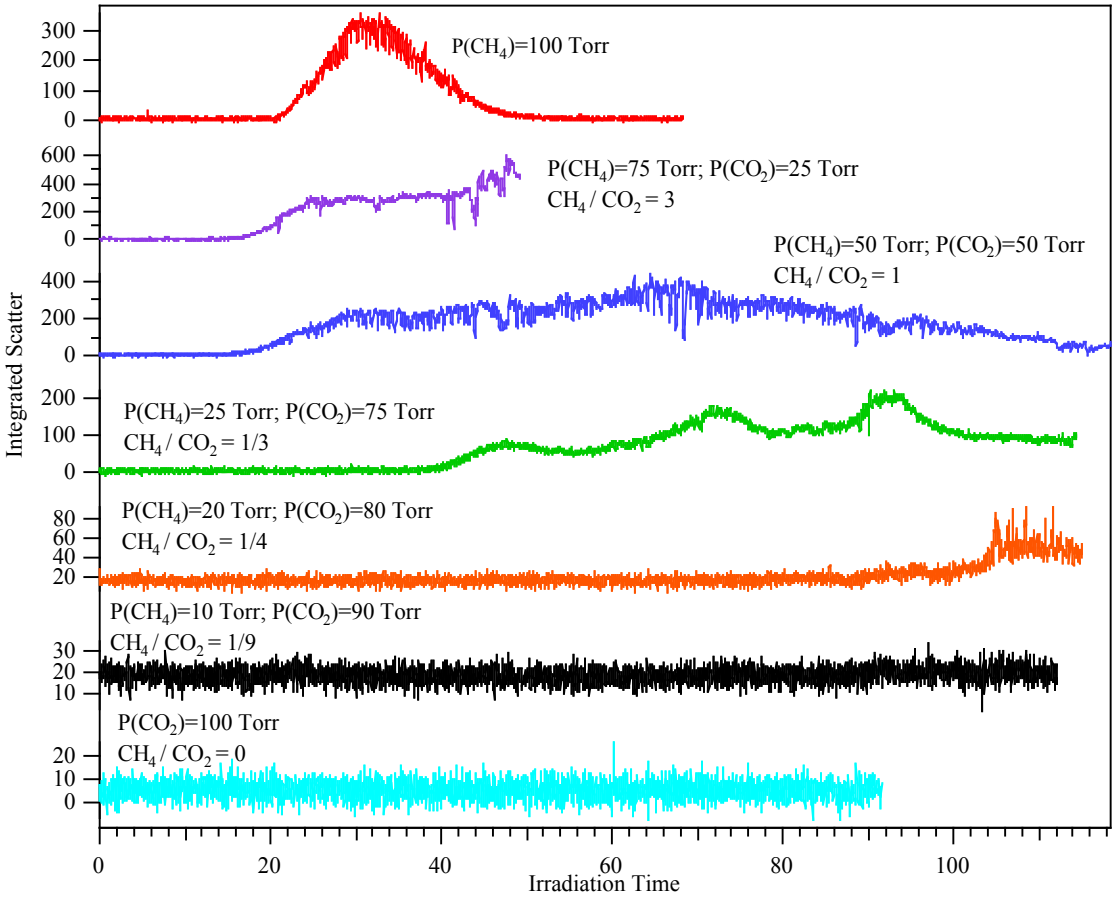

Figure 3.8: HeNe light scattering by particles for the experiments in which mixtures of CH_4 and CO_2 were irradiated, with partial pressures and the CH_4/CO_2 mixing ratios given as text in the figure. As in Figure 3.3, an 8 mW, 613 nm laser was used (see Methods). (Adapted from Figure 3.1 of Adamkovics [2004].)

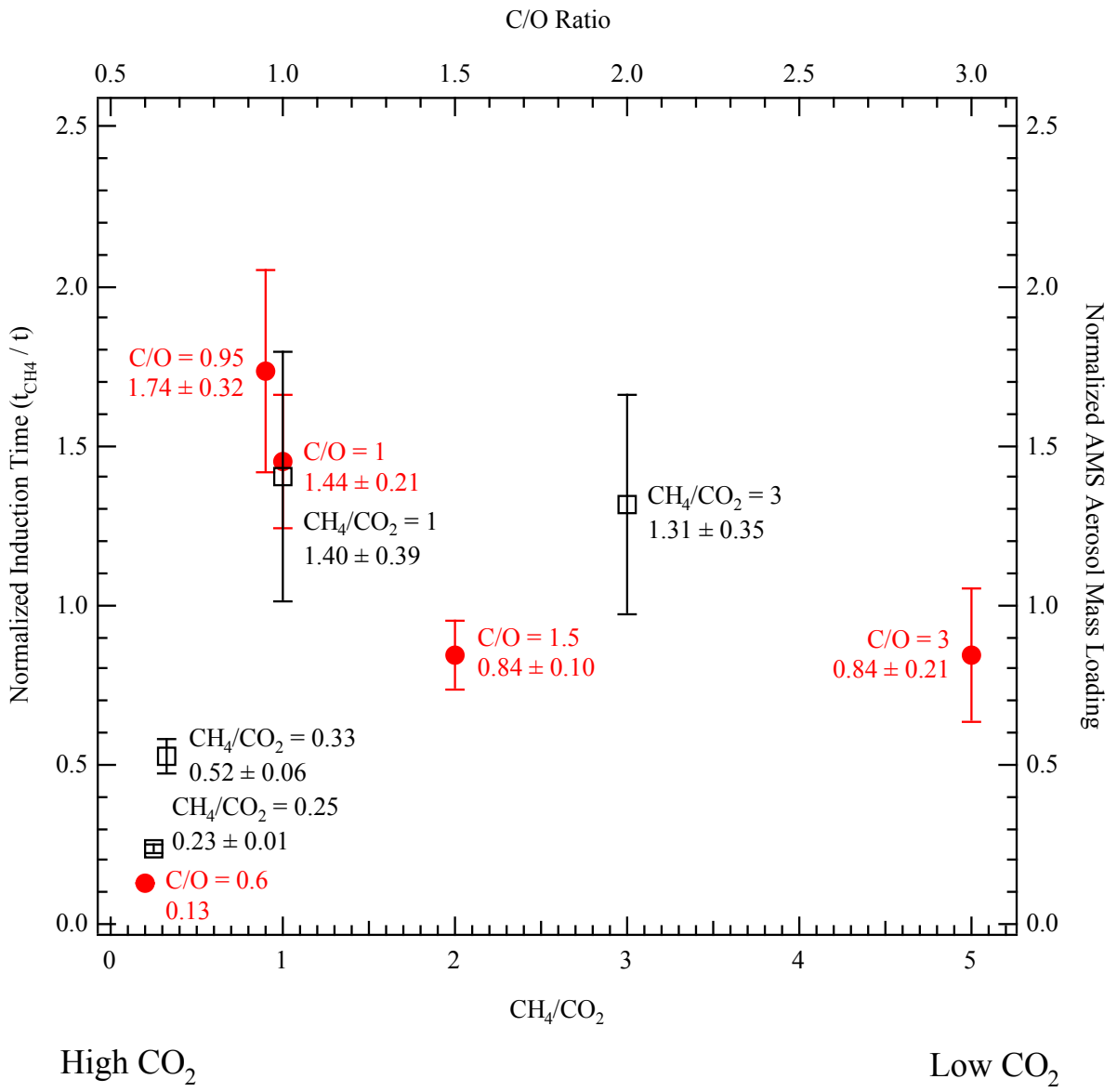

Figure 3.9: Experimental data for the normalized induction time for the HeNe light scattering measurements shown in Figure 3.8 (Open Black Squares) and the normalized AMS aerosol mass loading from Trainer *et al.* [2006] (Closed Red Circles) versus the CH_4/CO_2 ratio of the irradiated gas mixture. Each dataset is normalized with respect to the same experimental results for irradiation of pure CH_4, and error bars represent 1σ uncertainties.

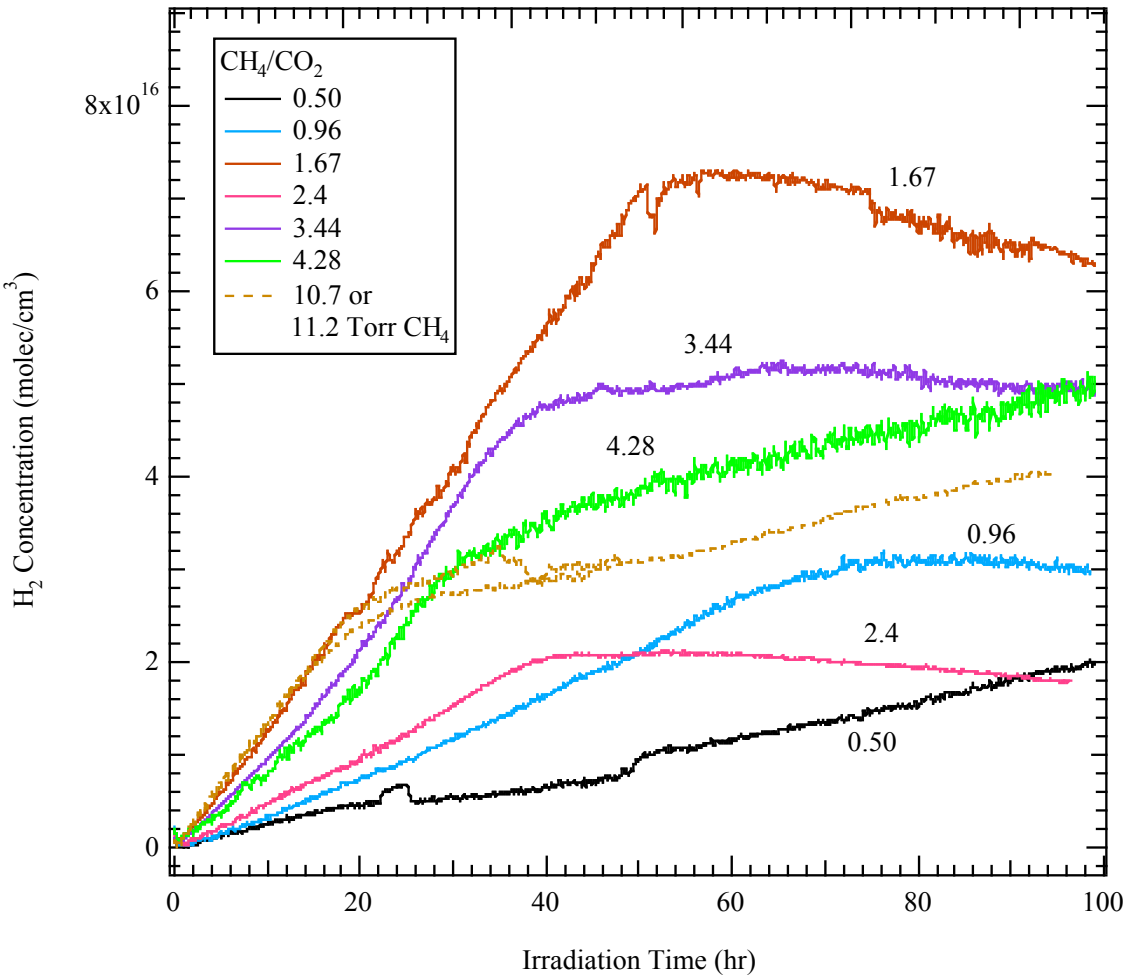

Figure 3.10: Time dependence of the net production of H_2 from a deconvolution of the RGA mass spectrometer data in experiments irradiating mixtures of 10 Torr CH_4 and addition of CO_2 to yield the CH_4/CO_2 ratios given in the legend. Also shown (dashed lines) are the correponding pure CH_4 irradiation results for comparison. The data have been smoothed with 4th order Savitzy-Golay for this figure and offset by the initial concentration values.

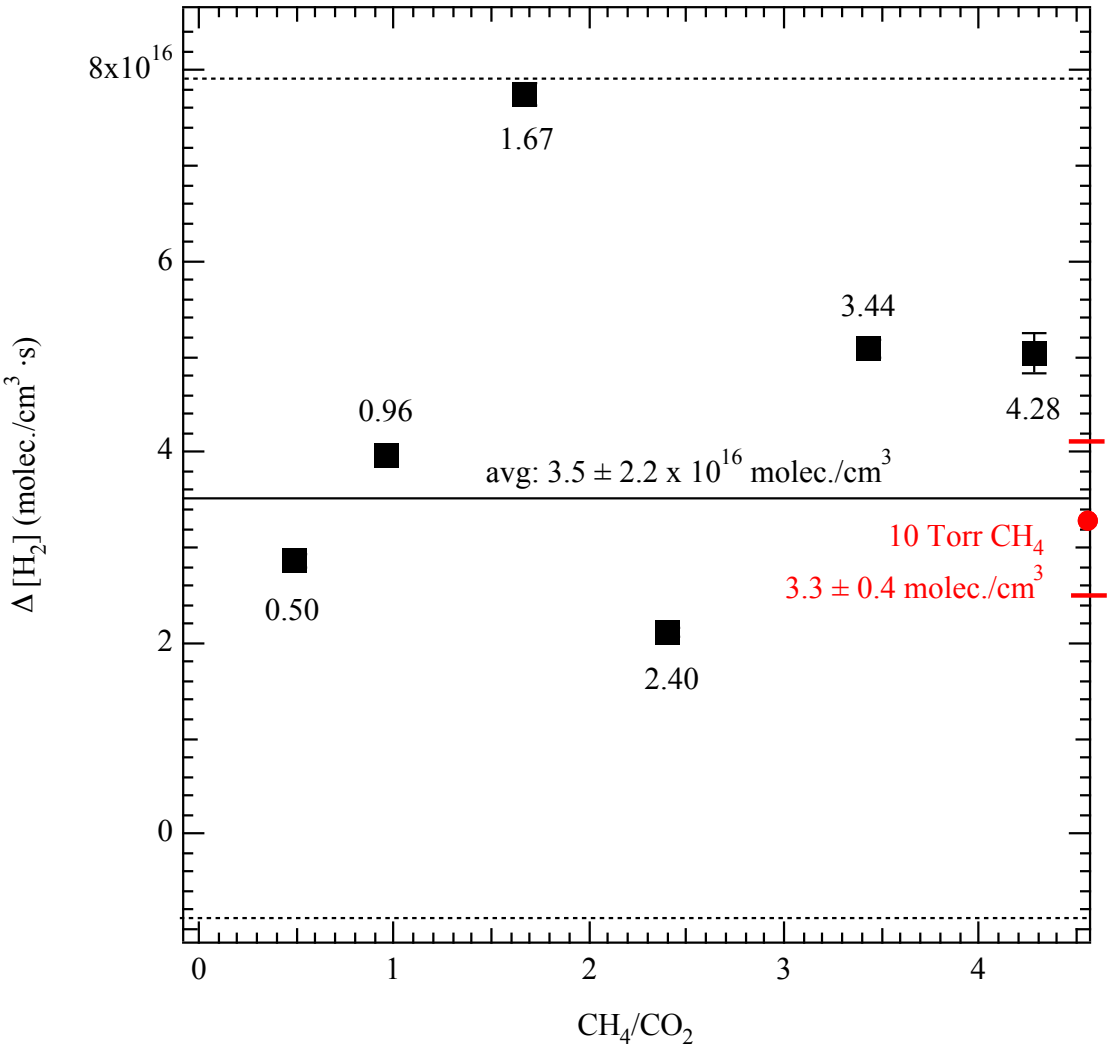

Figure 3.11: Net hydrogen production ($\Delta[H_2]$) as a function of the CH_4/CO_2 ratio at a CH_4 partial pressure of 10 Torr for the experiments shown in Figure 3.10. The horizontal lines represent the average of all the data points (solid) and the average ± 2σ (dashed).

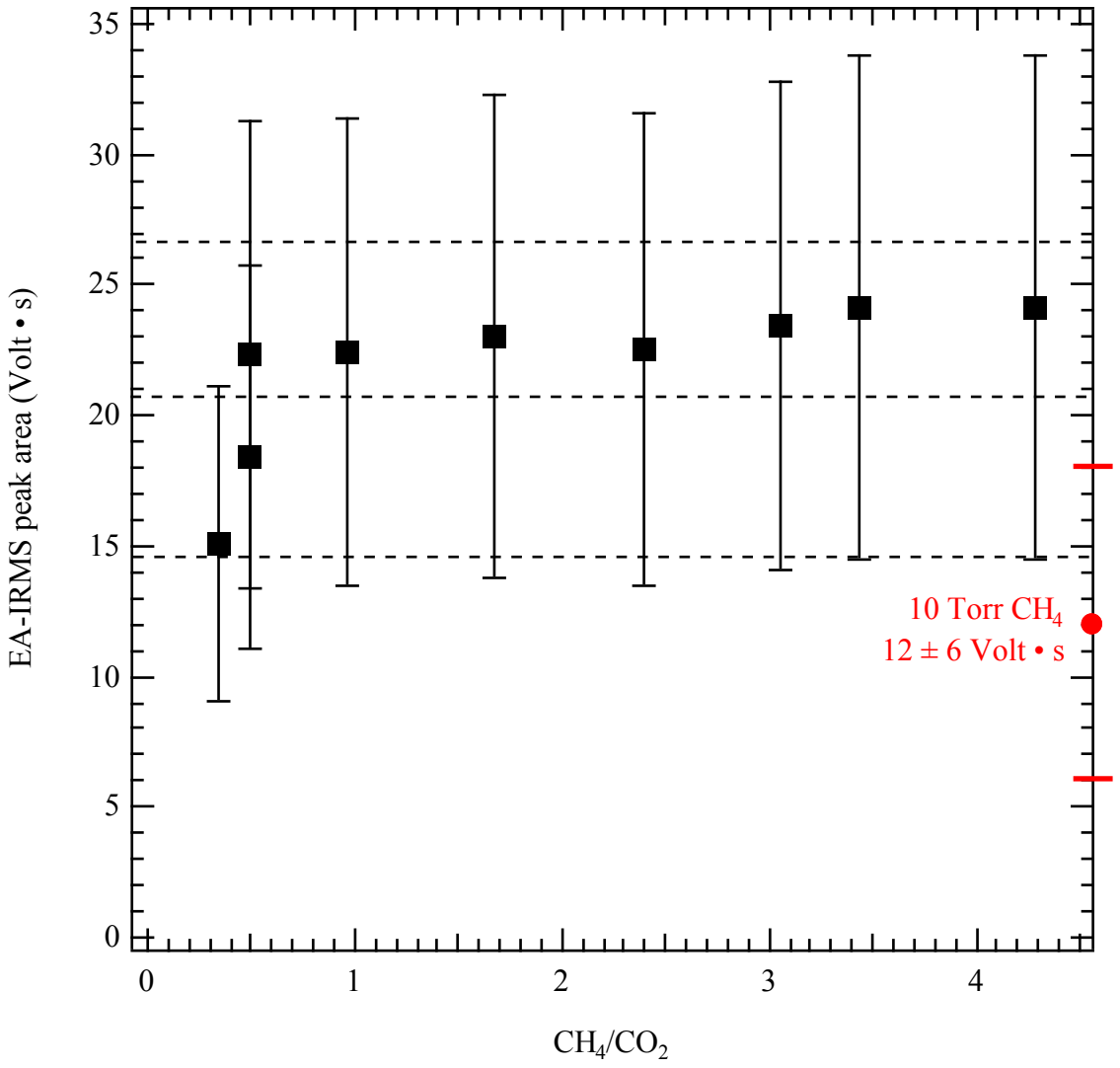

Figure 3.12: Peak areas for the EA-IRMS measurements on "offline" samples of particles collected over the course of an experimental run irradiating CH_4 at a partial pressure of 10 Torr with CO_2 to satisfy the CH_4/CO_2 ratio on the x-axis. The horizontal lines are the average of all the CH_4/CO_2 data points and the average ± 2σ. The red symbol and error bars show the average and the average ± 2σ, respectively, of the peak areas for the pure CH_4 experiments from 5 to 20 Torr shown in Figure 3.7.

Chapter 4

The carbon-13 isotopic composition of hydrocarbon aerosols formed from photolysis of CH_4 in the laboratory and applications to early Earth and Mars

4.1 Introduction

The isotopic compositions of atmospheric species as well as compounds preserved in rock and meteorites can provide insights into a planet's history of atmospheric, physical, and even biological processes. For example, the ratio of carbon-13 (^{13}C) to carbon-12 (^{12}C) has often been used as a biomarker since biological processes frequently discriminate against the heavier isotope, producing carbon compounds that are more depleted in ^{13}C relative to ^{12}C compared to the starting material [*Hayes*, 1983, 1994]. One interesting and important example in the Earth's distant past is that the carbon isotopic composition of kerogens (organic material) found in rocks dated between 2.5 and 3.0 billion years ago dropped to as low as −60‰ [*Schidlowski et al.*, 1983; *Rye and Holland*, 2000], where the carbon-13 isotopic composition, expressed in delta notation, or $\delta^{13}C$, is the part per thousand difference (‰) in the $^{13}C/^{12}C$ ratio in a sample versus the $^{13}C/^{12}C$ ratio in the Pee Dee Belemnite international standard:

$$\delta^{13}C = \left[\frac{\left(\frac{^{13}C}{^{12}C}\right)_{sample} - \left(\frac{^{13}C}{^{12}C}\right)_{standard}}{\left(\frac{^{13}C}{^{12}C}\right)_{standard}} \right] \times 1000 \qquad (4.1)$$

The minimum values observed during this time period near −60‰ are far lower than the minimum $\delta^{13}C$ values for similar kerogen samples that are both older (dating back to 3.5 billion years ago) and younger (dating 2.5 billion to 1.5 billion years ago), for which $\delta^{13}C$ values vary between −20 and −40‰. The most widely accepted explanation for the isotopically light carbon measured 2.5-3.0 billion years ago is that it represents the emergence of methanotrophic bacteria: the organic carbon incorporated into the rock record is even lighter than that produced by methanogenic bacteria due to the additional isotope fractionation produced by the methanotrophic bacteria which consume the methane produced by methanogens, thus discriminating against ^{13}C even further. Eventually, the rise of atmospheric O_2 levels were large enough by ~2.5 billion years ago that methanogenesis finally dominated over methanotrophy once again [*Hayes*, 1983, 1994].

An alternative hypothesis to the isotopically light organic rock record from 2.5-3.0 billion years ago, proposed by *Pavlov et al.* [2001], is that isotopically light carbon might have come from the settling or raining out of organic haze particles that formed abiotically in early Earth's atmosphere by the photochemical polymerization of atmospheric CH_4. This haze would have then dissipated after atmospheric O_2 levels rose significantly 2.5 billion years ago and, in response, both CH_4 emissions and atmospheric concentrations decreased (due to the new predominance of sulfate-reducing bacteria over methanotrophic bacteria as well as oxidation of atmospheric CH_4) so that haze formation was no longer favorable. These haze particles would be analogous to the ones present in Titan's atmosphere, formed at least in some regions of Titan's atmosphere from the UV irradiation of CH_4 and comprised of polycyclic aromatic hydrocarbons and polyacetylenes [*Hanel et al.*, 1981; *Kunde et al.*, 1981; *Maguire et al.*, 1981; *Khare et al.*,

1984; *Ehrenfreund et al.*, 1994; *Imanaka et al.*, 2004; *Israël et al.*, 2005; *Lavvas et al.*, 2008; *Cable et al.*, 2012]. If the aerosols that may have formed in early Earth's CO_2-rich atmosphere from the UV photolysis of CH_4 were significantly more depleted in ^{13}C relative to ^{12}C than the CH_4 from which they formed, then atmospheric photochemistry might therefore have been an source of isotopically light carbon that is now being mistaken as biologic in origin. The idea that an isotope signature from the atmosphere can indeed be preserved in the rock record is supported by the identification of oxygen and sulfur isotope signatures in the rock and meteorite records of Earth and Mars [*Farquhar et al.*, 1998, 2000; *Farquhar and Thiemens*, 2000] whose only origin is likely to be atmospheric photochemistry. To date, however, the hypothesis of *Pavlov et al.* [2001] that the formation of organic haze particles produced abiotically by the UV photolysis of CH_4 in Earth's atmosphere could have produced haze particles that are depleted enough in ^{13}C to account for the isotopically light kerogen in the rock record 3.0 to 2.5 billion years ago has not been tested systematically in the laboratory.

In this study, organic aerosol particles were formed by UV irradiation of CH_4 in the presence or absence of CO_2 and their bulk carbon isotopic composition was measured by Elemental Analyzer – Isotope Ratio Mass Spectrometery (EA-IRMS). These measurements were combined with Continuous-flow, Preconcentration, Gas Chromatography Isotope Ratio Mass Spectrometry measurements of the initial reactant CH_4 in the photolysis experiments to determine whether photochemical haze production can result in particles that are depleted in ^{13}C relative to the reactant CH_4. These new measurements provide constraints on the magnitudes of possible kinetic isotope effects in the chemical pathways from the initial CH_4 through to the formation of organic aerosols and, in turn, whether photochemically-generated organic hazes could indeed be an abiotic source of isotopically light organic matter that could be misinterpreted as a biomarker in any number of environments, including in the rock and meteorite records of early Earth and Mars.

4.2 Methods

The irradiation chamber and photolysis experiments are described in previous chapters. Briefly, the particles were formed in a 13 L cylindrical stainless steel reaction chamber (height of 36 cm and a diameter of 21 cm) using a deuterium lamp, installed in the top flange. Two types of D_2 lamps were used. Both lamps had a MgF_2 window that allowed transmittance of wavelengths longer than 110 nm into the chamber. The "high-brightness" D_2 lamp (Hamamatsu L9841) was measured to have a total lamp intensity from 120 to 300 nm of $5.4 \pm 0.4 \times 10^{15}$ photons s^{-1} with maximum output near 160 nm, determined in our experimental setup by using N_2O actinometry [*Greiner*, 1967]. The "low-brightness" D_2 lamp (Hamamatsu L7292), had a measured photon flux of $8.8 \pm 0.8 \times 10^{15}$ photons $^{-1}$ as reported by *Ádámkovics and Boering* [2003], approximately the same magnitude of the high-brightness D_2 lamp. The "low brightness" designation comes from the fact that its aperture of 1.0 mm is twice the size of the aperture for the "high-brightness" lamp and thus the photons are spread across a wider area. To collect aerosol particles produced during the irradiation experiments for offline EA-IRMS analysis, a square piece of tin (Sn) foil (30 mm x 30 mm) was placed on a 6 cm x 6 cm stainless steel platform within the chamber, approximately 16 cm below the window of the D_2 lamp. The chamber was then evacuated and baked out for 12 hours after which a background pressure of $\sim 10^{-8}$ Torr was attained. At the start of an irradiation experiment, the reaction chamber was isolated from the turbomolecular pump and CH_4 and/or CO_2 gases (CH_4, Scott Gas, 99.99%; CO_2, Scott Gas, 99.997%) were introduced through a valved inlet. The gas mixtures were then irradiated for 44 to 137 hours (90 hour

average). At the end of each experiment, the formation of particles was confirmed by the presence of a visible brown residue on the window of the D_2 lamp, which was subsequently cleaned with acetone and optical grade cloths (Fisher Scientific 06-665-29). The tin foil was collected from the chamber with a clean pair of tweezers and then wrapped in another piece of foil. The particle sample was kept in a vacuum desiccators until EA-IRMS analysis. Before the next experiment, another piece of foil was placed in the chamber and the chamber was evacuated and baked again.

4.2.1 EA-IRMS measurements of particulates

The carbon-13 isotopic composition of the collected aerosol particles formed by the irradiation of the CH_4 or CH_4/CO_2 gas mixtures was measured using a Finnigan Delta Plus XL isotope ratio mass spectrometer coupled to a Carlo Erba CHN 1108 Elemental Analyzer at the NASA Ames Astrobiology Institute in the laboratory of David Des Marais. Samples were analyzed between January 2010 and September 2012, with a desiccator storage time between sample collection during irradiation and analysis at NASA Ames of 5 weeks to 6 months. At NASA Ames, the particle samples were prepared by placing them in a tin foil cup with vanadium oxide (V_2O_5), used to promote clean, complete combustion. Within the EA, the particle samples underwent flash combustion between 1000 and 1050°C so that 100% of the carbon in various chemical forms in the sample was converted into CO_2. The resulting CO_2 sample was purified in a flow of helium, first through a series of oxidation and reduction steps and through a gas chromatography column before entering the IRMS for the bulk $\delta^{13}C$ measurement [*Matthews and Hayes*, 1978; *Brenna et al.*, 1997].

On a given analysis date, either one or two carbon-13 isotope standards were run along with the samples: sucrose ANU (−10.45‰ vs PDB) and/or NBS-22 (−30.03‰ vs PDB). Standards were selected that were expected to be relatively close in $\delta^{13}C$ values to those of the samples in order to avoid non-linearity effects on measured isotopic compositions. In addition, to correct for non-linearity effects due to sample size (i.e., total carbon content), the standards were run with varying amounts of carbon to try to bracket the sample sizes. However, it was often not known ahead of time how large the samples would be, as the laboratory was not set up to weigh or measure samples as small as those from the irradiation chamber. Therefore, for a significant fraction of the samples, the sample sizes are much smaller than the standards. This means that the 1σ $\delta^{13}C$ errors reported here, which range from ±0.06‰ to ±0.34‰, which are based on replicate runs for the standards, are probably an underestimate of the true uncertainty given the possible non-linearity effects and the corresponding systematic error for small sample sizes. In addition to $\delta^{13}C$ values for each sample, the EA-IRMS peak areas – i.e., the integrated IRMS voltages for m/z 44 as measured by a Faraday cup detector – are used as a measure of the relative amount of particulate carbon produced in the irradiation experiments under different conditions. The uncertainties in the relative carbon amounts from the peak areas are as large as 40% due to changes in, e.g., IRMS source parameters, both from run to run and over time. The large uncertainty is not particularly surprising since the EA-IRMS was not designed to measure the amount of carbon and the peak area is more of a housekeeping measurement to check, for example, the appropriateness of the relative standard and sample sizes and instrument performance in general, but is useful here nevertheless when comparing different CH_4 and CH_4/CO_2 runs and how serious non-linearity effects might be a problem for our small samples. Uncertainties of ±40% (±1σ) are therefore given in tables, figures, and the results and discussion below. Finally, we note that, due to the destructive analysis method, each particle sample from

an individual experiment could be combusted and analyzed only once. To check for overall repeatability (from gas mixture introduction into the chamber all the way through the EA-IRMS analysis of the particulate samples), some experimental conditions were performed in separate experimental runs more than once.

4.2.2 $\delta^{13}C$ measurements of reactant CH_4

Several aliquots of CH_4 taken directly from the gas cylinder as well as after introduction into the reaction chamber were measured for $\delta^{13}C$ using Continuous-flow, Preconcentration Gas Chromatography Isotope Ratio Mass Spectrometry using a custom-built gas processing system and a Thermo Scientific Delta V Advantage IRMS in the laboratory of Andrew Rice at Portland State University. Two aliquots were taken directly from the cylinder of CH_4 (Scott Gas, 99.99%) used in the UV irradiation experiments. To check for any possible isotope fractionation associated with filling the reaction chamber, a third aliquot came from the reaction chamber after filling it to 10 Torr CH_4 and a fourth and a fifth aliquot came from the reaction chamber after filling it to 200 Torr CH_4 in two separate fillings. All aliquots were acquired by attaching an evacuated 500 mL stainless steel flask (Swagelok 304L-HDF4-500 with needle valve SS-16DKM4-F4-1 and rupture disc SS-RDK-16-2850) to the gas cylinder or reaction chamber and opening a valve. The first two samples from the cylinder were allowed to equilibrate for 2 minutes and the samples from the chamber equilibrated for 3 hours before opening and then shutting the valve to the sample cylinder and then detaching it from the chamber. The IRMS instrumentation is described in detail in *Rice et al.* [2001] and *Tyler et al.* [2007]. As reported in *Rice et al.* [2001], the precision of replicate $\delta^{13}C$-CH_4 measurements can reach as low as ±0.5‰. However, since the apparatus at the time of our measurements was set-up for volatile organic compounds instead of CH_4, the precision for our measurements is lower, up to ±1.1‰. At least two replicate $\delta^{13}C$ measurements of the CH_4 samples were performed on different days for each sample. NBS-19 (1.95‰ VPDB) and IAEA-CO-9 (–47.12‰ VPDB) were both used as standards to bracket the $\delta^{13}C$ measurements for the samples of reactant CH_4 gas.

4.3 Results

Measurements of $\delta^{13}C$ for the particle samples from all the irradiation experiments and for the various reactant CH_4 aliquots described above are listed in Table 4.1. In Figure 4.1, the $\delta^{13}C$ values for the particles formed from the irradiation of CH_4 alone are plotted versus the pressure of CH_4 that was irradiated in each experiment. The average $\delta^{13}C$ value for the samples from the irradiation of more than 40 Torr CH_4 was -23.9 ± 1.6‰ (2σ), which is illustrated in Figure 4.1 with solid and dashed horizontal lines. The $\delta^{13}C$ values for CH_4 pressures less than 40 Torr show greater variability than the particles formed from higher CH_4 pressures and are outside the 2σ confidence interval for the average $\delta^{13}C$ values for particles formed from CH_4 pressures greater than 40 Torr. At lower initial CH_4 pressures, generally smaller amounts of aerosol are formed, as explored and discussed in Chapter 3, based on measurements of the EA-IRMS peak areas. To follow up in this chapter, the EA-IRMS peak areas are shown along with the $\delta^{13}C$ measurements versus initial CH_4 pressure in Figure 4.2. The greater variability in $\delta^{13}C$ values for experiments in which CH_4 is < 40 Torr may thus be at least in part related to the smaller aerosol sample sizes collected during the irradiation of the smaller absolute pressures of CH_4. Additional discussion appears in Section 4 below and supports the idea that the $\delta^{13}C$ measurements for initial CH_4 pressures < 40 Torr are likely to have one or more systematic errors and should be

discounted relative to the rest of the dataset. For comparison, $\delta^{13}C$ of the reactant CH_4 before irradiation is −18.4 ± 0.8‰ (2σ), shown as the solid green lines in Figure 4.1. Thus, under the experimental conditions of these runs and using the average isotopic composition of the particles for CH_4 pressures >40 Torr of −23.9 ± 1.6‰ (2σ; N=10), carbon isotope effects in the photolysis and reaction pathways from CH_4 to aerosol formation result in an isotope fractionation of −5.5 ± 1.8‰ (2σ; N=10), or about −6 ± 2‰ (2σ; N=10).

To measure whether the presence of CO_2 had any effect on $\delta^{13}C$ of the particulate matter formed from CH_4 photolysis and subsequent chemistry to form aerosols, varying amounts of CO_2 were added to either 10 Torr or 200 Torr CH_4 in the reaction chamber. In Figure 4.3, the $\delta^{13}C$ measurements of the particles from these experiments are plotted versus the CH_4/CO_2 ratio. For the 10 Torr data, $\delta^{13}C$ of the particles formed do not vary significantly as the CH_4/CO_2 ratio is changed. The $\delta^{13}C$ values for the datum at a CH_4/CO_2 ratio of 0.34 and for one of the two datapoints at a CH_4/CO_2 ratio of 0.50 are slightly lower than the rest; these two datapoints have the smallest EA-IRMS peak areas and are both ~3 times smaller than the smallest standard size run in their batch of samples (not shown), while the peak areas of the other samples fall closer to the standard peak areas; thus these two points may be biased low (see discussion below). They are still within a reasonable 2σ variation of all the 10 Torr CH_4 data with added CO_2, however, so we still include them in the overall average, yielding an average value of −22.8 ± 1.6‰ (2σ; N=9) for the 10 Torr CH_4 data irradiated in the presence of CO_2. This average and the average of the non-biased CH_4-only dataset −23.9 ± 1.6‰ (2σ; N=10) are within 1σ of each other, so there appears to be no significant difference in the $\delta^{13}C$ of aerosol formed when CO_2 is added to 10 Torr of CH_4 in the reaction chamber. Thus, given the $\delta^{13}C$ value for the reactant CH_4 before irradiation of −18.4 ± 0.8‰ (2σ) and under the experimental conditions of these runs, carbon isotope effects in the photolysis and reaction pathways from CH_4 to aerosols result in an isotope fractionation of −4.4 ± 1.8‰ (2σ; N=9), or about −4 ± 2‰ (2σ; N=9).

For the three 200 Torr datapoints at CH_4/CO_2 mixing ratios of 0.8 (N=1) and 1.0 (N=2), also shown in Figure 4.3, the average of the $\delta^{13}C$ values for the 3 particulate samples is −26.8 ± 1.8‰ (2σ); there are not enough data to discern whether $\delta^{13}C$ of the particles might be changing with the CH_4/CO_2 ratio or not. If we compare the average of these 3 datapoints with the average of the two 200 Torr CH_4-only points, the difference (i.e., added CO_2 − no CO_2) is −2.2 ± 3.0‰ (2σ), so no significant difference by adding CO_2 at the CH_4/CO_2 ratios measured of 0.8 and 1.0. Comparing these 3 datapoints with the other $\delta^{13}C$ averages yields slightly significant differences at the 2σ level: a difference of −2.9 ± 2.4‰ (2σ) with respect to the average of the CH_4-only data and a difference of −4.0 ± 2.4‰ (2σ) with respect to the average of the CH_4/CO_2 mixtures at 10 Torr CH_4. Whether to speculate on an origin for these potential differences or to assume they fall within the noise of all the measurements is discussed in Section 4 below. Finally, given the $\delta^{13}C$ value for the reactant CH_4 before irradiation of −18.4 ± 0.8‰ (2σ) and under the experimental conditions of these runs, carbon isotope effects in the photolysis and reaction pathways from CH_4 to aerosols from these 3 datapoints for CO_2 added to 200 Torr CH_4 result in an isotope fractionation of 8.4 ± 2.0 ‰ (2σ), or about 8 ± 2‰ (2σ).

Overall, our findings are that carbon isotope fractionation in the photochemical pathways from CH_4 photolysis to aerosol formation result in aerosol that is depleted in ^{13}C relative to the starting CH_4. The results are −6 ± 2‰ (2σ; N=10) from the CH_4-only experiments, −4 ± 2‰ (2σ; N=9) from the experiments on CH_4/CO_2 mixtures at 10 Torr CH_4, −8 ± 2‰ (2σ; N=3) from

experiments on the CH_4/CO_2 mixtures at 200 Torr CH_4 experiments, and, if all these results are combined, $-6 \pm 3‰$ (2σ; N=22). These are shown schematically in Figure 4.4.

4.4 Discussion

4.4.1 Uncertainties

There are several types of uncertainties that led us to discount some of the datapoints that are not included in the final estimates of carbon isotope fractionation from CH_4 photolysis to aerosol formation. The large variation in $\delta^{13}C$ for particles formed from irradiating smaller CH_4 pressures, for example, may come from two sources. The first is systematic error arising from the smaller sample sizes (corresponding to the EA-IRMS peak areas shown in addition to the $\delta^{13}C$ values as a function of CH_4 pressure in Figure 4.2). When the sample peak areas are much smaller than the smallest standard size run, the $\delta^{13}C$ values appear to be biased low. The larger the difference between the lowest standard peak size and the particulate sample size, the larger the bias (not shown). This is also true but on a less serious scale for several "replicate" experimental datapoints in which the smaller sample size has a slightly lower $\delta^{13}C$ value than the larger sample, all else being approximately equal (see Table 4.1). If the sample size is about 2 times smaller than the smallest standard size or larger, the bias appears to be small, and we have kept those data in the averages. However, the size bias appears to be large for the two 10 Torr and one 20 Torr datapoints in the CH_4-only runs, for which the sample size is 6 to 8 times smaller than the minimum standard size run in that batch, and we have therefore removed these datapoints from the averages, as noted above in the results section.

The second set of possible systematic, non-random biases affecting the data arise from examination of the 5 Torr data, which are significantly enriched in ^{13}C relative to all the other particulate measurements. First, there may be systematic error that could result from a "reservoir effect;" smaller standard sizes were run on those days, so the 5 Torr aerosol samples do not suffer from small sample size alone (although they are indeed quite small). Rather, at 5 Torr, a significantly larger fraction of the CH_4 could have been photolyzed relative to the other experiments, and/or, perhaps more importantly, lost through the leak valve over the course of the 50+ hour experiment. The result that the $\delta^{13}C$ values for the particles are much higher and close to the starting CH_4 concentration may therefore be a "reservoir" effect – as CH_4 is photolyzed, mass balance requires that, as CH_4 is used up, the products should become more enriched in ^{13}C, more like the starting material [e.g., *DesMarais et al.*, 1981; *Chang et al.*, 1983]. On the other hand, the pressure drops during the experiment from 5 Torr to 1 Torr, and, if this were all from conversion of CH_4 into higher hydrocarbons, we would see much larger gas phase non-methane hydrocarbon and particulate concentrations. Alternatively, and working in the same direction, there may be isotopic fractionation of CH_4 through the leak valve to the RGA mass spectrometer over the 50+ hours of the experiment. The effect would therefore be largest for the smallest CH_4 pressures of the 5 Torr run here and appear to be absent in the 10 Torr data (which suffer instead from small sample size relative to the smallest size standard run that day). A third possibility that is consistent with the unusually ^{13}C-enriched 5 Torr data is that the enrichments at this pressure result from optical self-shielding for $^{12}CH_4$ but not for $^{13}CH_4$. For example, once the initial CH_4 pressure is as low as 5 Torr, the chamber is still very optically thick with respect to $^{12}CH_4$ but the optical depth finally drops to 1 or less for $^{13}CH_4$ for the entire depth of the reaction chamber, as shown in Figure 4.5. This means that, at 5 Torr, $^{13}CH_4$ is preferentially photolyzed over the entire depth of the chamber while $^{12}CH_4$ is still photolyzed mostly within 0.3 cm of the D2 lamp. This large difference, much smaller at higher CH_4 pressures for which $^{13}CH_4$ is also optically thick,

could lead to enrichments in ^{13}C in the hydrocarbons and particulates that are formed due to this preferential photolysis of $^{13}CH_4$ over $^{12}CH_4$. Any of these 3 possibilities are qualitatively consistent with the ^{13}C enrichments measured at a CH_4 pressure of 5 Torr. Thus, the 5 Torr data are not likely to represent the "instantaneous" isotope fractionation that we are interested in.

Given all the uncertainties discussed here due to possible systematic biases, including sample size versus standard size effects, reservoir effects, and optical self-shielding, perhaps the most weight should be given to the 200 Torr CH_4 irradiation data, especially the 200-250 Torr CO_2 data for the CH_4/CO_2 runs since isotope fractionation effects through the leak valve for the highest total pressure of 400-450 Torr total are likely to be the smallest. Relative to the starting CH_4, the 200 Torr data suggest an overall carbon isotopic fractionation of -8.4 ± 2.0‰ (2σ; N=3). (It is also relevant to note as an aside here that, although the carbon isotopic composition of the CO_2 used was −43.8‰ vs VPDB, and that more CO_2 will be photolyzed at the higher pressures of CO_2 used in the CH_4/CO_2 experiments, it is the oxygen atom photoproducts of CO_2 photolysis that are incorporated into the higher hydrocarbons and aerosols [e.g., *Trainer et al.*, 2006] not the carbon from the CO photoproduct; the latter would require Fischer-Tropsch-type reactions which happen only at very high temperatures in the presence of special catalysts [*Olah*, 2003] and these conditions are not relevant for the experiments here. Thus, the carbon isotopic composition of the added CO_2 should not lower the particulate $\delta^{13}C$ values, even at the high CO_2 pressures of the 200 Torr CH_4 experiments.)

In addition, there may be other uncertainties with respect to other experimental parameters that were unintentionally varied in this dataset, including whether or not there are differences between the ~50 and 135 hour irradiation times, how many previous operational hours the D_2 lamps had on them for any given experiment (the lamps degrade after 1000 hours of operation but the degradation in time may be a function of wavelength and the Lyman-α lines may degrade more quickly), and the fact that a low brightness D_2 lamp was used for the 200 Torr CH_4 experiments, while a high-brightness D_2 lamp was used for all but one of the others. We cannot account for all these possibilities in the current dataset since there are more variables that could potentially affect the results than had been anticipated. Thus, averaging all the data together to yield an overall carbon isotopic fractionation -6 ± 3‰ (2σ; N=22) is the most reasonable approach to interpreting this dataset. While additional experiments might help resolve whether there are additional drivers for some of the variability measured, such as lamp variations and irradiation times, a much more important variable is likely to be temperature, which was not explored in this study and which is discussed in the following section.

4.4.2 Comparison with expectations and previous experiments and observations

The carbon isotope fractionation in the integrated photochemical pathways from CH_4 to organic aerosols of −3 to −9‰ in this study is consistent both with expectations from carbon kinetic isotope effects and with generalized results from other previous experiments. Substitution of a heavy isotope of an element in a molecule often results in a change in rate coefficient for that molecule for photolysis or a chemical reaction. For a "normal" primary kinetic isotope effect (KIE), bonds containing the lighter isotopes break at a faster rate than bonds containing the heavier isotopes due to differences in zero-point energies of the reactant or the transition state to form products for the different isotopologues so that $k_{light}/k_{heavy} > 1$ [*Lowry and Richardson*, 1981; *Lin et al.*, 2005]. Thus, the immediate reaction products are depleted in the heavier isotope relative to the reactants and, in a sequence of reactions with normal kinetic isotope effects, the subsequent products of each reaction become successively more isotopically

depleted in the heavy isotope. Indeed, this sequence of kinetically-controlled reactions is how the origin of small molecular weight hydrocarbons in geothermal systems can be determined [*DesMarais et al.*, 1981]: if the carbon isotopic composition becomes progressively depleted in ^{13}C as the number of carbon atoms in the hydrocarbon increases, then the polymerization of CH_4 is the process responsible for formation of the hydrocarbons. If, however, the carbon isotopic composition becomes progressively enriched in ^{13}C as the number of carbon atoms in the hydrocarbon increases, then the degradation of larger hydrocarbons in the geothermal system is the origin since the "normal" KIEs are operating in the opposite direction – that is, the products of the kinetically-controlled reactions become progressively depleted in ^{13}C but the sequence with respect to carbon number is opposite depending on whether smaller hydrocarbons are forming larger ones or vice versa. To demonstrate this experimentally, *DesMarais et al.* [1981] produced hydrocarbons from pure CH_4 in a plasma discharge and showed that higher hydrocarbons are produced that are progressively depleted in ^{13}C as the carbon number increases, while the thermal decomposition of hexane at 500°C produces smaller hydrocarbons that are progressively depleted in ^{13}C as the carbon number decreases (i.e., the opposite to the spark discharge results). For the spark discharge in CH_4, ethane is depleted by ~12‰, while propane and butane are depleted by ~15‰ relative to the starting CH_4 (No data on any solid matter formed are given). Similarly, both saturated and unsaturated hydrocarbons and carboxylic acids in the Murchison meteorite are progressively depleted in ^{13}C as the carbon number grows, suggesting an origin that involves progressive build-up from smaller species [*Yuen et al.*, 1984] (and relevant here since carboxylic acids are expected to be among the compounds in the particulate matter formed in the mixed CH_4/CO_2 experiments we describe here, as demonstrated by Trainer *et al.* [2006] with Aerosol Mass Spectrometry measurements of particulate chemical composition produced from the UV irradiation of CH_4/CO_2 mixtures).

Particularly relevant for our study is the work of *Chang et al.* [1983] in which the gaseous and solid products formed by a spark discharge in a gaseous mixture of CH_4, H_2O and NH_3 were analyzed: the larger hydrocarbons produced in the discharge were progressively more depleted in ^{13}C as the carbon number increased, in line with expectations; the largest molecular weight compound measured was glycine, with a $\delta^{13}C$ value relative to the initial CH_4 of –18‰. The "acid insoluble" solid matter from the discharge experiment was only –6‰ depleted relative to the starting CH_4 isotopic composition. The fact that the solid matter is enriched in ^{13}C relative to the highest molecular weight gaseous products formed reflects a typical "inverse" KIE (for which $k_{light}/k_{heavy} < 1$); this is the type of KIE expected in condensation (i.e., vapor to liquid or solid) reactions, with the KIE favoring incorporation of the heavy isotope into the condensed phase rather than the gas phase, which favors the lighter isotope [*Jancso and Van Hook*, 1974]. Overall, the magnitude of the isotope fractionation going from CH_4 to particulate matter in this spark discharge study is the same as ours, at –6‰. Chang *et al.* [1983] also measured the isotopic composition of products from the UV photolysis at 254 nm of a mixture of CH_4, C_2H_6, NH_3, H_2S and H_2O; the benzene-insoluble solid product was 9‰ depleted in ^{13}C relative to the initial average $\delta^{13}C$ of the reactants. Thus, the $\delta^{13}C$ values of the solid product formed in both their spark discharge and 254 nm photolysis experiments were 6 to 9‰ depleted relative to the starting CH_4 isotopic composition, very similar to our results but in a complex mixture also containing significant amounts of water.

The similarities of the Chang *et al.* [1983] results with our results are important: they all suggest that it is indeed a combination of the normal primary KIEs in the formation of progressively larger hydrocarbons and inverse KIEs in the condensation of these species from

the gas phase to form the aerosol that controls the overall isotopic composition of the aerosol formed. The magnitude of the isotope fractionation does not appear to depend significantly on light source (narrowband 254 nm from a Hg lamp versus broadband UV extending to much lower UV wavelengths for a D_2 lamp) nor on the method of CH_4 decomposition to form radicals (e.g., photolysis versus plasma discharge). The magnitude of the isotope fractionation also does not appear to depend sensitively on temperature given the expected temperature differences in the plasma discharge versus the photolysis experiments, at least from room temperature to higher temperatures. Importantly, however, atmospheric temperatures in Earth's upper atmosphere where the photolysis of CH_4 on the Early Earth would have occurred can be much lower than room temperature, and it is possible that the KIEs could be much larger at lower temperatures, given the exponential dependence of rate coefficients on activation energy barriers and ambient temperatures through the Arrhenius equation [*Lowry and Richardson*, 1981] as well as various more sophisticated theoretical calculations of the temperature dependence of KIEs for small molecules [*Lin et al.*, 2005]. Thus, it will be important to devise similar experiments to those presented here at much colder temperatures relevant for the upper atmosphere.

4.4.3 Applications to early Earth, Mars, and Titan

The carbon isotope fractionation derived in this study from broadband UV photolysis of CH_4 and mixtures of CH_4 and CO_2 of -6 ± 3‰ does not appear to be large enough to explain the low $\delta^{13}C$ excursions in Earth's early rock record about 2.7 billion years ago as large as -30 to -40‰, although experiments at low temperatures relevant for the upper atmosphere are needed to more convincingly rule out the hypothesis of *Pavlov et al.* [2001] as a possibility. Likewise, it does not appear likely from these results that abiotic atmospheric photochemistry producing organic aerosols from CH_4 photolysis would have been capable of producing large $\delta^{13}C$ excursions in, e.g., martian meteorites from Mars [*McKay et al.*, 1996], although this apparent negative result also does not confirm that such signals are in fact biologic in origin. Again, lower temperature laboratory measurements are needed to confirm these implications for the isotopic composition of photochemical organic aerosol formation. Interestingly, the composite infrared spectrometer (CIRS) on the Cassini spacecraft orbiting Titan has measured the $^{12}C/^{13}C$ ratios of methane, acetylene, and ethane, finding that methane is more enriched in ^{13}C than acetylene, and that acetylene is more enriched than ethane [*Nixon et al.*, 2008], similar ratios to those from CIRS have been derived from high spectral resolution ground-based observations [*Jennings et al.*, 2009]. The difference between methane and ethane is -80‰, a much larger apparent fractionation than measured in room temperature photolysis and spark discharge experiments [*DesMarais et al.*, 1981; *Chang et al.*, 1983]. And this difference may be much *smaller* on Titan than it might have been on Earth or Mars since on Titan ethane may be depleted in ^{13}C relative to what KIEs in its photochemical production could produce due to inverse KIEs associated with ethane condensation in Titan's atmosphere where it is cold enough for ethane to condense [*Nixon et al.*, 2008], which not have occurred in the atmospheres of Earth and Mars. Thus the potential exists for the photochemical production of at least ethane from methane to have an extremely large carbon isotope fractionation of much larger than -80‰ given the very cold stratospheric temperatures there (e.g., 120K). Such large potential KIEs at the low temperatures in Titan's stratosphere further suggest the need to measure the isotopic composition of particulates formed from CH_4 photolysis at much lower temperatures than room temperature. Finally, we note that such results may also be relevant for the isotopic composition of aerosols thought to be deposited on Titan's surface, perhaps in large amounts [e.g., *Lorenz et al.*, 2006] and will be particularly

relevant, especially lower temperature results, if a future mission is designed to analyze these surface solids [*Atreya*, 2007].

4.5 Summary

In this experimental study, CH_4 and mixtures of CH_4 and CO_2 were irradiated with a deuterium lamp (120-300 nm) for ~50 to 135 hours in a static stainless steel reaction chamber, forming organic aerosol particles that were then collected and measured for the carbon-13 isotopic composition using EA-IRMS. Relative to the initial isotopic composition of the reactant CH_4, the particle samples were depleted in ^{13}C by 6 ± 3‰ and showed little sensitivity to the pressure of CH_4 irradiated from 10 Torr to 200 Torr and for CH_4/CO_2 ratios down to 0.34. There is some sensitivity observed, however, between −4‰ and −8‰ that may be real but still close to the statistical uncertainties within this particular set of experiments, and additional experiments are suggested to test the robustness of some of these smaller possible influences.

An overall isotope fractionation of −6 ± 3‰ is significantly smaller than the ^{13}C depletions observed in the geological record 2.8 billion years ago for which *Pavlov et al.* [2001] were seeking an abiotic explanation. Thus, unless the normal kinetic isotope effects in the formation of increasingly large and increasingly depleted carbon-13 hydrocarbons initiated by CH_4 photolysis are much larger at the much lower temperatures in the upper atmosphere than in our room temperature laboratory experiments, the abiotic production of photochemical haze in Earth's early atmosphere is not likely to account for observations of the isotopically light carbon in Earth's rock record from 2.5 to 3.0 billion years ago. Measurements of the isotopic composition of particles formed by the UV irradiation of CH_4 at lower temperatures are therefore critically needed to address this remaining uncertainty.

Chapter 4 References

Ádámkovics, M., and K. A. Boering (2003), Photochemical formation rates of organic aerosols through time-resolved in situ laboratory measurements, *J. Geophys. Res. E: Planets*, *108*(E8), 5092, doi:10.1029/2002JE002028.

Atreya, S. (2007), Titan's Organic Factory, *Science*, *316*, 843, doi:10.1126/science.1141869.

Brenna, J. T., T. N. Corsco, H. J. Tobias, and R. J. Caimi (1997), High-precision continuous-flow isotope ratio mass spectrometry, *Mass Spectrom. Rev.*, *16*(5), 227–258, doi:10.1002/(SICI)1098-2787(1997)16:5<227::AID-MAS1>3.0.CO;2-J.

Cable, M. L., S. M. Horst, R. Hodyss, P. M. Beauchamp, M. A. Smith, and P. A. Willis (2012), Titan Tholins: Simulating Titan Organic chemistry in the Cassini-Huygens Era, *Chem. Rev.*, *112*, 1882–1909, doi:dx.doi.org/10.1021/cr200221x.

Chang, S., D. DesMarais, R. Mack, S. L. Miller, and G. E. Strathearn (1983), Prebiotic Organic Syntheses and the Origin of Life, in *Earth's earliest biosphere*, pp. 53–92, Princeton University Press, Princeton, N.J.

DesMarais, D. J., J. H. Donchin, N. L. Nehring, and A. H. Truesdell (1981), Molecular carbon isotopic evidence for the origin of geothermal hydrocarbons, *Nature*, *292*, 826–828, doi:10.1038/292826a0.

Ehrenfreund, P., J. J. Boon, J. Commandeur, C. Sagan, W. R. Thompson, and B. N. Khare (1994), Analytical Pyrolysis Experiments of Titan Aerosol Analogues in Preparation for the Cassini Huygens Mission, *Adv. Space Res.*, *15*(3), 335–342, doi:10.1016/S0273-1177(99)80105-7.

Farquhar, J., and M. H. Thiemens (2000), Oxygen cycle of the Martian atmosphere-regolith system: 17O of secondary phases in Nakhla and Lafayette, *J. Geophys. Res.*, *105*(E5), 11991–7, doi:10.1029/1999JE001194.

Farquhar, J., M. H. Thiemens, and T. Jackson (1998), Atmosphere-surface interactions on Mars: Δ17O measurements of carbonate from ALH 84001, *Science*, *280*(5369), 1580–1582, doi:10.1126/science.280.5369.1580.

Farquhar, J., J. Savarino, T. L. Jackson, and M. H. Thiemens (2000), Evidence of atmospheric sulphur in the martian regolith from sulphur isotopes in meteorites, *Nature*, *404*, 50–52, doi:10.1038/35003517.

Greiner, N. R. (1967), Photochemistry of N2O Essential to a Simplified Vacuum-Ultraviolet Acintometer, *J. Chem. Phys.*, *47*(11), 4373–4377, doi:10.1063/1.1701640.

Hanel, R. et al. (1981), Infrared Observations of the Saturnian System from Voyager 1, *Science*, *212*(4491), 192–200, doi:10.1126/science.212.4491.192.

Hayes, J. M. (1983), Geochemical evidence bearing on he origin of aerobiosis, a speculative hypothesis, in *Earth's earliest biosphere*, pp. 291–301, Princeton University Press, Princeton, N.J.

Hayes, J. M. (1994), Global methanotrophy at the Archean-Proterozoic transition, in *Early life on Earth*, pp. 220–236, Columbia University Press, New York.

Imanaka, H., B. N. Khare, J. E. Elsila, E. L. O. Bakes, C. P. McKay, D. P. Cruikshank, S. Sugita, T. Matsui, and R. N. Zare (2004), Laboratory experiments of Titan tholin formed in cold plasma at various pressures: implications for nitrogen-containing polycyclic aromatic compounds in Titan haze, *Icarus*, *168*, 344–366, doi:10.1016/j.icarus.2003.12.014.

Israël, G. et al. (2005), Complex organic matter in Titan's atmospheric aerosols from in situ pyrolysis and analysis, *Nature*, *438*, 796–799, doi:10.1038/nature04349.

Jancso, G., and W. A. Van Hook (1974), Condensed Phase Isotope Effects (Especially Vapor Pressure Isotope Effects), *Chem. Rev.*, *74*(6), 689–750, doi:10.1021/cr60292a004.

Jennings, D. E., P. N. Romani, G. L. Bjoraker, P. V. Sada, C. A. Nixon, A. W. Lunsford, R. J. Boyle, B. E. Hesman, and G. H. McCabe (2009), 12C/13C Ratio in Ethane on Titan and Implications for Methane's Replenishment, *J. Phys. Chem. A*, *113*(42), 11101–11106, doi:10.1021/jp903637d.

Khare, B. N., C. Sagan, E. T. Arakawa, F. Suits, T. A. Callcott, and M. W. Williams (1984), Optical Constants of Organic Tholins Produced in a Simulated Titanian Amtosphere: From Soft X-Ray to Microwave Frequencies, *Icarus*, *60*, 127–137, doi:10.1016/0019-1035(84)90142-8.

Kunde, V. G., A. C. Aiken, R. A. Hanel, D. E. Jennings, W. C. Maguire, and R. E. Samuelson (1981), C4H2, HC3N and C2N2 in Titan's atmosphere, *Nature*, *292*, 686–688, doi:10.1038/292686a0.

Lavvas, P. P., A. Coustenis, and I. M. Vardavas (2008), Coupling photochemistry with haze formation in Titan's atmosphere, Part II: Results and validation with Cassini/Huygens data, *Planet Space Sci.*, *56*(1), 67–99, doi:10.1016/j.pss.2007.05.027.

Lin, H., B. A. Ellingson, J. Pu, and D. G. Truhlar (2005), Temperature Dependence of Carbon-13 Kinetic Isotope Effects of Importance to Global Climate change, *J. Am. Chem. Soc.*, *127*, 2830–2831, doi:10.1021/ja0434026.

Lorenz, R. D. et al. (2006), The sand seas of Titan: Cassini RADAR observations of longitudinal dunes, *Science*, *312*, 724–727, doi:10.1126/science.1123257.

Lowry, T. H., and K. S. Richardson (1981), *Mechanism and Theory in Organic Chemistry*, 2nd Edition., Harper and Row Publishers, New York.

Maguire, W. C., R. A. Hanel, D. E. Jennings, V. G. Kunde, and R. E. Samuelson (1981), C3H8 and C3H4 in Titan's atmosphere, *Nature*, *292*, 683–686, doi:10.1038/292683a0.

Matthews, D. E., and J. M. Hayes (1978), Isotope-Ratio-Monitoring Gas Chromatography-Mass Spectrometry, *Anal. Chem.*, *50*(11), 1465–1473, doi:10.1021/ac50033a022.

McKay, D. S., E. K. Gibson Jr., K. L. Thomas-Keprta, H. Vali, C. S. Romanek, S. J. Clemett, X. D. F. Chillier, C. R. Maechling, and R. N. Zare (1996), Search for Past Life on Mars: Possible Relic Biogenic Activity in Martian Meteorite ALH84001, *Science*, *273*(5277), 924–930, doi:10.1126/science.273.5277.924.

Nixon, C. A. et al. (2008), The 12C/13C isotopic ratio in Titan hydrocarbons from Cassini/CIRS infrared spectra, *Nature*, *195*(2), 778–791, doi:10.1016/j.icarus.2008.01.012.

Olah, G. (2003), *Hydrocarbon Chemistry*, 2nd ed., John Wiley & Sons, Hoboken, New Jersey.

Pavlov, A. A., J. F. Kasting, J. L. Eigenbrode, and K. H. Freeman (2001), Organic haze in Earth's early atmosphere: Source of low-13C Late Archean kerogens?, *Geology*, *29*(11), 1003–1006, doi:10.1130/0091-7613(2001)029<1003:OHIESE>2.0.CO;2.

Rice, A. L., A. A. Gotoh, H. O. Ajie, and S. C. Tyler (2001), High-Precision Continuous-Flow Measurement of d13C and dD of Atmospheric CH4, *Anal. Chem.*, *73*(17), 4104–4110, doi:10.1021/ac0155106.

Rye, R., and H. Holland (2000), Life associated with 2.76 Ga ephemeral pond?: Evidence from Mount Roe #2 paleosol, *Geology*, *28*(6), 483–486, doi:10.1130/0091-7613(2000) 28<483:LAWAGE>2.0.CO;2.

Schidlowski, M., J. M. Hayes, and I. R. Kaplan (1983), Isotopic Inferences of Ancient Biochemistries: Carbon, Sulfur, Hydrogen, and Nitrogen, in *Earth's earliest biosphere*, pp. 149–186, Princeton University Press, Princeton, N.J.

Trainer, M. G., A. A. Pavlov, H. L. DeWitt, J. L. Jimenez, C. P. McKay, O. B. Toon, and M. A. Tolbert (2006), Organic haze on Titan and the early Earth, *Proc. Natl. Acad. Sci. U.S.A.*, *103*(48), 18035–18042, doi:10.1073/pnas.0608561103.

Tyler, S. C., A. L. Rice, and H. O. Ajie (2007), Stable isotope ratios in atmospheric CH4: Implications for seasonal sources and sinks, *J. Geophys. Res.*, *112*, D03303, doi:10.1029/2006JC007231.

Yuen, G., N. Blair, D. J. DesMarais, and S. Chang (1984), Carbon isotopic composition of low molecular weight hydrocarbons and monocarboxylic acids from Murchison meteorite, *Nature*, *307*, 252–254, doi:10.1038/307252a0.

Table 4.1: Measurements of $\delta^{13}C$ for reactant CH_4 and for the particles formed from the irradiation of CH_4 and mixtures of CH_4 and CO_2.

Reactant CH_4 Samples	CH_4 (Torr)	$\delta^{13}C$ (‰) *	Peak Area (Volt · s)	IRMS Analysis Date
Aliquots of Reactant CH_4				
CH_4 tank aliquot		−18.29 ± 0.53		Jul 2012
		−18.13 ± 0.33		Nov 2012
10 Torr CH_4 in chamber		−19.13 ± 0.50		Nov 2012
200 Torr CH_4 in chamber		−18.70 ± 0.89		Jul 2012
		−18.53 ± 1.1		Nov 2012
Average		−18.4 ± 0.4		
Particles from the CH_4 irradiation experiments				
	4.9	−19.61 ± 0.13	14.141	12/11/11
	4.9	−20.76 ± 0.13	12.191	9/10/12
	5.0	−18.21 ± 0.13	13.848	9/10/12
	10.7	−27.64 ± 0.06	7.511	9/13/11
	11.2	−26.05 ± 0.06	6.601	9/13/11
	20.5	−26.48 ± 0.13	6.584	12/11/11
	41.5	−23.24 ± 0.06	27.123	9/13/11
	70 †	−23.3	-------	2004†
	70 †	−23.17	-------	2004†
	70 †	−23.76	-------	2004†
	70.8	−23.97 ± 0.13	19.012	9/13/11
	71.8	−24.59 ± 0.34	-------	1/26/10 †
	102.1	−24.23 ± 0.06	40.647	9/13/11
	149.9	−24.57 ± 0.13	46.941	9/10/12
	200.2	−23.79 ± 0.16	50.774	7/20/10
	200.7	−25.45 ± 0.34	-------	1/26/10 †
Average (N=16)		−25 ± 2		
Average (≥ 40 Torr) (N=10)		−23.9 ± 0.8		

Particles from the CH_4/CO_2 irradiation experiments at 10 Torr CH_4					
CH_4/CO_2 ratio	**CH_4 (Torr)**	**CO_2 (Torr)**	**$\delta^{13}C$ (‰) ***	**Peak Area (Volt · s)**	**IRMS Analysis Date**
0.34	10.3	30.3	−24.23 ± 0.13	15.093	9/10/12
0.50	10.7	21.5	−22.54 ± 0.13	22.337	12/11/11
0.50	10.7	21.5	−23.82 ± 0.13	18.424	12/11/11
0.96	10.3	10.7	−22.68 ± 0.13	22.425	12/11/11
1.67	10.7	6.4	−21.97 ± 0.06	23.038	9/13/11
2.40	10.3	4.3	−22.57 ± 0.13	22.575	12/11/11
3.06	10.7	3.5	−22.87 ± 0.13	23.438	12/11/11
3.44	11.7	3.4	−22.55 ± 0.06	24.136	9/13/11
4.28	10.7	2.5	−22.05 ± 0.13	24.096	12/11/11
Average (N=9)			−22.8 ± 0.8	21 ± 3	
Particles from the CH_4/CO_2 irradiation experiments at 200 Torr CH_4					
0.8	200	250	−27.8 ± 0.16	81.391	4/15/10
1	200.2	200.2	−26.64 ± 0.16	48.676	4/15/10
1	201.2	201.1	−26.04 ± 0.16	86.361	4/15/10
Average (N=3)			−26.8 ± 0.9	72 ± 20	

* For the reactant CH_4 samples, the 1σ errors for $\delta^{13}C$ are based on the standard deviation of replicate measurements. For the particles samples, the 1σ errors for $\delta^{13}C$ are based on the single measurement precision of runs of the standards sucrose ANU (−10.45 ‰ VPDB) or NBS-22 (−30.03 ‰ VPDB) and do not include possible systematic errors due to sample sizes being smaller than the standards for the smallest samples.

† IRMS peak areas are not available for the 26 January 2010 nor the 2004 analyses.

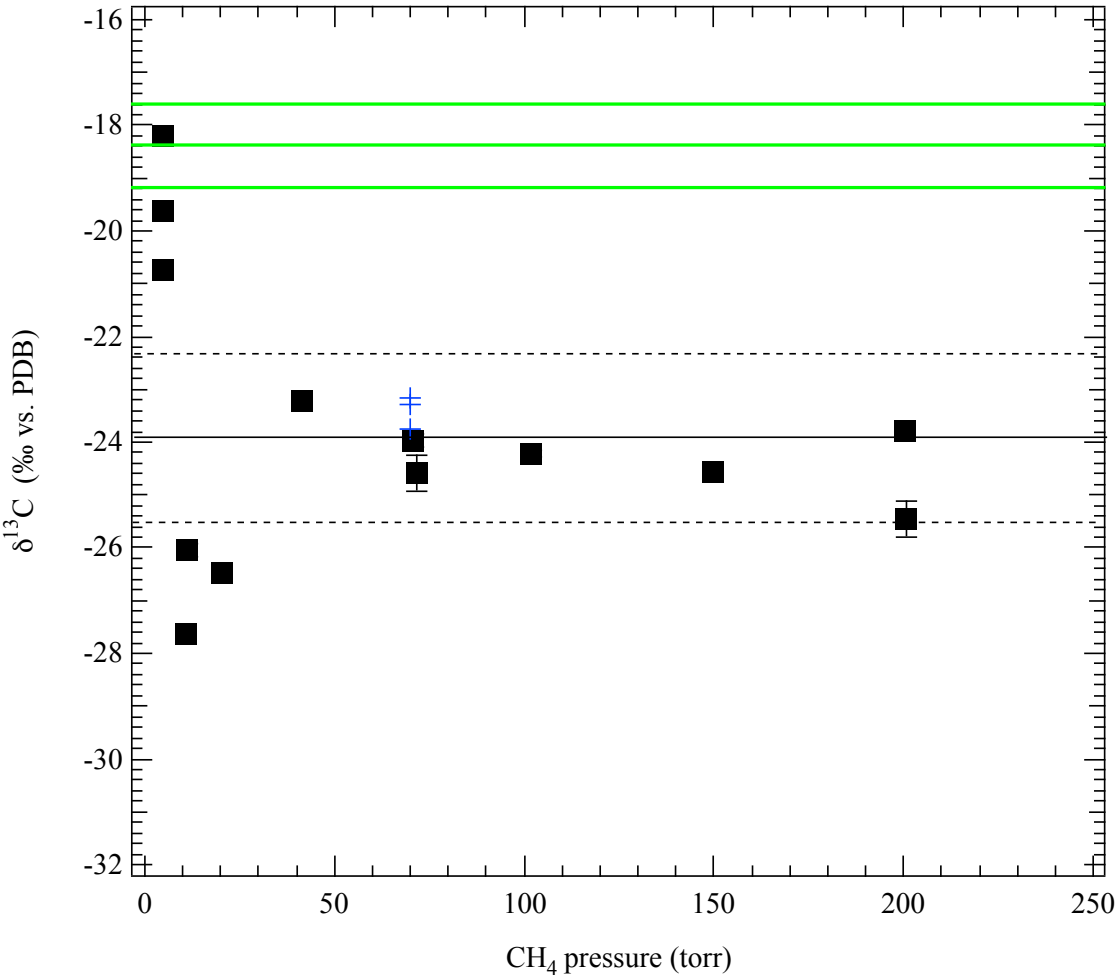

Figure 4.1:Measurements of $\delta^{13}C$ of aerosol particles formed from the irradiation of pure CH_4 as a function of the initial pressure of CH_4 in the chamber for each experimental run. The horizontal lines represent the average (solid) and the average ± 2σ (dashed) for the experiments irradiating CH_4 for initial pressures ≥ 40 Torr (−23.9 ± 1.6‰ VPDB). Black squares are measurements from over the period from 2010-2012; blue crosses are measurements from 2004. For comparison, the green thick lines shows the isotopic composition of the reactant CH_4 before irradiation of −18.4 ± 0.8‰ VPDB (2σ).

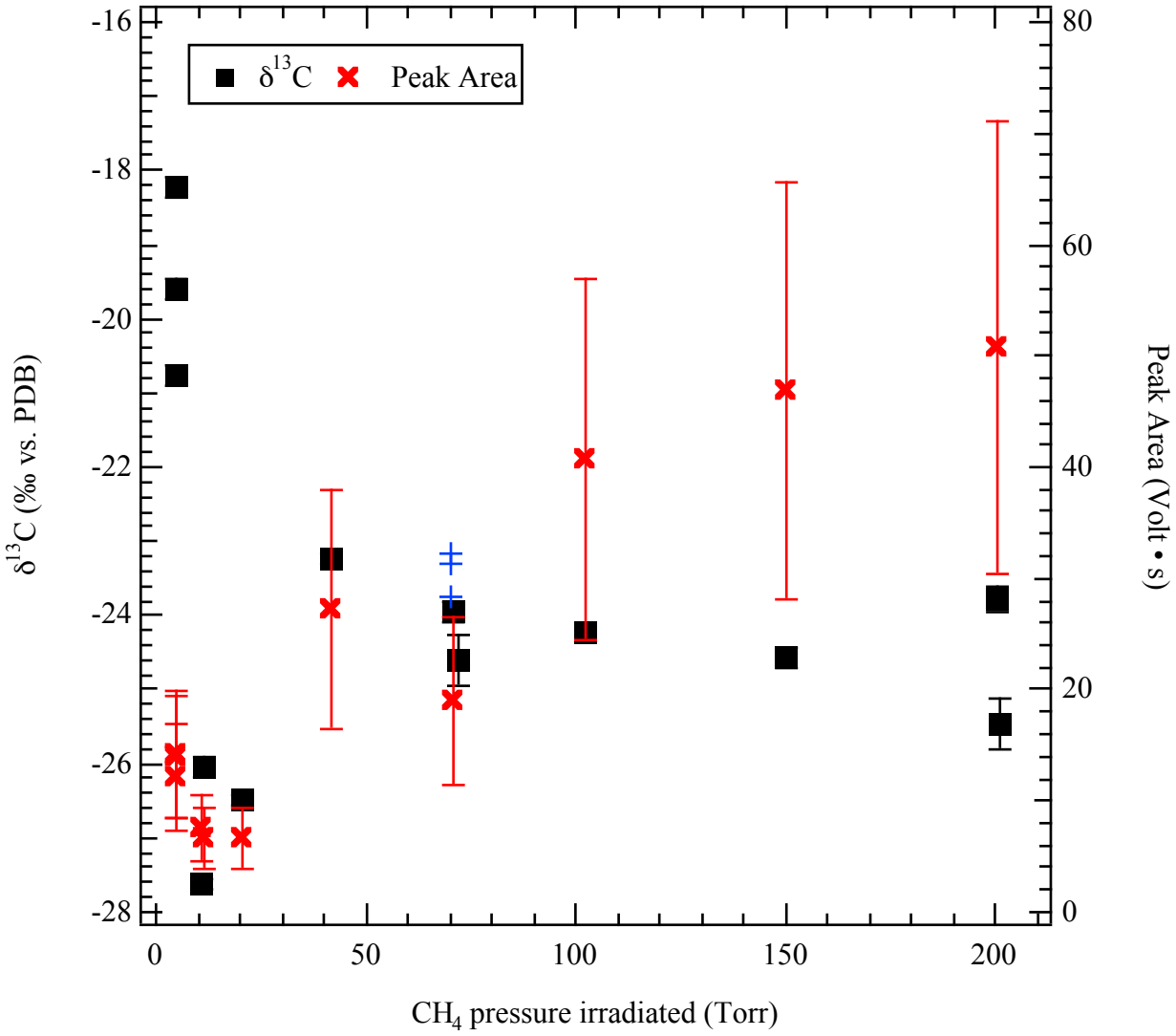

Figure 4.2: Same as for Figure 4.1 but with the corresponding EA-IRMS peak area measurements plotted as red crosses. Error bars for the peak areas represent their ±40% (1σ) uncertainty (see Methods).

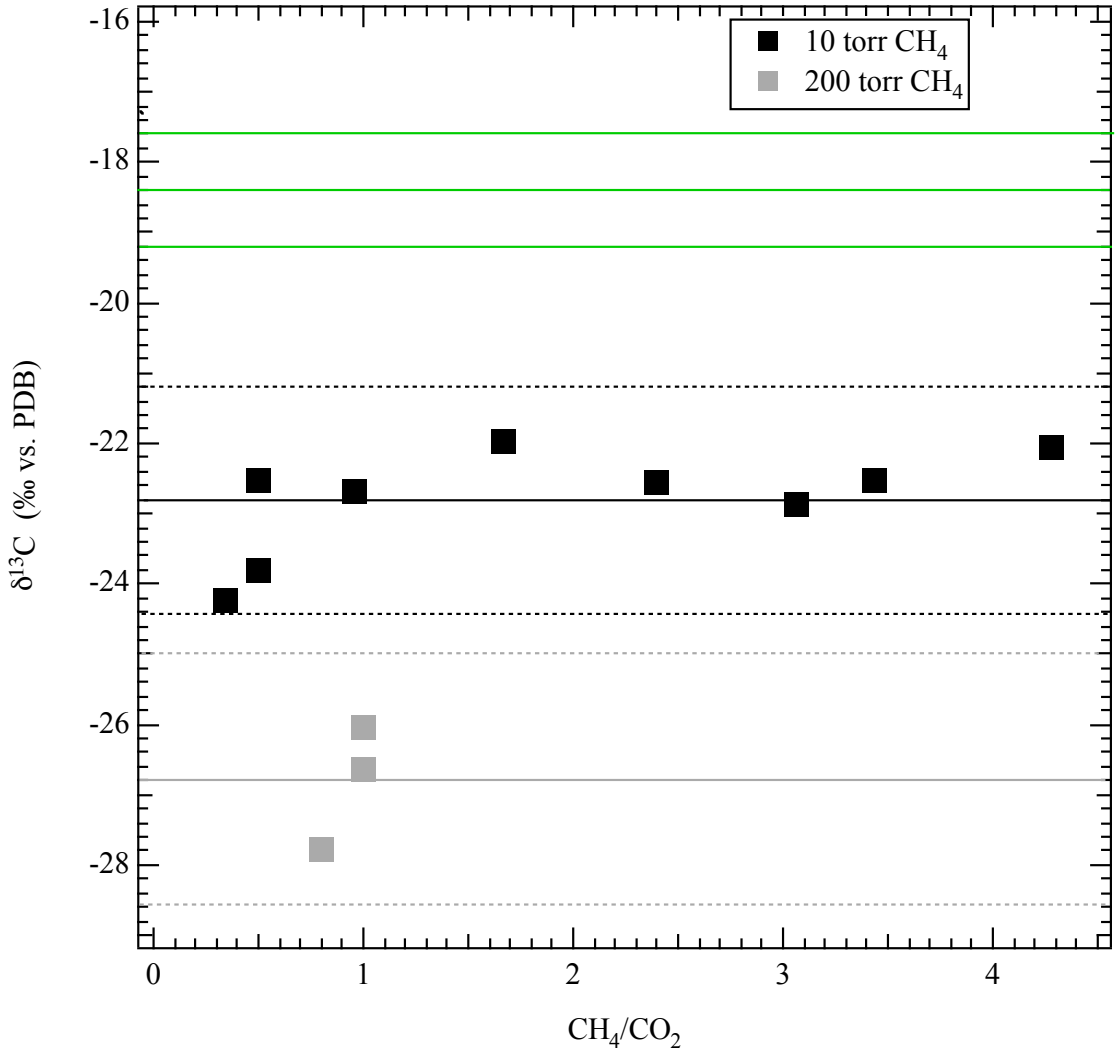

Figure 4.3: $\delta^{13}C$ of particles formed from the irradiation of mixtures of CH_4 and CO_2. Two sets of experiments were conducted with either 10 Torr or 200 Torr of CH_4. The separate averages of $\delta^{13}C$ from the two sets of experiments are noted with the solid lines; the dashed lines represent the averages ± 2σ. For comparison, the thick green lines show the isotopic composition of the reactant CH_4 before irradiation of −18.4 ± 0.8‰ VPDB (2σ).

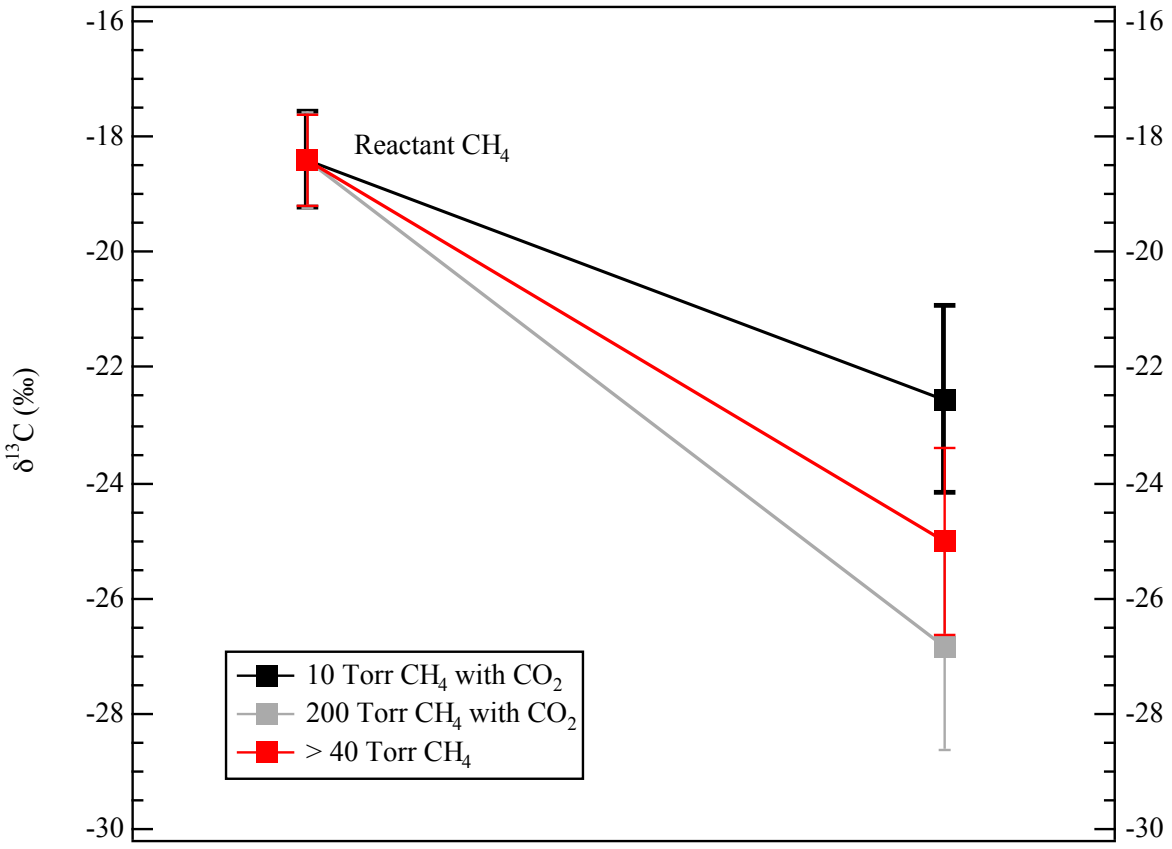

Figure 4.4: Comparison of measurements of $\delta^{13}C$ of the reactant CH_4 with those of the particles produced in the different sets of experiments. The particles are depleted in ^{13}C relative to the reactant CH_4. Error bars represent 2σ; see text.

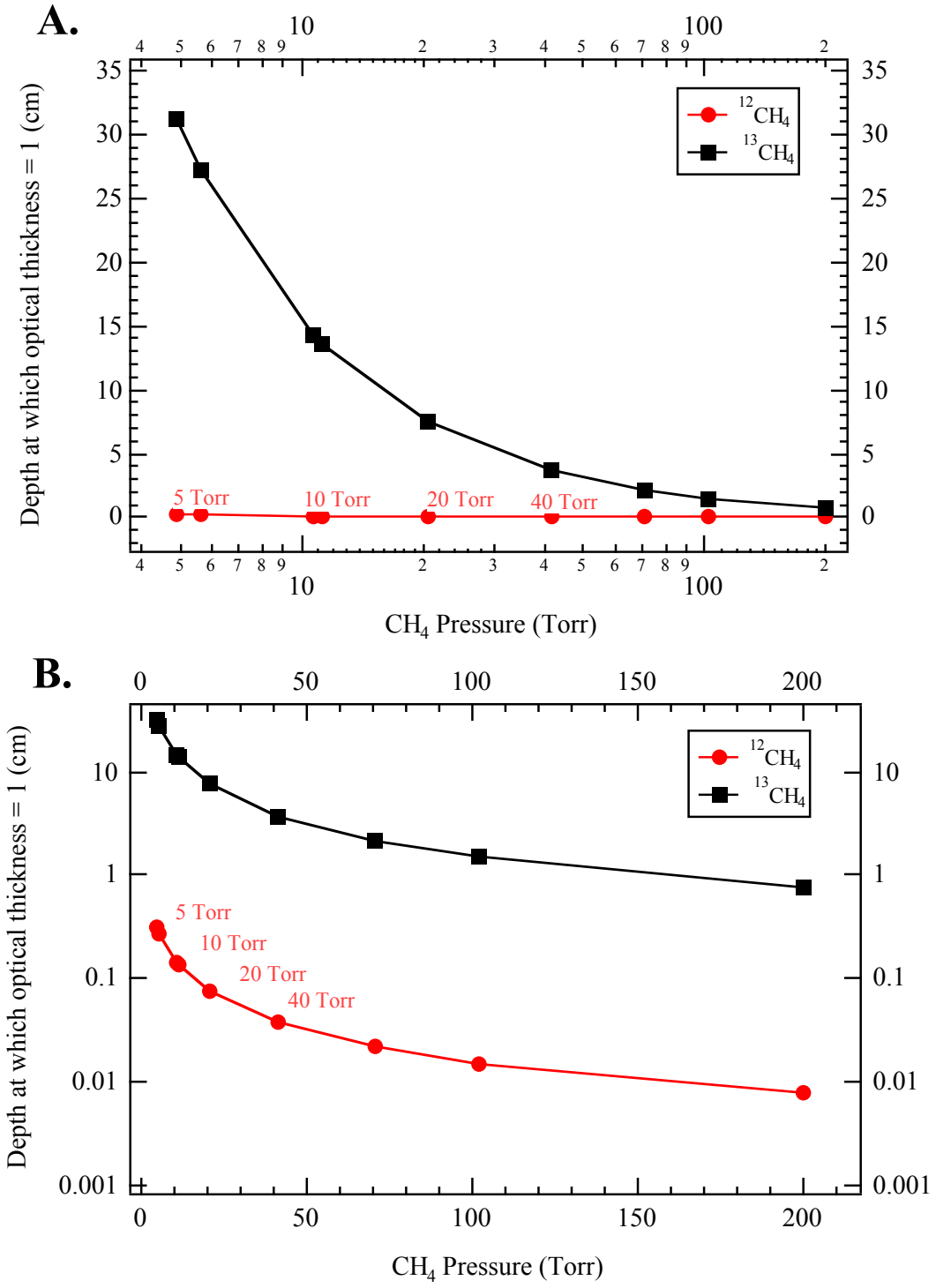

Figure 4.5: Distance from D_2 lamp window (in cm) at which the optical depth for $^{12}CH_4$ (red circles) and $^{13}CH_4$ (black squares) is 1, versus experimental CH_4 pressures (from experiments shown in Figure 4.1), calculated using an absorption cross-section for CH_4 of 2 x 10^{-17} cm^2 at 120 nm [*Yung and DeMore*, 1999] and making the simplifying assumption that there is not an isotope shift in cross-section for $^{13}CH_4$. (A) shows log(distance from window) vs CH_4 pressure while (B) shows distance from window vs log(CH_4 pressure). The height of the chamber is 36 cm.